Geological Survey of Canada
Commission geologique du Canada

ECONOMIC GEOLOGY REPORT 35

PETROLOGY AND ECONOMIC GEOLOGY OF THE DUMONT SILL: AN ARCHEAN INTRUSION OF KOMATIITIC AFFINITY IN NORTHWESTERN QUEBEC

J. M. DUKE

1986

Canada

86-04081/

GEOLOGICAL SURVEY OF CANADA
ECONOMIC GEOLOGY REPORT 35

PETROLOGY AND ECONOMIC GEOLOGY OF THE DUMONT SILL: AN ARCHEAN INTRUSION OF KOMATIITIC AFFINITY IN NORTHWESTERN QUEBEC

J. M. DUKE

1986

© Minister of Supply and Services Canada 1986

Available in Canada through

authorized bookstore agents and other bookstores

or by mail from

Canadian Government Publishing Centre
Supply and Services Canada
Ottawa, Canada K1A 0S9

and from

Geological Survey of Canada offices:

601 Booth Street
Ottawa, Canada K1A 0E8

3303-33rd Street N.W.,
Calgary, Alberta T2L 2A7

A deposit copy of this publication is also available
for reference in public libraries across Canada

Cat. No. M43 35/1986E Canada: $6.00
ISBN 0-660-12062-3 Other countries: $7.20

Price subject to change without notice

Critical Reader

O.R. Eckstrand

Original manuscript received – 1983-06-24
Final version approved for publication 1983-08-11

Preface

The Dumont Sill, a differentiated ultramafic to mafic sill of Archean age in the Abitibi greenstone belt of the Superior Province, Canadian Shield, was first reported in 1925. Over the last 60 years the intrusion has been the focus of limited and largely unsuccessful prospecting for asbestos, base metals and precious metals. Exploration carried out between 1969 and 1972, however, resulted in the discovery of an extensive zone of low grade nickel mineralization within the sill. Although this mineralization has not yet proved to be an economically viable ore deposit, it is a significant nickel resource.

This report describes the mineralogy, petrology, and economic geology of the Dumont intrusion, with particular emphasis on the magmatic stage of its development. The study would not have been possible without the complete co-operation of industry. Less than 2 per cent of the bedrock surface of the intrusion outcrops, the remainder being covered by up to 45 m of overburden. Most of the material used in this study was derived from core samples from 57 holes drilled by industry.

An understanding of the petrogenesis of the sill and especially of the factors that controlled the distribution of nickel sulphides is of fundamental importance in guiding any further exploration of the body. Perhaps of greater significance is the likelihood that the Dumont intrusion is not unique and that knowledge acquired here will provide criteria for the identification and exploration of other similar bodies.

R.A. Price
Director General
Geological Survey of Canada

Préface

Le sill de Dumont, intrusion différenciée ultramafique à mafique d'âge archéen dans la zone de roches vertes d'Abitibi de la province du lac Supérieur du Bouclier canadien, a été idenfitié pour la première fois en 1925. Au cours des soizante dernières années, l'intrusion a fait l'objet de travaux de prospection limités et en grande partie infructueux visant à découvrir l'amiante, les métaux communs et les métaux précieux. Cependant, les travaux d'exploration effectués entre 1969 et 1972 ont abouti à la découverte, dans le sill, d'une vaste zone à faible teneur en nickel. Bien que ce gisement ne se soit pas encore avéré rentable, il représente une importante source de nickel.

Le présent rapport décrit la minéralogie, la pétrologie et la géologie économique de l'intrusion de Dumont, notamment la phase magmatique de son évolution. Cette étude n'aurait pas été possible sans l'entière collaboration de l'industrie. Moins de 2% de la surface rocheuse de l'intrusion affleure en surface, le reste étant caché par une couverture de dépôts meubles dont l'épasseur peut atteindre 45 m. La plupart des données utilisées au cours de cette étude ont été prises à partir de carottes provenant de 57 trous forés par l'industrie.

Il est essentiel de connaître la pétrogénèse du sill et notamment les facteurs qui ont contrôlé la répartition des sulfures de nickel avant d'entreprendre d'autres travaux d'exploration de cette intrusion. En outre, l'intrusion de Dumont n'est vraisemblablement pas unique et les connaissances acquises lors de son étude permettront d'établir des critères pour l'identification et l'exploration d'autres masses similaires.

Le directeur général de la
Commission géologique du Canada
R.A. Price

CONTENTS

1 Abstract/Résumé
1 Summary/Sommaire
3 Introduction
3 Purpose of the investigation
3 Previous studies
4 Access, exposure, and sampling
4 Acknowledgments
4 General description of the Dumont Sill
4 Regional geological setting
6 Contact relations, areal extent, and age of the intrusion
8 Petrography of the intrusion
8 Magmatic textures and modal composition
8 Introduction
12 Ultramafic Zone
14 Mafic Zone
16 Secondary textures and modal composition
16 Ultramafic Zone
19 Mafic Zone
19 Mineral compositions
19 Analytical method
19 Primary minerals
22 Secondary minerals
24 Sulphides and alloys
26 Economic geology
26 Introduction
27 Intermineral distribution of nickel
28 Composition of magmatic sulphide grains
29 Assay data and resource estimation
30 Petrogenesis
30 Nature of the parent and derivative magmas
31 Emplacement and differentiation of the intrusion
40 Computer simulation of the differentiation of the intrusion
43 Nature of the alteration processes
44 Composition – volume relationships during serpentinization
45 Discussion
45 Comparison with other layered komatiitic intrusions
47 Nickel sulphide deposits associated with komatiitic rocks
47 Exploration guidelines
48 References

Appendices

52 1. Diamond-drill hole data
53 2. Chemical analyses of whole-rocks

Tables

5 1. Chemical compositions of volcanic host rocks of the Dumont and Landrienne (Amos) intrusions
18 2. Representative olivine analyses – arranged in order of increasing stratigraphic height
21 3. Representative average clinopyroxene compositions – arranged in order of increasing stratigraphic height
24 4. Representative chromite analyses – arranged in order of increasing stratigraphic height
25 5. Representative serpentine analyses
26 6. Representative analyses of secondary chlorite, diopside and actinolite
27 7. Representative analyses of sulphides and alloys
30 8. Magmatic sulphide grains: grain size, modal and chemical composition and distribution coefficient
31 9. Average grades and true thicknesses of upper, middle and lower nickel-enriched layers
32 10. Compositions of spinifex-textured peridotites and model parent magma of Dumont Sill
35 11. Composition of noncumulate rocks from the Dumont intrusion and overlying sills
35 12. Bulk composition of the Dumont Sill calculated from average compositions of subzones
37 13. Average composition of orthocumulate rocks from the basal Lower Peridotite Subzone
41 14. Compositions of silicate liquid, olivine and sulphide calculated using computer model

Figures

5 | 1. Location of the Dumont sill within the Abitibi greenstone belt
6 | 2. Magnetometer survey of the Dumont intrusion
7 | 3. Geological map of the Dumont intrusion
8 | 4. Cross-section showing positions of three nickel-enriched layers in the Dunite Subzone
9 | 5. Modal, cryptic, and grain size variation across the Dumont Sill
10 | 6. Photomicrographs showing primary igneous textures in the Dumont Sill
(a) Fine grained olivine-chromite orthocumulate, base of Lower Peridotite Subzone
(b) Fine grained olivine-chromite adcumulate, top of Lower Peridotite Subzone
(c) Medium grained olivine adcumulate, lowermost Dunite Subzone
(d) Clinopyroxene oikocryst enclosing partly serpentinized olivine, Dunite Subzone
(e) Medium grained olivine-chromite orthocumulate, Upper Peridotite Subzone
(f) Fine grained clinopyroxene adcumulate, Clinopyroxenite Subzone
(g) Subophitic texture, Gabbro Subzone
(h) Part of irregular plagioclase-rich layer, Gabbro Subzone
(i) Plagioclase-pyroxene cumulate, Quartz Gabbro Subzone
(j) Noncumulate texture, Quartz Gabbro Subzone
13 | 7. Opaque minerals in the Ultramafic Zone of the Dumont Sill
(a) Large chromite oikocryst enclosing serpentinized cumulus olivine, Dunite Subzone
(b) Cumulus chromite, Upper Peridotite Subzone
(c) Olivine + sulphide cumulate in Dunite Subzone
(d) Typical magmatic sulphide grain composed of pentlandite, magnetite and awaruite
(e) Magmatic sulphide grain composed of pentlandite, magnetite and awaruite
14 | 8. Variation of specific gravity with modal per cent of primary minerals (= olivine + clinopyroxene + chromite)
15 | 9. Distribution of specific gravities and serpentine textures in cross-section 36 + 00 West
16 | 10. Features related to serpentinization in the Ultramafic Zone
(a) Incipient serpentinization with development of lizardite
(b) Lizardite mesh texture, pseudomorphous after olivine
(c) Lizardite hourglass texture with brucite + magnetite veinlets
(d) Typical development of antigorite around rims of lizardite pseudomorphs after olivine
(e) Nonpseudomorphic ribbon texture of serpentinization
(f) Nonpseudomorphic interpenetrating texture
19 | 11. Variation of the forsterite content of olivine in drillholes E5, E16, E21, and W13
20 | 12. Compositions of Dumont clinopyroxenes plotted in the pyroxene quadrilateral
21 | 13. Analyses across a single clinopyroxene oikocryst illustrating crystal zoning
22 | 14. Correlation between chromium and aluminum of Dumont clinopyroxenes
23 | 15. Histograms showing frequency distribution of oxide concentrations in analyzed chromites
25 | 16. Composition of serpentine minerals in terms of the number of Si and Fe atoms in the structural formula
25 | 17. Variation of the chlorine concentration and specific gravity of whole-rock samples from the Ultramafic Zone. Ratios across the Ultramafic Zone in drillhole E21
26 | 18. Compositions of primary and secondary clinopyroxenes, Lower Peridotite Subzone
28 | 19. (a) Whole-rock nickel concentration, recalculated on an anhydrous basis plotted against nickel content of contained olivine in unmineralized samples
(b) Concentration of nickel in primary olivine and secondary serpentine and magnetite
29 | 20. Nickel content of whole-rock and contained olivine and forsterite content of olivine in drillhole E16
33 | 21. Nickel assay profiles of sections along the length of the sill
36 | 22. Depiction of proposed model of intrusion, crystal settling, filter pressing, magma mixing, bottom crystallization and sulphide saturation
38 | 23. Possible thermal regimes in the zone of mixing at the onset of accumulation of the Dunite Subzone
42 | 24. Variation of Al_2O_3 and FeO/FeO+MgO in the Dumont rocks
42 | 25. Variation of Zr and TiO_2 in the Dumont rocks
43 | 26. Variation of V and TiO_2 in the Dumont rocks
43 | 27. Variation of nickel and forsterite contents of olivines
44 | 28. Compositions of samples from the Ultramafic Zone plotted in a portion of the $CaO-MgO-SiO_2$ system
46 | 29. Synoptic histograms of zero change volume factors for each of two serpentinized dunites

PETROLOGY AND ECONOMIC GEOLOGY OF THE DUMONT SILL: AN ARCHEAN INTRUSION OF KOMATIITIC AFFINITY IN NORTHWESTERN QUEBEC

Abstract

The komatiitic, synvolcanic Dumont Sill occurs within a sequence of iron-rich tholeiite lavas in the Abitibi greenstone belt. Its Ultramafic Zone comprises the Lower Peridotite Subzone, an olivine+chromite cumulate, the Dunite Subzone, an olivine ± sulphide cumulate, and the Upper Peridotite Subzone, an olivine+chromite cumulate. The overlying Mafic Zone comprises the Clinopyroxenite Subzone, a clinopyroxene cumulate, the Gabbro Subzone, a clinopyroxene+plagioclase cumulate, and the Quartz Gabbro which includes plagioclase + pyroxene cumulates as well as noncumulate gabbros. The parent magma was a peridotitic komatiite liquid (27.5% MgO) that carried 12.5% olivine crystals in suspension. The Lower Peridotite formed by the settling and accumulation of these intratelluric phenocrysts whereas the overlying cumulates accumulated by a bottom crystallization process. Olivine+sulphide cumulate layers occur in the Dunite and formed by the accumulation of olivine and molten sulphide in their "cotectic" proportions. Sulphide saturation occurred when fractionated, sulphur-enriched intercumulus liquid was expelled upward by filter-pressing of the partially molten Lower Peridotite and mixed with less evolved liquid at the floor of the magma chamber. The intrusion is pervasively altered with the development of lizardite+brucite+magnetite+diopside+chlorite in the Ultramafic Zone and actinolite+epidote+chlorite assemblages in the Mafic Zone. The secondary textures and assemblages are indicative of nonequilibrium, retrograde, low-temperature alteration which probably resulted from an influx of water during initial cooling of the sill.

Résumé

Le sill komatiitique synvolcanique de Dumont se présente dans une séquence de laves tholéiitiques riches en fer dans la zone de roches vertes d'Abitibi. La zone ultramafique se compose d'un cumulat à olivine+chromite, sous-zone inférieure de péridotite, d'un cumulat à olivine+sulfure, sous-zone de dunite, et d'un cumulat à olivine+chromite, sous-zone supérieure de péridotite. La zone mafique sus-jacente comprend un cumulat à clinopyroxène, sous-zone de clinopyroxénite, un cumulat à clinopyroxène+plagioclase, sous-zone de gabbro, ainsi que des cumulats à clinopyroxène+plagioclase et des gabbros sans cumulats, sous-zone de gabbro quartzique. Le magma originel était un liquide komatiitique péridotitique (27,5 % de MgO) comportant 12.5% de cristaux d'olivine en suspension. La péridotite inférieure à été formée par décantation et accumulation de ces phénocristaux intratelluriques, tandis que les cumulats sus-jacents se sont accumulés par cristallisation basale. Des couches de cumulats à olivine+sulfure trouvées dans la dunite ont été formées par accumulation, en proportions <<cotectiques>>, d'olivine et de sulfure en fusion. La saturation en sulfure a eu lieu lorsqu'un liquide intercumulus fractionné riche en soufre a été expulsé par l'effet de filtre-presse de la péridotite inférieure partiellement fondue et mélangé à un liquide moins évolué au fond de la chambre magmatique. L'altération répandue de l'intrusion a produit un assemblage de lizardite+brucite+magnétite+diopside+chlorite dans la zone ultramafique et des assemblages d'actinote+épidote+chlorite dans la zone mafique. Les structures et assemblages secondaires indiquent qu'il y a eu altération régressive non équilibrée à faible température, vraisemblablement à la suite d'une entrée d'eau lors du refroidissement initial du sill.

Summary

The Dumont Sill, situated 62 km northeast of Rouyn in northwestern Quebec, is a synvolcanic, komatiitic intrusion of Archean age occurring within the Abitibi greenstone belt in the Superior Province of the Canadian Shield. The sill intrudes subaqueous, iron-rich tholeiite lavas which are approximately 2.7 Ga old. The sill is poorly exposed over a strike length of 6.5 km and comprises a lower Ultramafic Zone which averages 450 m in true thickness and an upper Mafic Zone about 250 m thick. The Ultramafic Zone is subdivided into the Lower Peridotite, Dunite and Upper Peridotite subzones. The Lower and Upper Peridotite subzones are olivine+chromite cumulates with variable amounts of intercumulus clinopyroxene. The Dunite Subzone is an extreme olivine adcumulate containing very small amounts of intercumulus chromite and clinopyroxene. Cumulus sulphide occurs in certain parts of the Dunite Subzone and also locally in the Lower Peridotite. The Mafic Zone comprises three subzones which are; from the base upwards, the Clinopyroxenite, the Gabbro and the

Sommaire

Le sill de Dumont, situé à 62 km au nord-est de Rouyn, dans le nord-ouest québécois, est une intrusion komatiitique synvolcanique d'âge archéen. Il se présente dans la zone de roches vertes d'Abitibi dans la province du lac Supérieur du Bouclier canadien. Le sill a pénétré des laves tholéiitiques subaquatiques riches en fer qui datent d'environ 2,7 Ga. Il est mal exposé sur une distance de 6,5 km parallèlement à sa direction et comporte une zone ultramafique inférieure, dont l'épaisseur réelle moyenne est de 450 m, et une zone mafique supérieure d'environ 250 m d'épaisseur. La zone ultramafique se subdivise en trois sous-zones, la sous-zone inférieure de péridotite, la sous-zone de dunite et la sous-zone supérieure de péridotite. Les sous-zone inférieure et supérieure de péridotite se composent de cumulats à olivine-chromite et de quantités variables de clinopyroxène intercumulus. La sous-zone de dunite est un adcumulat très riche en olivine qui contient de très petites quantités de chromite et de clinopyroxène intercumulus. Du sulfure cumulus se présente dans certaines parties de la sous-zone de dunite et par endroits dans la sous-zone inférieure de péridotite. La zone

Quartz Gabbro. The Clinopyroxenite Subzone is an extreme clinopyroxene adcumulate at its base but grades into clinopyroxene+plagioclase cumulate rocks in the overlying Gabbro Subzone. The Quartz Gabbro Subzone includes both plagioclase+clinopyroxene cumulates and noncumulate gabbros that contain modal and normative quartz. Olivine and chromite are restricted to the Ultramafic Zone whereas plagioclase occurs only in the Mafic Zone.

The Mg/Mg+Fe ratios of the ferromagnesian cumulus phases increase gradually from the base of the sill upwards across the Lower Peridotite, undergo an abrupt increase at or just above the base of the Dunite, remain essentially constant through the upper part of the Dunite and into the base of the Upper Peridotite, and then follow a normal iron enrichment trend upward through the overlying part of the intrusion.

The parent magma of the intrusion was a peridotitic komatiite liquid containing about 27.5% MgO and carrying about 12.5% olivine (Fo_{93}) in suspension. The Lower Peridotite Subzone represents the accumulation of these intratelluric phenocrysts and variable proportions of trapped intercumulus liquid. The cumulus chromite in the Lower Peridotite may also have been carried into the magma chamber in suspension or may have crystallized during settling of the olivine. The increase of forsterite content of olivine upwards across the Lower Peridotite reflects the amount of reaction of the cumulus olivine with intercumulus liquid before and during expulsion of the liquid from the crystal mush by filter pressing. The Dunite, Upper Peridotite, Clinopyroxenite and Gabbro subzones accumulated by crystallization at or near the upward-migrating base of the convecting magma chamber. The base of the Mafic Zone represents a reaction relationship or distribution point whereby olivine and chromite are replaced as liquidus phases by clinopyroxene. Coarse grained, noncumulate gabbros and pegmatoidal gabbro schlieren within the Quartz Gabbro Subzone demonstrate that fractional crystallization of peridotitic komatiite magma can produce liquids containing as little as 5.5% MgO. Moreover, the presence of thin sills of similar evolved composition overlying the Dumont body indicates that these liquids were mobile and mass balance considerations suggest that an amount of differentiated liquid equivalent to about 10% of the initial mass of magma was tapped off the main chamber. Some of the noncumulate rocks are very iron-rich (about 15% FeO), and differ in this respect from typical extrusive basaltic komatiites.

Magmatic sulphides are restricted to the Lower Peridotite and Dunite subzones, although in the former they represent mainly a post cumulus phase. In the Dunite Subzone olivine and sulphide are present in approximately their "cotectic" proportions and molten sulphide was apparently a cumulus phase. Three olivine-sulphide cumulate layers occur within the Dunite Subzone but do not extend over the entire strike length of the sill.

mafique comporte les trois sous-zones suivantes, données par ordre ascendant: la sous-zone de clinopyroxénite, la sous-zone de gabbro et la sous-zone de gabbro quartzique. La base de la sous-zone de clinopyroxénite est un adcumulat très riche en clinopyroxène qui se transforme en roches à cumulats à clinopyroxène+orthopyroxène+plagioclase dans la sous-zone de gabbro sus-jacente. La sous-zone de gabbro quartzique comprend à la fois des cumulats à plagioclase+clinopyroxène et des gabbros sans cumulats contenant du quartz modal et normatif. L'olivine et la chromite se trouvent uniquement dans la zone ultramafique tandis que la plagioclase se présente seulement dans la zone mafique.

Les proportions Mg/Mg+Fe des phases cumulus ferromagnésiennes augmentent graduellement de la base du sill jusqu'au sommet de la sous-zone inférieure de péridotite. Elles s'accroissent brusquement à la base de la sous-zone de dunite ou imméridatement au-dessus de celle-ci, demeurent plus ou moins constantes dans la partie supérieure de la sous-zone de dunite et jusque dans la partie inférieure de la péridotite supérieure, puis suit la tendance normale à l'enrichissement en fer dans la partie sus-jacente de l'instrusion.

Le magma à l'origine de l'intrusion était un liquide komatiitique péridotitique contenant environ 27,5 % de MgO et environ 12,5 % d'olivine (Fo_{93}) en suspension. La sous-zone inférieure de péridotite représente l'accumulation de ces phénocristaux intratelluriques et de proportions variables de liquide intercumulus piégé. La chromite cumulus dans la sous-zone inférieure de péridotite a peut-être transportée en suspension dans la chambre magmatique ou cristallisée lors de la décantation de l'olivine. L'accroissement, dans l'olivine, de la teneur en forstérite vers le sommet de la sous-zone inférieure de péridotite reflète l'importance de la réaction entre l'olivine cumulus et le liquide intercumulus avant et durant l'expulsion, par l'effet de filtre-presse, du liquide de la bouillie cristalline. La sous-zone supérieure de péridotite et les sous-zone de dunite, de clinopyroxénite et de gabbro se sont accumulées par cristallisation près de la base ascendante de la chambre magmatique en convection. La base de la zone mafique représente un lien réactionnel ou un point de distribution grâce auquel l'olivine et la chromite sont remplacées en tant que phases liquides par la clinopyroxène. La présence de gabbros fortement grenus et sans cumulats et de schlieren à gabbro pegmatoïdique dans la sous-zone de gabbro quartzique indique que la cristallisation fractionnée d'un magma à komatiite péridotitique peut donner des liquides contenant aussi peu que 5,5 % de MgO. En outre, la présence de minces sills de matériau à évolution similaire au-dessus de l'intrusion de Dumont indique que ces liquides étaient mobiles, tandis que l'étude de l'équilibre des masses porte à croire qu'une quantité de liquide différenciée équivalant à environ 10 % de la masse initiale du magma a été enlevée de la chambre principale. Certaines roches sans cumulats ont une très forte teneur en fer (environ 15 % de FeO) et, à cet égard, diffèrent des komatiites basaltiques extrusives typiques.

Les sulfures magmatiques se présentent seulement dans la sous-zone inférieure de péridotite, où ils représentent surtout une phase cumulus, et dans la sous-zone de dunite. Dans cette dernière sous-zone, l'olivine et le sulfure sont présents plus ou moins dans leurs proportions «cotectiques», le sulfure en fusion représentant vraisemblablement une phase cumulus. Trois couches à cumulats à olivine-sulfure se présentent dans la sous-zone de dunite, mais non pas sur

The middle layer has the highest average nickel grade (0.50%) and is the most laterally extensive, persisting over a strike of 2400 m with an average true thickness of 24 m. A higher grade zone within the middle layer averages 0.71% Ni over a strike length of 730 m and has a true thickness of 14 m. Evidently the magma was somewhat undersaturated with sulphide at the time of emplacement but became saturated over part of the strike length of the sill during accumulation of the Dunite Subzone. Sulphide saturation occurred when fractionated, sulphur-enriched intercumulus liquid was expelled by filter pressing of the partially molten Lower Peridotite and mixed with more primitive liquid in the zone of crystallization at the base of the main body of magma.

The ultramafic rocks are pervasively serpentinized. Serpentinization is overprinted by talc-carbonate alteration in places along the basal contact of the sill. The predominant secondary assemblage is lizardite + magnetite + brucite + chlorite + diopside ± chrysotile ± pentlandite ± awaruite ± heazlewoodite. Antigorite is developed locally, particularly in the uppermost Ultramafic Zone. Native copper occurs in some samples but not in those containing awaruite. Millerite occurs in steatitized rocks. The Mafic Zone rocks are ubiquitously altered to the assemblage actinolite + epidote + chlorite ± quartz. Primary textures are pseudomorphously preserved throughout most of the intrusion. Serpentinization proceeded isovolumetrically on the microscopic scale. On the mesoscopic scale, serpentinization was isochemical aside from the addition of significant amounts of hydrogen and chlorine, and the loss of some calcium.

The textures and assemblages of the secondary minerals are indicative of nonequilibrium, retrograde, low temperature (<350°C) alteration which may well have occurred as a result of an influx of water during the initial cooling of the intrusion. The sill was faulted and tilted into a steeply inclined attitude during the Kenoran event but no penetrative deformational fabric is evident, and the effects of regional metamorphism are minimal.

toute la longueur du sill. La couche du milieu a la plus forte teneur moyenne en nickel (0,50 %), ainsi que la plus vaste étendue latérale, et se prolonge sur une distance de 2 400 m; son épaisseur réelle moyenne est de 24 m. Une zone plus riche dans la couche du milieu contient en moyenne 0,71 % de Ni sur une distance de 730 m; son épaisseur réelle est de 14 . Le magma a dû être plutôt sous-saturé en sulfure au moment de sa mise en place, mais est devenu saturé sur une partie de la longueur du sill durant l'accumulation de la sous-zone de dunite. La saturation en sulfure s'est produite lorsqu'un intercumulus fractionné riche en soufre a été expulsé par l'effet de filtre-presse de la péridotite inférieure partiellement fondue et mélangé à un liquide plus primitif dans la zone de cristallisation à la base de la masse magmatique principale.

Les roches ultramafiques sont partout serpentinisées; par endroits, le long du contact inférieur du sill, il y a eu altération avec formation de talc. L'assemblage secondaire principal se compose de lizardite + magnétique + brucite + chlorite + diopside ± chrysotile ± pentlandite ± awaruite ± heazlewoodite. L'antigorite se présente par endroits, notamment dans la partie supérieure de la zone ultramafique. Du cuivre natif se trouve dans certains échantillons, mais non dans ceux qui contiennent de l'awaruite. La millérite se présente dans les roches altérées dans lesquelles il y a eu formation de talc. Les roches de la zone mafique ont partout été altérées à l'assemblage actinote + épidote + chlorite ± quartz. Les structures primaires sont conservées sous forme de pseudomorphes dans la plus grande partie de l'intrusion. La serpentinisation a procédé isovolumétriquement à l'échelle microscopique et isochimiquement à l'échelle mésoscopique sauf pour l'addition d'importantes quantités d'hydrogène et de chlore et pour la perte d'une certaine quantité de calcium.

Les structures et assemblages des minéraux secondaires indiquent qu'il y a eu altération régressive non équilibrée à faible température (<350°C), peut-être à cause de l'arrivée d'une quantité d'eau lors du refroidissement initial de l'intrusion. Le sill a été faillé et basculé et a adopté une attitude fortement inclinée lors de l'orogène du Kénoranien. Il ne présente aucune structure de déformation par pénétration et les effets du métamorphisme régional sont minimes.

INTRODUCTION

Purpose of the investigation

The Dumont intrusion is a differentiated, ultramafic to mafic sill of Archean age in the Abitibi greenstone belt of the Superior Province, Canadian Shield. It is located in Launay and Trecesson townships (NTS 32 D/9) in northwestern Quebec, about 62 km northeast of Rouyn and 26 km west of Amos. The body has been the focus of limited and largely unsuccessful prospecting for asbestos, base, and precious metals over the past 60 years. However, exploration carried out by the Dumont Nickel Corporation between 1969 and 1972 resulted in the discovery of an extensive zone of low grade nickel mineralization within the sill. Although the Dumont occurrence has not yet proved to be an economically viable ore deposit, it is nevertheless a significant nickel resource and is prototypical of a distinct class of nickel sulphide deposit. An understanding of the petrogenesis of the sill and especially of the factors that controlled the distribution of nickel sulphides is of fundamental importance in guiding any further exploration of the body. Perhaps of greater significance is the likelihood that the Dumont intrusion is not unique and that knowledge acquired here will provide criteria for the identification and exploration of other similar bodies. Finally, the intrusion presents an opportunity to gain insight into some important aspects of Archean ultramafic magmatism and greenstone belt evolution. This paper describes the mineralogy, petrology, and economic geology of the intrusion with particular emphasis on the magmatic stage of its development.

Previous studies

The intrusion was first reported by James and Mawdsley (1925), and parts of it were mapped subsequently by Weeks (1935), Ross (1939), MacLaren (1953), and Vogel (1979). Besson and Capitant (1976), Besson (1979), and Duke (1980, 1982) have discussed aspects of the petrology and petrochemistry of the sill. Eckstrand (1975) and Bonneau (1977) have described the opaque minerals which occur in the ultramafic rocks, while Rucklidge (1972), Rucklidge and Patterson (1977), Miura et al. (1979, 1981), and Duke (1978) have reported on aspects of the serpentinization of the body. Jambor (1975), and Crook and Jambor (1979) have described the occurrence of some unusual secondary minerals in drill core samples. Harris and Nickel (1972) tabulated analyses of Dumont pentlandites as part of their study of the association-dependence of pentlandite composition. The distribution of iron and nickel between

olivine and sulphide in the Dumont body has been discussed by Thompson et al. (1984). Duke and Naldrett (1983) have discussed the nickel resources contained in intrusions of the Dumont type.

Access, exposure, and sampling

The Dumont Sill is situated immediately north of Quebec Highway 11 and the Canadian National railway line which run between Amos and La Sarre. The area is readily accessible by motor vehicle and no part of the body is more than about 4 km from a good quality road. The area is rather flat lying with elevations in the range of 300 to 365 m above sea level, and the maximum relief over the intrusion is about 30 m. Less than 2 per cent of the bedrock surface of the intrusion outcrops, and most of the exposure occurs at the extreme ends of the body. The remainder is covered by overburden which ranged in thickness from 12 to 45 m in those parts where drilling was carried out. None of the zones of nickel sulphide enrichment are exposed in outcrop.

Fifty-seven holes were drilled on behalf of Dumont Nickel Corporation and it is from these cores that most of the sample material used in this study was derived. The sampling was carried out by J.L. Jambor and O.R. Eckstrand prior to initiation of this project and the Dumont Nickel Corporation has retained only abbreviated cores. Consequently, I have not had the opportunity to examine complete drill core intersections. This limitation has meant that it has not been possible to locate with precision certain internal contacts or to observe structural and textural features which would only be apparent in uninterrupted sections of drill core. In this report, most samples are enumerated according to their location within a particular drillhole. For example, sample E16-1415 was recovered from drillhole E16 at a depth of 1415 ft (430 m). The locations and other details of the drillholes are tabulated in Appendix 1. The locations are referred to the co-ordinate system established by Dumont Nickel Corporation; that is, the distance (in feet) east or west of the Launay-Trecesson township boundary and the distance north of a given range line. The drillholes lie in essentially vertical north-south planes and it is important to note that since the sill has a northwesterly strike, except at the extreme southeast end, most of the holes intersect the plane of the body at an oblique angle.

Acknowledgments

This investigation could not have been carried out without the co-operation of the Dumont Nickel Corporation which allowed free access to diamond-drill core, drill logs, and other exploration records. Thorough sampling of the drill core was undertaken by J.L. Jambor and O.R. Eckstrand. A.G. Plant, M. Bonardi, and G.J. Pringle guided the author in electron microprobe analytical procedures. S. Green carried out mineral separations and X-ray diffractometry of the serpentine minerals and also assisted in fieldwork. F.J. Wicks kindly verified some of the serpentine mineral identifications using the microbeam camera technique. W. Petruk undertook some modal and grain size analyses using the Quantimet image analyzer. Whole-rock chemical analyses were carried out under the supervision of J.L. Bouvier and H. Champ. G.A. Lachance performed some of the trace element determinations using nonroutine X-ray fluorescence methods. J. Shaw, G. Wine, and Nguyen K. Kim assisted with petrography and drafting. E.C. Appleyard of the University of Waterloo provided a set of computer programs for the metasomatic mass balance calculations. R.I. Thorpe and O.R. Eckstrand offered constructive comments on the manuscript.

GENERAL DESCRIPTION OF THE DUMONT SILL

Regional geological setting

A thick supracrustal succession of volcanic and sedimentary rocks underlies about 65 per cent of the Abitibi belt as shown in Figure 1 (Goodwin and Ridler, 1970). A number of lines of evidence suggest that these supracrustal rocks lie unconformably upon a basement complex of sialic composition (Baragar and McGlynn, 1976). An implication of ongoing geochronological studies is that the entire supracrustal sequence may have been deposited in a relatively short period of time, perhaps as little as 50 Ma. Zircon U-Pb ages from the Timmins, Kirkland Lake and Noranda areas range from 2701 to 2725 Ma whereas a single determination from the Chibougamau area yielded a 2739 Ma age (Nunes and Pyke, 1980; Nunes and Jensen, 1980; Krogh and Davis, 1971). The volcanic rocks are mainly of mafic composition although ultramafic, intermediate and felsic types are also present. A number of volcanic centres have been identified. Within a given volcanic pile, the oldest lavas tend to be the most primitive and there is an upwards progression towards more felsic compositions. The abundance of pillowed and nonvesicular lavas together with the flyschoid character of much of the sedimentary component, demonstrate the prevalence of deep submarine conditions. However, the occurrence of some fluvial sedimentary rocks as well as airfall tuffs attest to occasional, local nonmarine conditions (Hyde and Walker, 1977). Numerous small to medium sized synvolcanic intrusions reflect the range of compositions of the lavas themselves.

The supracrustal rocks were deformed and intruded by granitic stocks and batholiths during the Kenoran event about 2680 to 2700 Ma ago. Folding about generally east-trending axes has commonly produced isoclinal structures. The greenschist and prehnite-pumpellyite facies of regional metamorphism predominate except in the contact aureoles of the Kenoran granites where amphibolite grade is usually attained (Jolly, 1978). The sedimentary rocks of the Pontiac Group are also in the amphibolite facies. Two main sets of diabase dykes occur in the Abitibi belt. The north-trending Matachewan swarm and northeast-trending Abitibi swarm have Rb-Sr ages of 2690 and 2147 Ma, respectively (Gates and Hurley, 1973). The latter are prominent in the vicinity of the Dumont intrusion although none are known to cut the body.

The Dumont Sill is hosted by lavas and volcaniclastic rocks that have been assigned to the Kinojevis Group by Latulippe (1972) and, more recently, to the Amos Group by Imreh (1980). The lavas may be traced eastwards through Amos and are part of what Goodwin and Ridler (1970) termed the Barraute volcanic complex. Three cycles of mafic to felsic volcanism are recognized and the Dumont intrusion is one of at least five ultramafic-mafic complexes in the Amos area which occur at approximately the same stratigraphic level within the mafic lavas of the middle cycle. The Amos (Landrienne) sill was recently described by Hébert (1982). The host rocks of the intrusion are for the most part basaltic lavas although some intermediate rocks were intersected in drilling of the footwall of the body at its eastern end. The basalts, as indicated by the chemical analyses in Table 1, are characterized by relatively high concentrations of $FeO+Fe_2O_3$ (>12%), TiO_2 (>1%), and V (>0.03%), and low values of SiO_2 (<52%) and Al_2O_3 (<14%). Therefore, they are similar to iron-rich tholeiites reported from elsewhere in the Abitibi belt (Pearce and Birkett, 1974; Arndt et al., 1977; Goodwin, 1979). Although the volcanic rocks have been folded and now dip rather steeply, a penetrative deformational fabric is only locally developed. In the vicinity

Table 1. Chemical compositions of volcanic host rocks of the Dumont and Landrienne (Amos) intrusions

	1.	2.	3.	4.	5.		6.	7.
	DBA-76 -109	DBA-76 -110	DBA-76 -30	DBA-77 -16	$\bar{X}$	σ	DBA-76 -28	DBA-76 -29
SiO_2	50.3	48.9	44.7	49.8	49.3	1.9	37.1	40.7
TiO_2	1.4	1.4	1.5	1.5	1.2	0.2	1.2	0.9
Al_2O_3	12.2	13.4	13.0	13.1	13.2	0.8	10.9	12.7
Fe_2O_3	1.3	2.3	nd	2.5	3.3	0.7	0.70	nd
FeO	11.1	12.5	12.9	10.4	10.0	0.6	11.2	16.9
MnO	0.23	0.23	0.28	0.18	0.25	0.04	0.45	0.21
MgO	5.9	6.5	5.9	7.2	5.9	0.5	6.3	10.0
CaO	8.9	7.9	9.5	7.4	9.5	0.8	9.8	5.9
Na_2O	2.0	1.9	2.3	3.2	2.4	0.9	3.6	0.36
K_2O	0.12	0.80	0.14	0.33	0.14	0.09	1.9	0.13
P_2O_5	0.12	0.13	0.15	0.10	0.07	0.02	0.12	0.10
H_2O	5.0	3.0	4.6	4.3	3.3	0.3	1.7	7.5
CO_2	2.2	nd	5.2	0.9	1.0	0.7	15.1	5.5
Ni	0.0080	0.0070	0.0060	0.0040	0.0066	0.0007	0.0070	0.0060
Cr	0.010	0.0080	0.0040	0.0040	0.0060	0.0020	0.0030	0.0030
V	0.039	0.040	0.044	0.036	0.034	0.0020	0.031	0.044
Co	0.0050	0.0060	0.0050	0.0050	0.0068	0.0004	0.0050	0.0060
Cu	0.011	0.011	0.013	0.0090	0.012	0.0020	nd	0.013
Total	100.84	99.03	100.24	100.97	99.62		100.11	100.97

1,2 Basalts from surface exposure, stratigraphic hangingwall, east end of Dumont intrusion
3 Basalt from D.D.H. W-14, 1660 ft, stratigraphic footwall, west end of Dumont intrusion
4 Basalt from surface exposure, stratigraphic footwall, west end of Dumont intrusion
5 Means and standard deviations of 8 analyses of basalts collected in vicinity of the Landrienne (Amos) sill (Alsac, 1977)
6,7 Highly altered and, in part, brecciated volcanic rocks from D.D.H. W-14 1505 and 1575 ft, stratigraphic footwall, west end of Dumont intrusion
nd - not detected

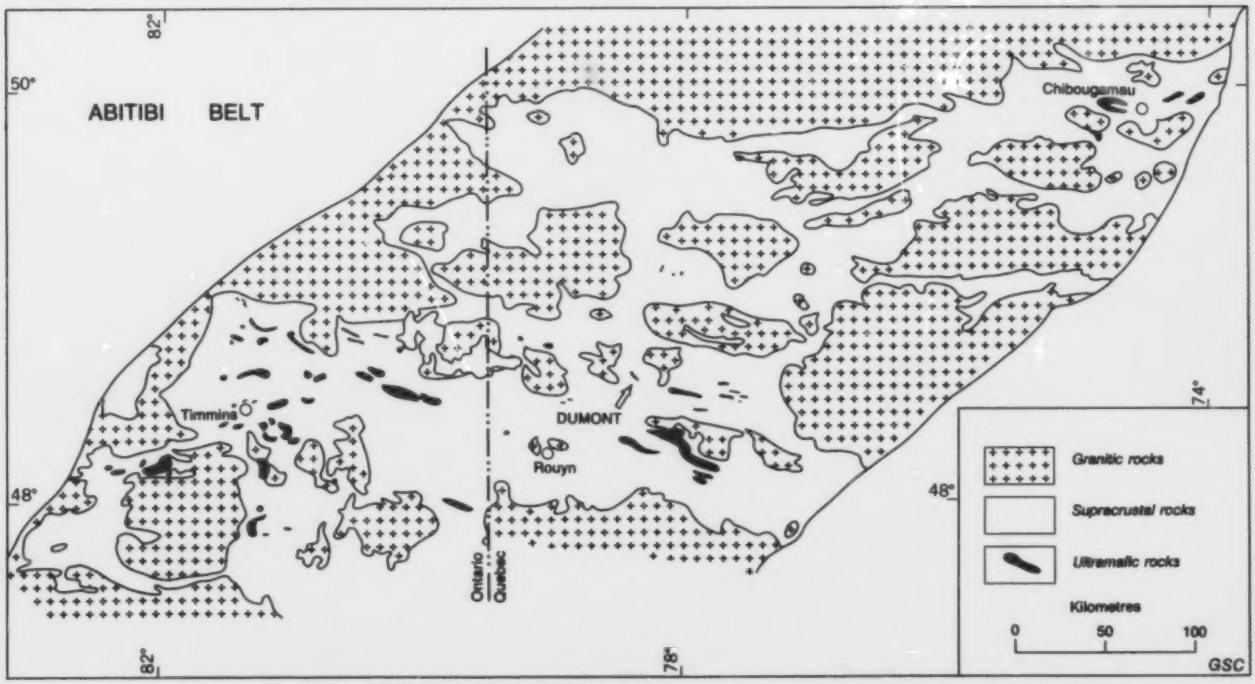

Figure 1. Location of the Dumont Sill within the Abitibi greenstone belt.

of the Dumont intrusion, pillows in the lavas are not greatly deformed and primary textures such as "swallow-tail" plagioclase microlites are preserved. However, the chemical compositions of many of the rocks are much altered, and many rocks contain significant levels of CO_2 (Table 1, analyses 6 and 7). Three main directions of faulting were recognized in the Amos area by Weber and Latulippe (1964). The earliest is the east-trending set of "bedding plane" faults which they believed developed during the major period of folding. The intrusion of the granitic rocks was accompanied by the development of steeply dipping faults that strike north to northwest. The most prominent faults strike northeast and probably postdate the granitic plutonism. The Dumont body is cut by a number of these northeast-trending faults (see below).

Contact relations, areal extent, and age of the intrusion

The contacts between the intrusion and its host rocks have not been observed in outcrop but in overall attitude the body appears to be conformable to the layering of the volcanic rocks and there is little doubt that it is a sill. Pillowed basalts exposed at the eastern end of the sill clearly indicate a northeast facing direction in contrast to the description by Vogel (1979). The sill comprises a lower Ultramafic Zone and an upper Mafic Zone. Although less than about 2 per cent of the bedrock surface of the intrusion is exposed in outcrop, the boundaries of the Ultramafic Zone can be drawn with some confidence on the basis of a ground magnetometer survey (Fig. 2) and diamond drilling (Fig. 3). The western end of the body has not been precisely outlined. Thus the Ultramafic Zone is a lenticular mass at least 6600 m

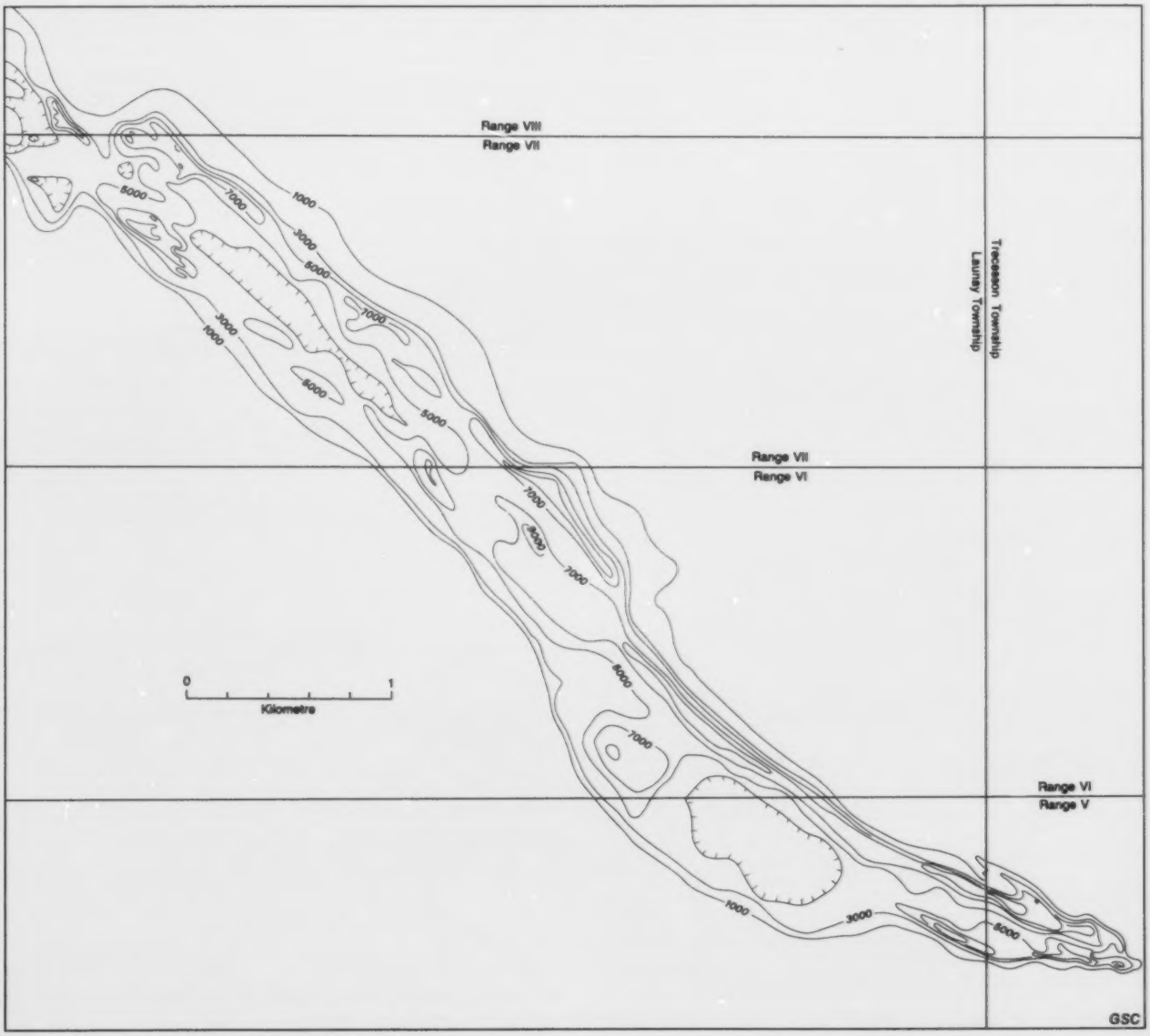

Figure 2. Magnetometer survey of the Dumont intrusion compiled from data provided by the Dumont Nickel Corporation. Contour interval = 2000 gammas.

in length with an average true thickness of 450 m. The true dip of the zone as determined in three cross-sections where either contact was intersected in two or more drillholes is 60 to 70° northeast (Fig. 4). The extent of the Mafic Zone is much less well defined and its top has not been observed in either outcrop or drill core. A drillhole near the middle of the sill intersected a true thickness of 175 m of the Mafic Zone, and outcrop constraints would allow a maximum of 400 m. I believe that 250 m is a reasonable estimate of the average true thickness of the Mafic Zone, and therefore the average true thickness of the sill as a whole would be 700 m. A number of faults at a high angle to the long axis of the sill are suggested by offsets in the magnetic contours and also by the internal stratigraphy of the Ultramafic Zone. However, the inferential nature of these faults is emphasized and there are undoubtedly other faults which have not been shown. A dyke-like apophysis of peridotite, 30 m wide, occurs between the Mafic Zone and the overlying lavas at the eastern end of the intrusion. The contact between the gabbro and peridotite in this location is marked by a mylonite zone about a centimetre in width and it is believed that the apophysis is a fault slice from the top of the Ultramafic Zone. This interpretation is supported by the composition and petrography of the peridotite. Two poorly exposed sills of gabbro occur about 1 km to the northeast of the Dumont body (Vogel, 1979) and I will argue below that these are consanguineous with the main sill. No feeder to the Dumont Sill has been observed.

The age of the intrusion is not explicitly known. No radiometric age determination has yet been undertaken and there is little in the way of direct geological evidence. The conformable nature of the body together with the character of its differentiation documented below leave little doubt that it was emplaced as a virtually horizontal sill that was folded and faulted during the Kenoran event. It is reasonable to conclude that the Dumont Sill is of late Archean age but is only slightly younger than the enclosing lavas; that is, about 2.7 Ga.

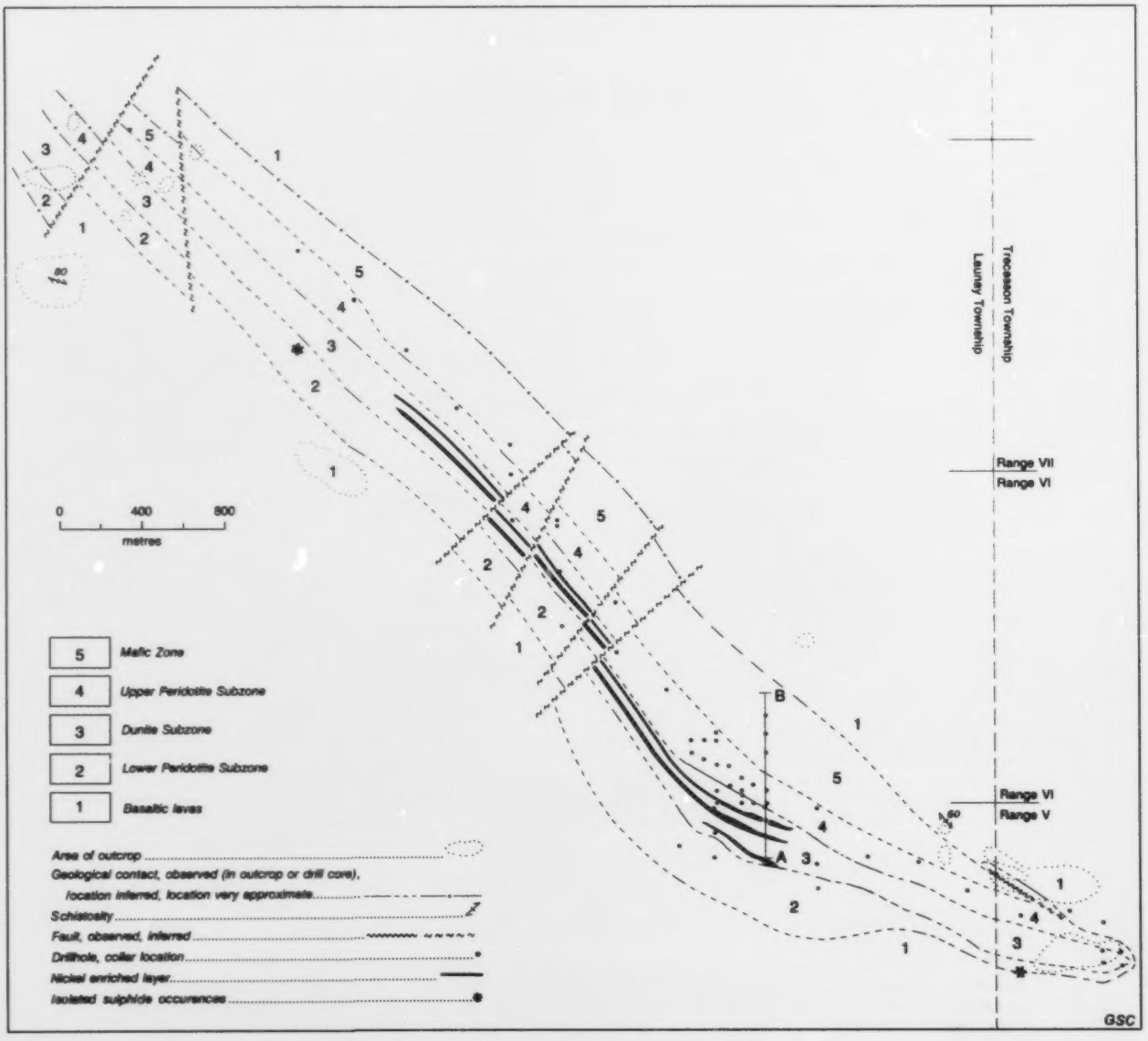

Figure 3. Geological map of the Dumont intrusion.

PETROGRAPHY OF THE INTRUSION

Magmatic textures and modal composition

Introduction

The Dumont intrusion has been pervasively altered. The rocks of the Ultramafic Zone have undergone variable amounts of serpentinization and local steatitization. Relict magmatic chromite occurs in most samples, and calcic clinopyroxene and olivine are preserved in many others. Even in completely serpentinized peridotite pseudomorphic textures are common and it is usually possible to discern the constituent minerals and igneous texture of the unaltered precursor. The preservation of primary features in the Mafic Zone is less complete. Relict clinopyroxene occurs in a few samples but pyroxene has generally been altered to actinolite and it is not clear to what extent the amphibole mimics the primary grain boundaries of the pyroxene. Plagioclase has been almost completely saussuritized but the primary crystal shapes are preserved. The disposition of the plagioclase pseudomorphs gives the best indication of the nature of the igneous texture of the rocks of the Mafic Zone. The subsequent discussion deals with the magmatic minerals, but

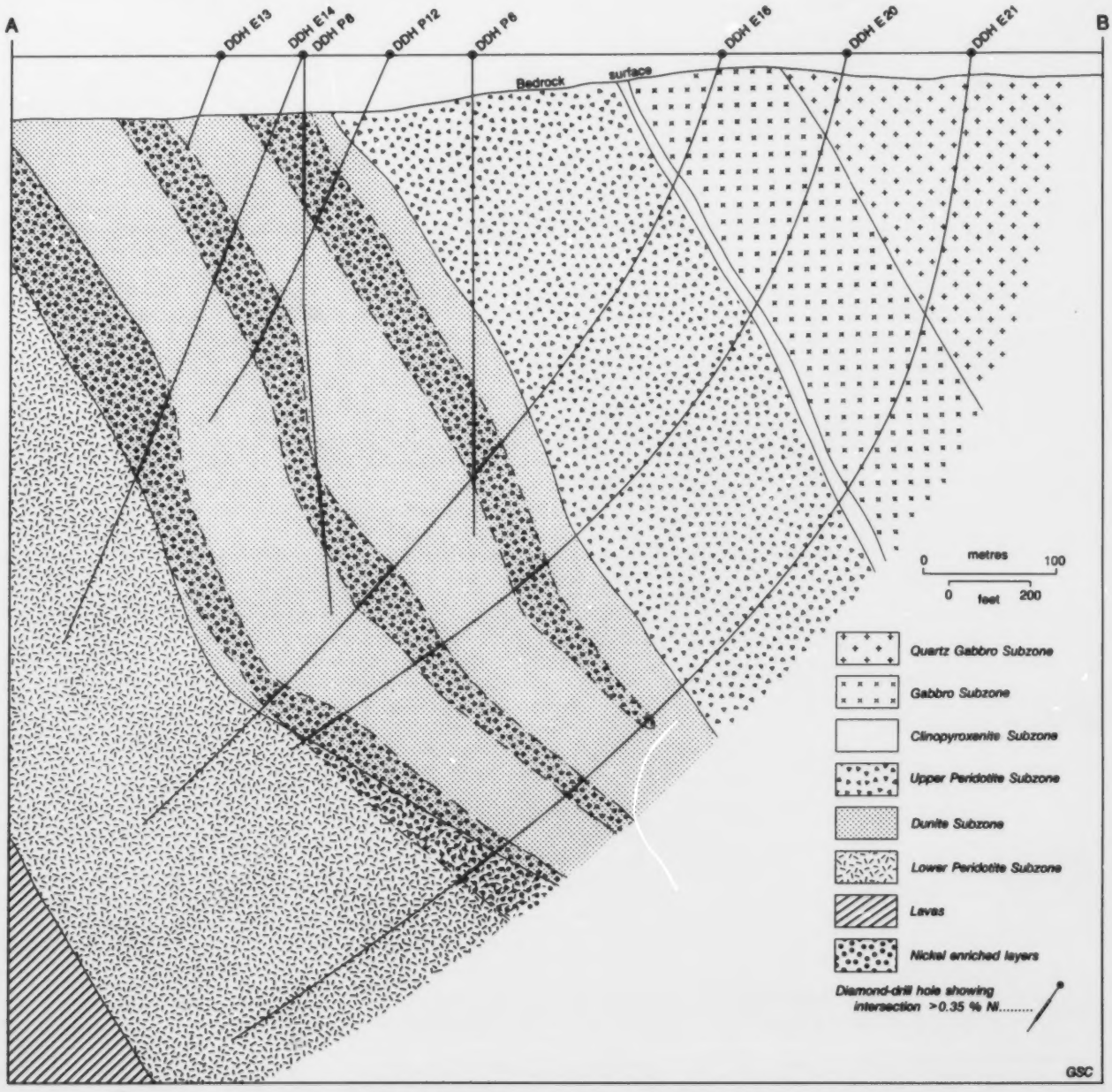

Figure 4. Cross-section 36+00 West showing positions of the three nickel-enriched layers in the Dunite Subzone. The position of the basal contact of the intrusion is projected from off-section. Note that the lowermost nickel enriched layer is not exactly conformable to the subzone boundary.

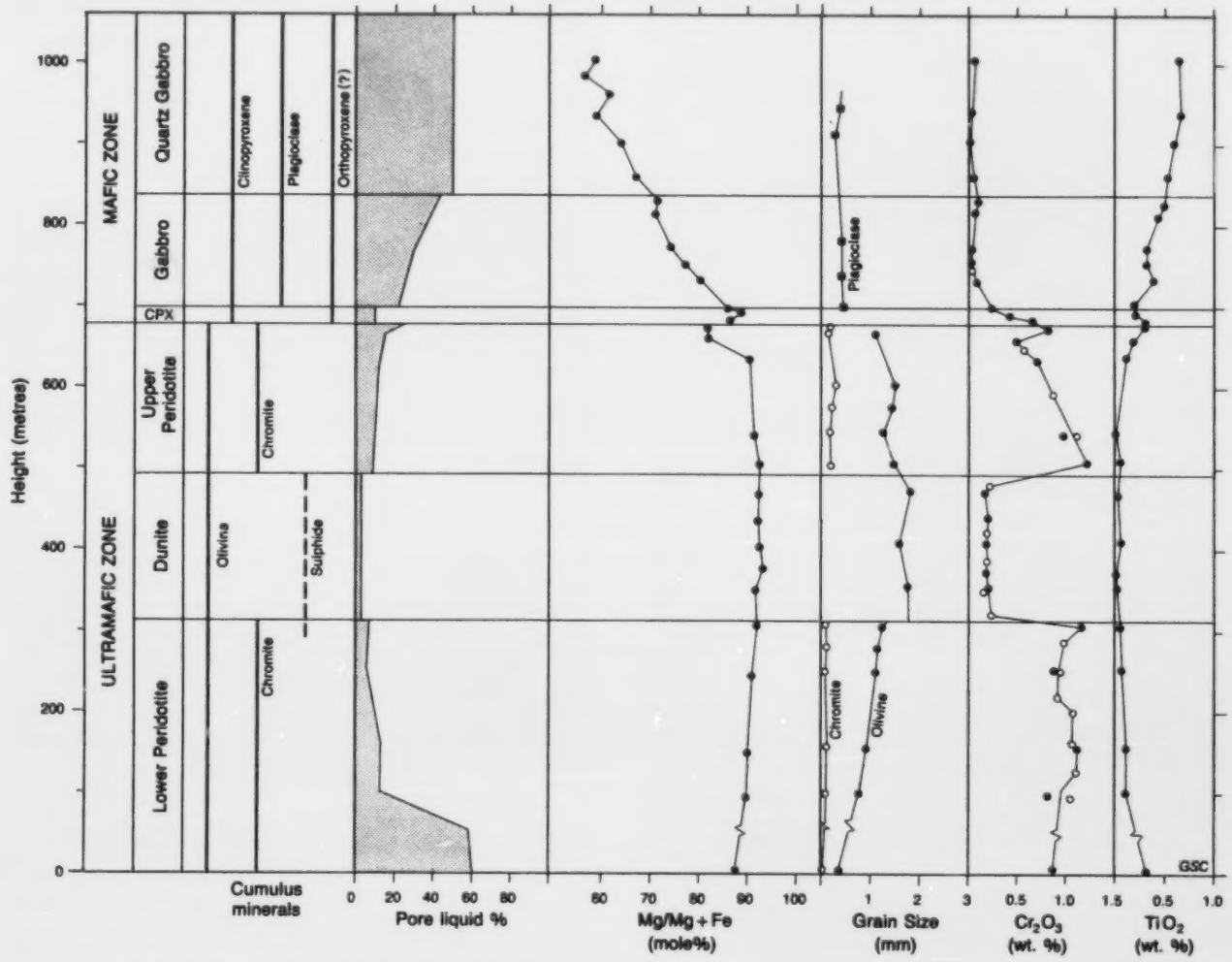

Figure 5. Modal, cryptic and grain size variation across the Dumont Sill. The chemical and grain size data were measured in samples from drillhole E21. The lowermost sample is from drillhole E8 and is included because drillhole E21 did not reach the basal contact of the intrusion. These drillholes were oblique to the plane of the Sill and so the total height represented on the vertical axis is greater than the true thickness. The cumulus range of sulphide is shown as a dashed line because its occurrence is not continuous along strike. The pore liquid % was calculated by dividing the concentrations of incompatible elements in the rocks by their inferred concentrations in the melt. The Mg/Mg+Fe ratio is the value for the whole rock: however, in the Ultramafic Zone this is normally equivalent to the forsterite content of the contained olivine. The whole rock Cr_2O_3 profile includes data from the present study as filled circles and that of Bonneau (1977) as open circles. In the Ultramafic Zone, the Cr_2O_3 concentrations reflect the modal amount of chromite whereas in the Mafic Zone, where chromite does not occur, chromium occurs mainly in clinopyroxene. The whole rock TiO_2 content generally reflects the amount of intercumulus material.

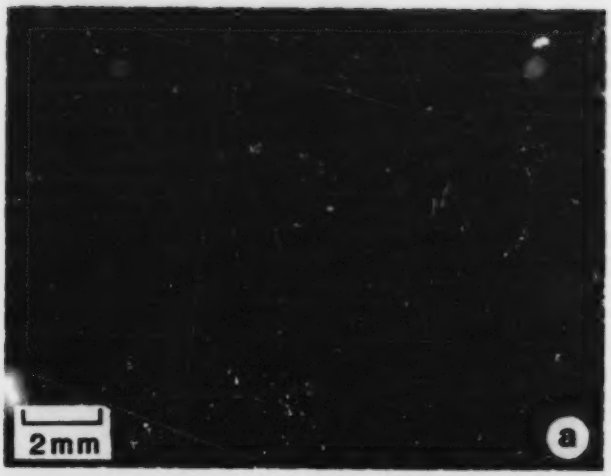

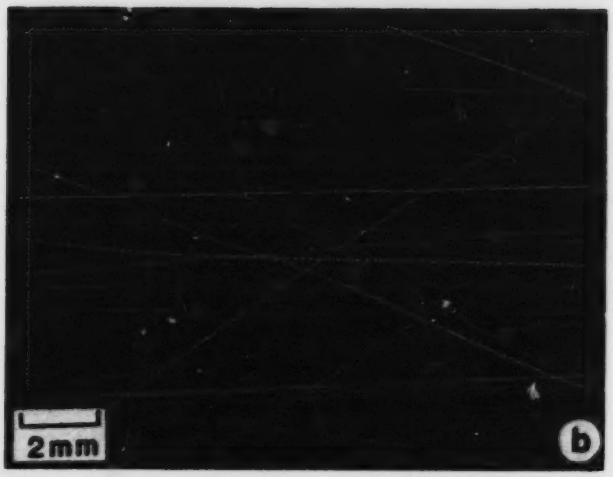

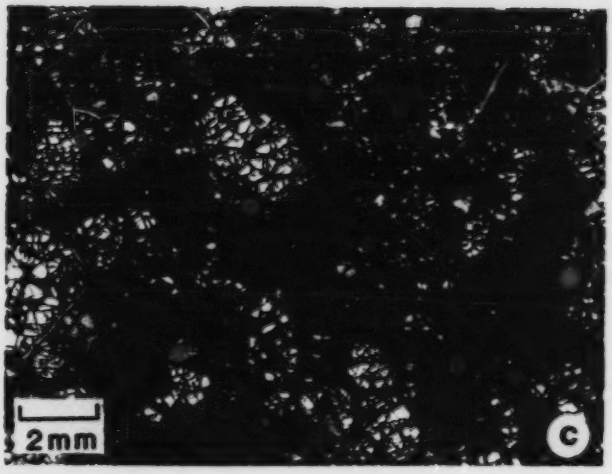

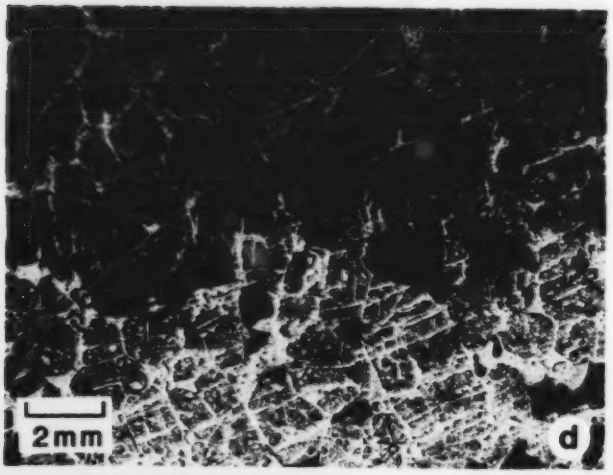

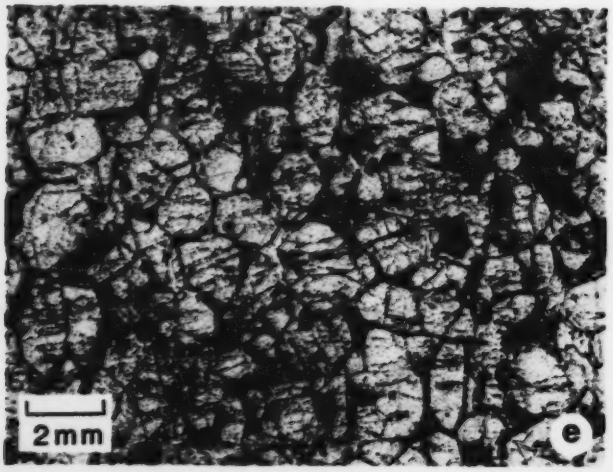

Figure 6. Primary igneous textures in the Dumont Sill. Photomicrographs are arranged in order of increasing stratigraphic height and are reproduced at the same scale.

(a) Fine grained olivine-chromite orthocumulate (poikilitic wehrlite) from the base of the Lower Peridotite Subzone. Euhedral to subhedral olivine (serpentinized) and chromite are enclosed by oikocrysts of clinopyroxene. Sample W12-2010, transmitted polarized light.

(b) Fine grained olivine-chromite adcumulate from the upper part of the Lower Peridotite Subzone. Anhedral olivine is serpentinized along grain boundaries. Sample E21-2886, transmitted partially polarized light.

(c) Medium grained olivine adcumulate from lowermost Dunite Subzone. The opaque grain in the centre is intercumulus chromite. This is among the least altered specimens observed with only limited development of serpentine occurring along the boundaries between the olivine anhedra. Sample E16-1830, transmitted polarized light.

(d) Clinopyroxene oikocryst enclosing partly serpentinized olivine in the Dunite Subzone. The opaque grain (top centre) is cumulus sulphide. Only rarely is this much intercumulus material observed in the Dunite. Sample E16-1245, transmitted plane light.

(e) Medium grained olivine-chromite mesocumulate from the middle part of the Upper Peridotite Subzone. Subhedral olivine (completely serpentinized) and euhedral chromite poikilitically enclosed by clinopyroxene (largely altered). Sample W7-415, transmitted plane light.

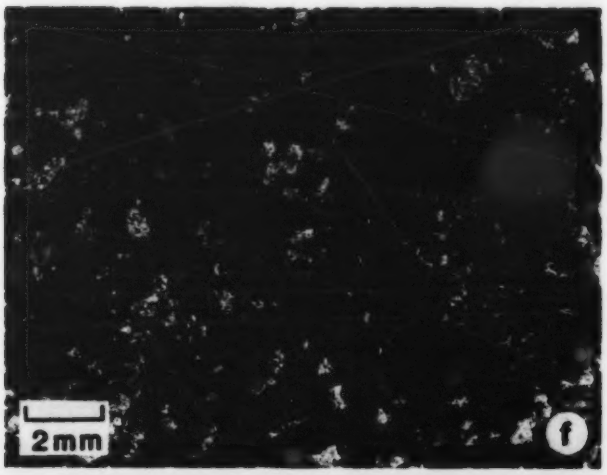

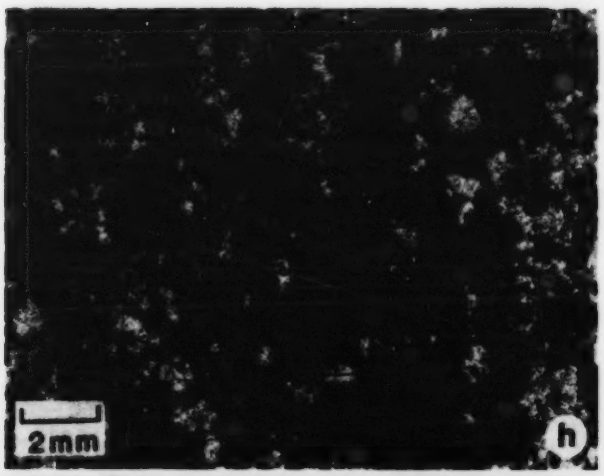

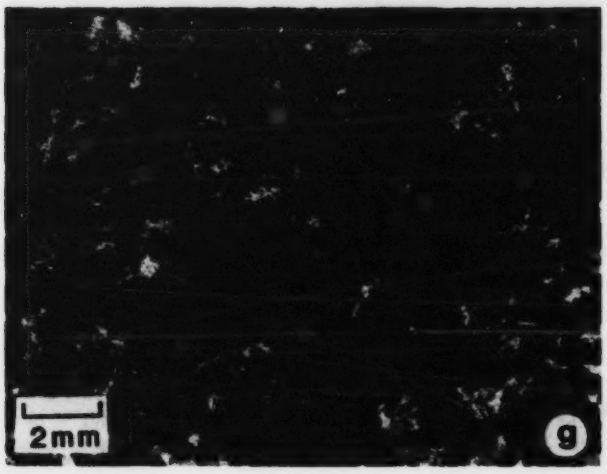

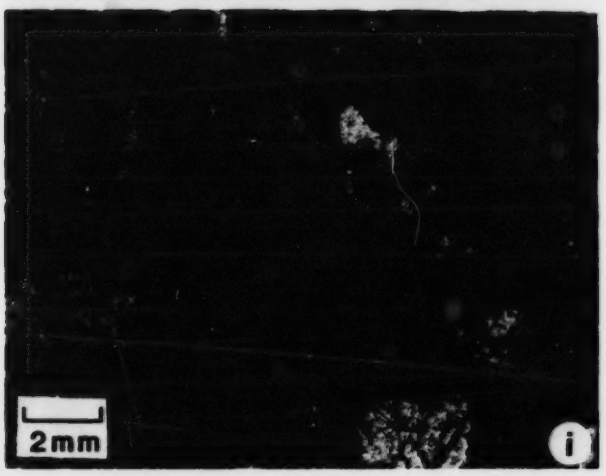

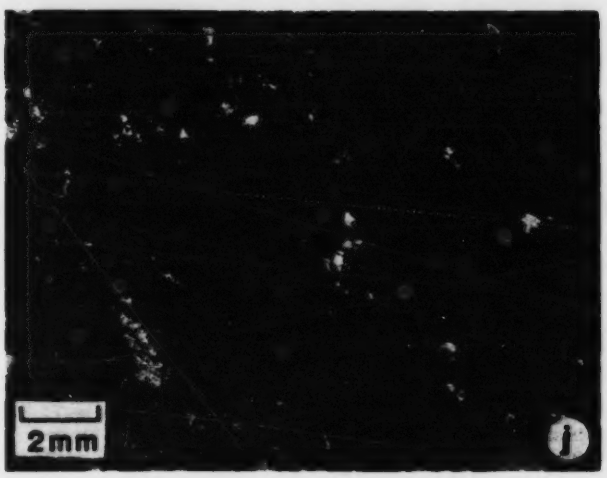

Figure 6 (cont.)

(f) Fine grained clinopyroxene adcumulate from Clinopyroxenite Subzone. Note the sutured or interlocking nature of the grain boundaries between clinopyroxene anhedra. Sample E21-1135, transmitted polarized light.

(g) Subophitic texture in Gabbro Subzone. Actinolite, presumed to be replacing primary clinopyroxene, is partially interstitial to, and partially encloses, euhedral to subhedral laths of plagioclase (nearly opaque due to saussuritization). Sample E21-830, transmitted polarized light.

(h) Part of irregular plagioclase-rich layer in Gabbro Subzone. The large, square-shaped actinolite pseudomorph is probably after orthopyroxene. Sample E21-690, transmitted plane light.

(i) Plagioclase-pyroxene cumulate from Quartz Gabbro Subzone. Plagioclase laths (saussuritized) occur in clusters and the disposition of actinolite pseudomorphs suggests a subophitic primary texture. Note the granophyric intergrowth at the right. Sample E21-290, transmitted plane light.

(j) Noncumulate texture in Quartz Gabbro Subzone. Note the relatively coarse grain size of plagioclase laths (saussuritized) and abundance of interstitial quartz. Sample E21-160, transmitted plane light.

it is emphasized that the altered character of the rocks has necessitated a large degree of inference from relict textures and bulk chemical composition.

The rocks of the Ultramafic Zone and much of the Mafic Zone have cumulus textures and I have adopted the terminology of Irvine (1982). The descriptive connotations of this terminology are useful and widely understood, notwithstanding the fact that the genetic implications of such textures (Wager et al., 1960) have changed dramatically in light of recent studies (McBirney and Noyes, 1979; Irvine, 1980). The grain sizes of cumulus minerals discussed below are the averages of the maximum and minimum dimensions of 75 randomly selected grains in each thin section. These averages will be slightly less than the "true" values owing to the effects of sectioning.

Ultramafic Zone

Olivine, chromite and calcic clinopyroxene are the essential magmatic minerals throughout the Ultramafic Zone. The zone has been subdivided into the Lower Peridotite Subzone, the Dunite Subzone and the Upper Peridotite Subzone with the contacts between the units being defined by an abrupt change in the abundance and texture of chromite which is readily discernible in hand specimen. The variation in modal composition through the intrusion is illustrated in Figure 5: the change in the modal proportion of chromite is reflected in the cryptic variation of Cr_2O_3.

The lowermost 30 to 50 m of the Lower Peridotite Subzone is an olivine-chromite orthocumulate made up of about 70% olivine, 28% clinopyroxene and 2% chromite. The olivine grains are generally euhedral, equant to moderately elongated and average 0.4 mm in size, although a few grains as large as 1 mm are present (Fig. 6a). Some very elongated crystals occur and there is a tendency for these to be rudely aligned. The chromite is also idiomorphic but is much finer grained, averaging only 0.04 mm. Clinopyroxene is the only apparent intercumulus phase, forming relatively large oikocrysts that enclose both olivine and chromite. The grain size of these oikocrysts is difficult to determine but probably falls in the range of 3 to 10 mm. Very fine lamellae of calcium-poor pyroxene occur in patches in the central portions of some clinopyroxene grains. Except at the narrow eastern end of the intrusion where the entire thickness of the Lower Peridotite is an orthocumulate, the texture grades upwards through mesocumulate to adcumulate textures at the top of the unit. The proportion of clinopyroxene decreases to about 2% and it is observed as small cuspate grains in the interstices of the cumulus olivine. The average olivine grain size increases to 1.2 mm and the crystals become anhedral in outline (Fig. 6b). The proportion of chromite is virtually constant at 2% across the Lower Peridotite, and its grain size in the middle and upper parts of the subzone averages about 0.08 mm. The chromite grains occur individually or in clusters in the interstices of the olivine grains and there is a tendency for the larger crystals to be somewhat subhedral. Tiny (<0.025 mm), idiomorphic crystals of nearly transparent chromite occur as inclusions in olivine throughout the Ultramafic Zone but are nowhere abundant.

The Dunite Subzone is an extreme olivine adcumulate being composed on average of 98% cumulus olivine, 1.5% intercumulus clinopyroxene, and 0.5% intercumulus chromite. Cumulus sulphide occurs locally in the unit (see below). Olivine forms equant, xenomorphic grains that average from 1.5 to 2 mm in size (Fig. 6c). Rare crystals as large as 10 mm across have been observed. The increase in average olivine grain size across the Lower Peridotite – Dunite contact is subtle but apparently abrupt. Both clinopyroxene and chromite are typically observed as small, cuspate interstitial grains but an oikocrystic character is evident in thin sections where either mineral is particularly abundant (Fig. 6d). Spectacular chromite oikocrysts as large as 3 mm have been observed (Fig. 7a).

The Upper Peridotite Subzone is an olivine-chromite cumulate. The modal composition grades from 95% olivine, 2.5% chromite and 2.5% clinopyroxene at the base to 84% olivine, 15% clinopyroxene and 1% chromite at the top. The increase in the proportion of intercumulus clinopyroxene is accompanied by a decrease in olivine grain size from 2 to 1.1 mm and a gradation of olivine texture from xenomorphic towards idiomorphic. The olivine crystals appear slightly rounded against clinopyroxene at the top of the subzone which may be indicative of resorption (Fig. 6e). The average grain size of chromite, 0.16 mm, is virtually constant across the subzone. Chromite-rich layers occur in the upper parts of the ultramafic zones of similar sills in Réaume township, Ontario (Duke and Bonardi, 1982) and the Amos sill (Hébert, 1982). Some samples of chromite-rich olivine-chromite cumulate have been observed in the Upper Peridotite (Fig. 7b) but the existence of layers cannot be confirmed due to the limitations on sampling described above. At first inspection, the Upper Peridotite may appear to be a mirror image of the Lower Peridotite Subzone. However, the coarser grain size of the cumulus phases and the distinct upwards decrease in the proportion of chromite in the former unit are significant differences.

Magmatic sulphides occur in both the Dunite and Lower Peridotite subzones but are neither ubiquitous nor homogeneously distributed within these units. It is noteworthy that no unequivocal examples of magmatic sulphides have been observed in the Upper Peridotite or, for that matter, in the overlying Mafic Zone described below. Five zones of relative sulphide enrichment have been identified. Two of these zones occur within the Lower Peridotite but since they have each been intersected in only a single drillhole in areas where drillholes are rather widely spaced (250 m), very little may be concluded in respect to their lateral extent. One occurs immediately above the basal contact of the intrusion towards its eastern end (section 4+00 E) and has a true thickness of about 3 m. The sulphide textures in this zone, as described in the core logs and as observed in the single specimen available for study, are apparently of secondary origin, and the ultimate magmatic origin of this zone is uncertain. The other was intersected towards the western end of the sill (section 108+00 W) in the upper part of the Lower Peridotite, and because the hole was terminated within the zone, its thickness is unknown. There has been more complete exploration of three generally parallel and conformable layers occurring in the central part of the Ultramafic Zone (Fig. 3, 4). The abundance of magmatic sulphides within these three layers is variable but generally falls within the range of 1 to 3%. Magmatic sulphides also occur above and below the enriched layers but usually in amounts much less than 1 modal per cent.

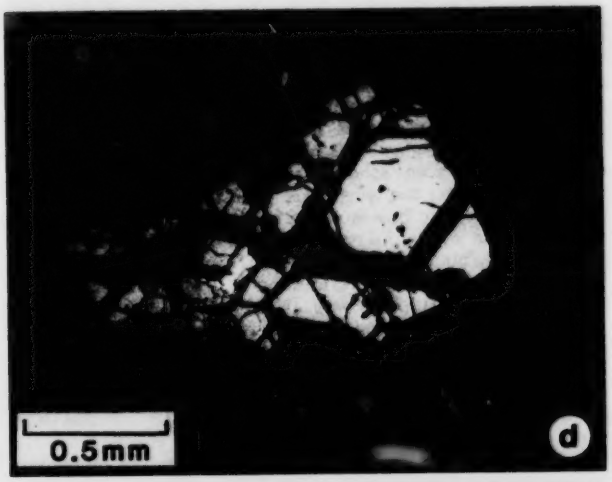

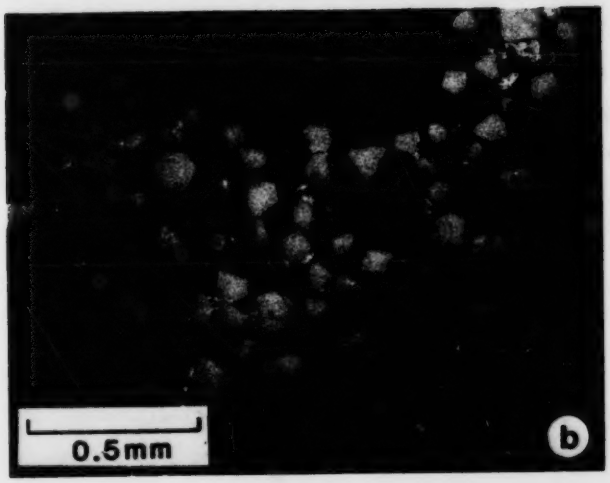

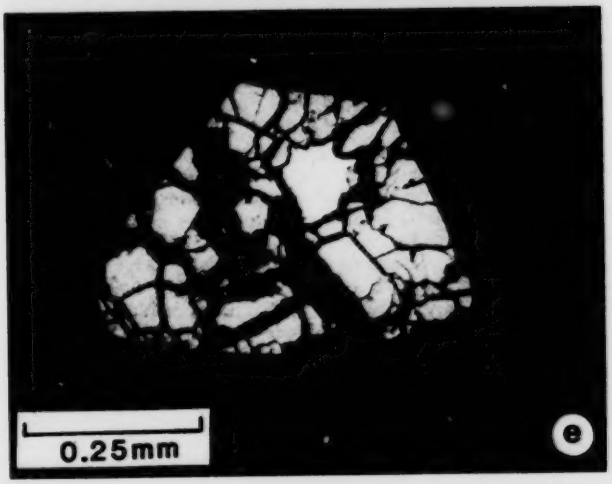

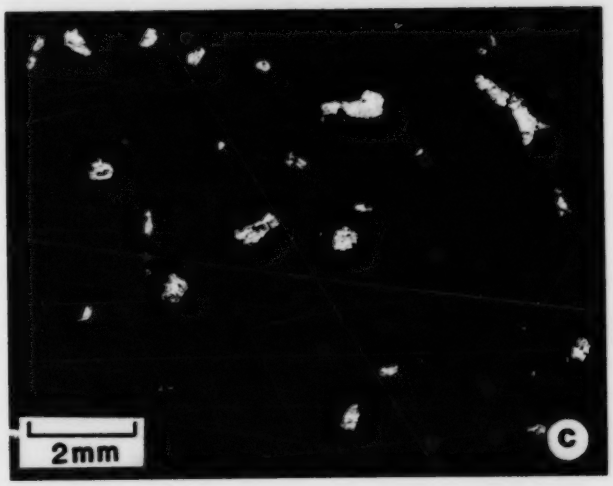

Figure 7. Opaque minerals in the Ultramafic Zone of the Dumont Sill.

(a) Large chromite oikocryst (medium grey) enclosing serpentinized cumulus olivine (dark grey), Dunite Subzone. The thin rim of magnetite (light grey) on the chromite and the magnetite "vein" on the left are typical secondary features. Sample W10-555, reflected plane light.

(b) Cumulus chromite euhedra poikilitically enclosed by clinopyroxene, upper part of Upper Peridotite Subzone. Sample W7-300, reflected plane light.

(c) Olivine + sulphide cumulate, Dunite Subzone. Magmatic sulphide grains retain their primary morphology but have been altered to the secondary assemblage pentlandite + magnetite + awaruite. Sample E20-2045, reflected plane light.

(d) Typical magmatic sulphide grain with magnetite (dark grey) developed along (111) cleavage in pentlandite (medium grey), and a small grain of awaruite (white) near middle. Sample E20-1550, reflected plane light.

(e) Magmatic sulphide grain with pentlandite (medium grey), magnetite (dark grey) and awaruite (white). The external morphology of the grain reflects its position interstitial to five olivine crystals. Sample P4-1029, reflected plane light.

Both magmatic and secondary sulphide grains are present in the ultramafic rocks. The relict magmatic grains are identified by their size and external morphology, their relationship to the primary silicates, and by the fact that they are typically polymineralic. The magmatic grains occur in the interstices of the cumulus olivine and exhibit a variety of shapes characteristic of liquid immiscibility (Fig. 7c-e). Some very small grains (<0.1 mm) are nearly spherical and in a few samples such spheres are included within cumulus olivine. However, the magmatic grains most typically have the appearance of droplets which have been deformed by the crystallization of the surrounding olivine, yielding a variety of ellipsoidal, bulbous, and subangular shapes and indicating that the silicate matrix crystallized at a higher temperature than the molten sulphide (e.g., Naldrett, 1969). A further characteristic is the tendency for the droplets to coalesce and to be concentrated within patches in a given specimen. These patches in some cases appear to be small domains of net-textured sulphide but do not satisfy the criterion of electrical conductivity (e.g. Kanehira, 1966). Within the zones of magmatic sulphide enrichment, the grains typically have mean sizes in the range of 0.4 to 0.7 mm, but elsewhere tend to be less than 0.2 mm. The modal composition of the magmatic sulphides is a result of conditions that prevailed during serpentinization (Eckstrand, 1975), and is therefore dealt with below.

Mafic Zone

The sharp transition between the Upper Peridotite Subzone and the overlying Mafic Zone is marked by the disappearance of modal olivine and chromite. The Mafic Zone has also been subdivided into three subzones: the Clinopyroxenite Subzone, the Gabbro Subzone, and the Quartz Gabbro Subzone. The basal part of the Clinopyroxenite Subzone is made up of about 85% cumulus clinopyroxene and possibly 15% intercumulus Ca-poor pyroxene (bronzite) which is completely altered to actinolite. Clinopyroxene is preserved in the unit although it is mostly altered to actinolite (Fig. 6f). It forms equant to slightly elongated, xenomorphic grains that average 0.5 mm in size. Very fine exsolution lamellae of what is presumably Ca-poor pyroxene occur in their central portions. No relict Ca-poor pyroxene grains have been observed but it is believed that the generally square patches of amphibole are pseudomorphs of bronzite oikocrysts. These patches are about 3 mm in size and include subhedral grains of unaltered calcic pyroxene.

The appearance of plagioclase marks the upward transition into the Gabbro Subzone which is interpreted to be a clinopyroxene-plagioclase-orthopyroxene cumulate. It is composed on average of about 40% clinopyroxene, 40% plagioclase and 20% orthopyroxene although individual samples are often heterogeneous with plagioclase-rich and pyroxene-rich domains. The nature of the domains is unclear owing to the sampling limitations described above; however, in some specimens they have the appearance of irregular layers 5 to 10 mm in thickness. Plagioclase occurs as lath-shaped crystals that range in average size from 0.45 mm at the base of the subzone to 0.30 mm at the top. Although clinopyroxene is almost completely altered, the disposition of saussuritized pseudomorphs of plagioclase gives an indication of its shape. Thus it would have formed slightly to very elongated grains averaging about 2 mm in size (Fig. 6g). In one sample where clinopyroxene is preserved, cumulus clinopyroxene in the pyroxene-rich portion is optically continuous with intercumulus clinopyroxene infilling between cumulus plagioclase in the plagioclase-rich portion, suggesting substantial adcumulus growth of the pyroxene. The texture may be described as subophitic. Generally square patches of amphibole are common in the plagioclase-rich portions and are interpreted to be pseudomorphs of cumulus bronzite (Fig. 6g,h). There is a crude alignment of the elongated plagioclase and clinopyroxene grains in the Gabbro Subzone. Both the Clinopyroxenite and Gabbro subzones are olivine normative.

The Quartz Gabbro Subzone is defined by the presence of conspicuous modal quartz and the rocks are also quartz normative. Plagioclase makes up on average about 45 modal per cent of the rocks. There is no unaltered pyroxene but orthopyroxene is more abundant in the norm than is clinopyroxene. Two distinct rock textures occur in the Quartz Gabbro. The first is regarded as a plagioclase-pyroxene cumulate and the second as a noncumulate gabbro. The textures in the cumulus material are quite similar to those in the underlying Gabbro Subzone (Fig. 6i). The lath-shaped plagioclase averages 0.30 to 0.35 mm in size while the pyroxenes were probably on the order of 2 to 3 mm. The principal difference is the abundance of quartz, both as intercumulus material between the plagioclase crystals and as larger (2-3 mm) grains of quartz or patches of granophyric intergrowth. The noncumulate rocks of the Quartz Gabbro are much coarser grained than the cumulates (Fig. 6j). Plagioclase is more equant than in the cumulates and averages at least 1 mm in size, and the amphiboles are more

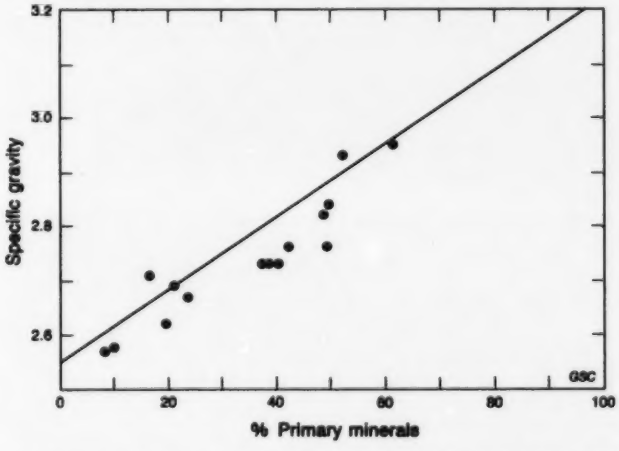

Figure 8. Variation of specific gravity with modal per cent of primary minerals (olivine+clinopyroxene+chromite). The solid line joins the specific gravities of olivine (Fo_{99}) and lizardite.

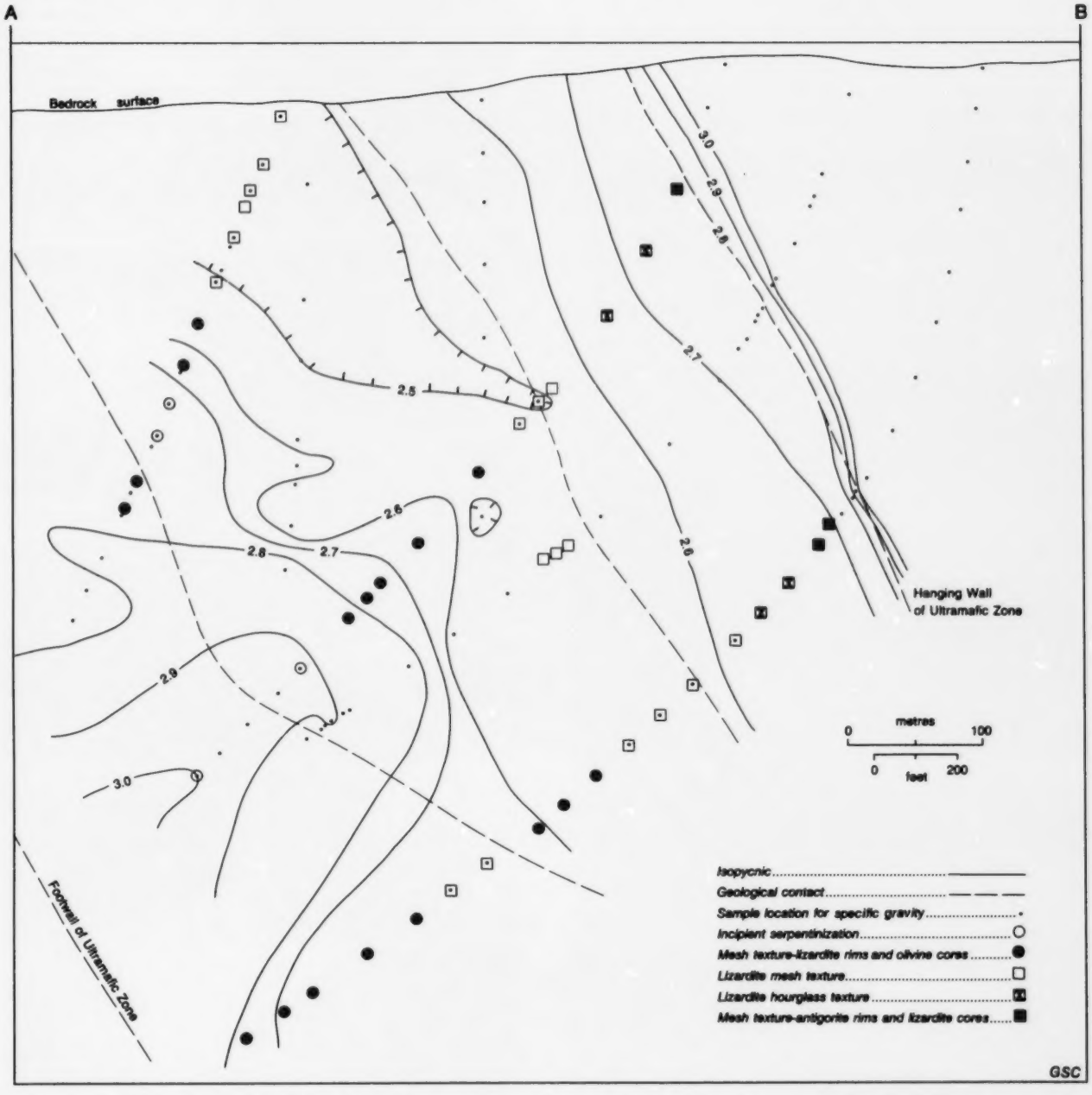

Figure 9. Distribution of specific gravities and serpentine textures in cross-section 36+00 West. The highest specific gravities indicate the least altered ultramafic rocks.

strongly coloured indicating their iron-rich composition (see below). The abundance of quartz, as well as the accessory minerals titanomagnetite (altered to leucoxene), apatite and sphene, also suggest that these rocks are enriched in residual constituents.

Secondary textures and modal composition

Ultramafic Zone

There are no completely unaltered rocks in the Ultramafic Zone. Most are serpentinites which contain less than about 25% relict primary minerals. Serpentinized peridotite or dunite having from 25 to 75% magmatic minerals is observed, however, and is concentrated in two main zones outlined by the magnetite depressions in Figure 2. The specific gravity of the serpentinized rock varies directly as the proportion of relict minerals as illustrated in Figure 8. The distribution of specific gravities in cross-section 36+00W is shown in Figure 9 and, when considered in conjunction with the magnetic pattern, suggests that the least altered rocks form a rod-shaped zone displaced towards the lower margin of the intrusion.

The only significant development of steatite occurs in isolated locations at the basal contact of the Ultramafic Zone. The contact was penetrated by drilling in only nine places along the length of the intrusion and steatite was observed in two of these, sections 17+00E and 136+00W. These zones of talc-carbonate rocks were about 30 and 50 m in true thickness, respectively, and amount to about one-quarter of the total thickness of the Ultramafic Zone.

The identification of the various serpentine minerals is not an entirely straightforward procedure and it is appropriate to outline the criteria used here. The general approach and terminology described by Wicks et al. (1977),

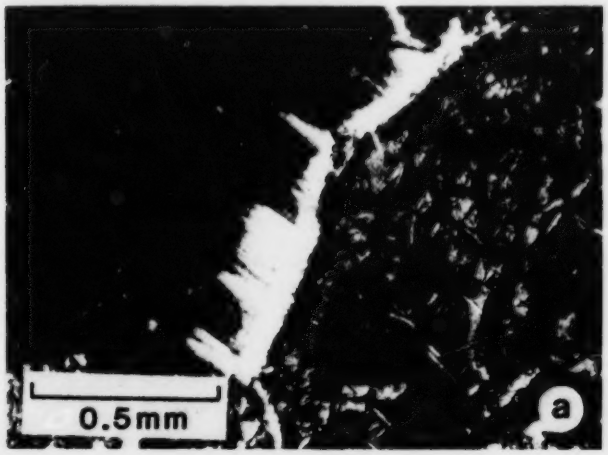

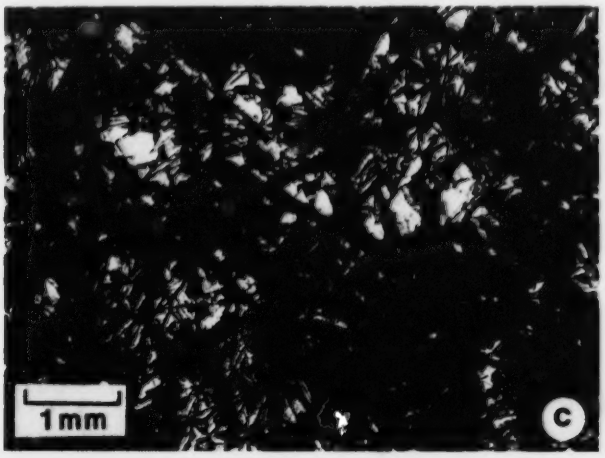

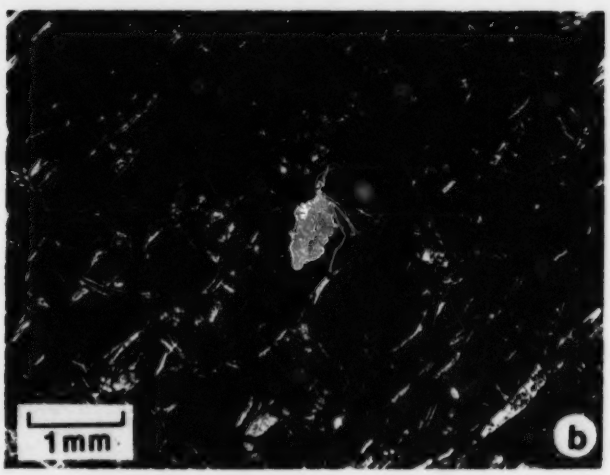

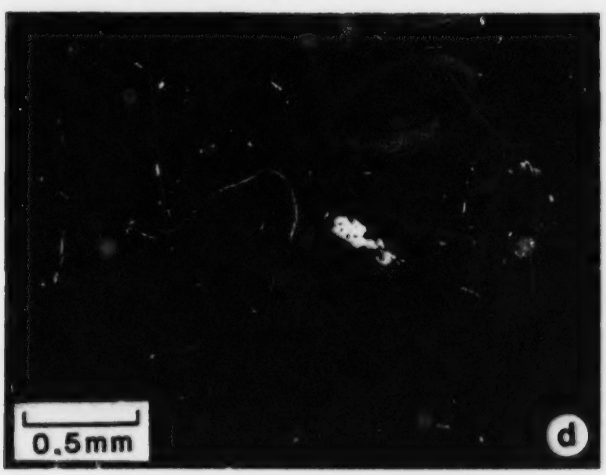

and Wicks and Whittaker (1975, 1977) has been adopted. It was found that the three serpentine polytypes could be distinguished optically in polished thin section. In transmitted light, lizardite "apparent fibres" were length fast (α-serpentine) whereas both antigorite and chrysotile were length slow (γ-serpentine). In reflected light, lizardite and chrysotile were observed to have similar polishing hardness whereas antigorite is distinctly harder. Microbeam X-ray diffraction patterns were determined for a number of typical specimens by F.J. Wicks and these confirmed the optical observations. In addition, X-ray diffraction powder patterns were measured for light mineral separates of ten samples.

The most commonly observed secondary assemblage is lizardite + chrysotile + brucite + agnetite + diopside + chlorite. Lizardite is almost always more abundant than chrysotile, and the amount of diopside and chlorite is directly proportional to the quantity of calcic clinopyroxene in the protolith. A less frequently observed assemblage is lizardite+antigorite+magnetite+diopside+chlorite. Chrysotile and brucite are only occasionally observed in the presence of antigorite and never in abundance. The assemblage present in steatite is talc+magnesite. It is noteworthy that magnetite is typically absent from steatite.

Most samples contain at least trace amounts of various secondary sulphide and alloy minerals, either as discrete grains intergrown with secondary oxide and silicate minerals or polymineralic pseudomorphs of magmatic sulphides. Pentlandite, heazlewoodite and awaruite are common in the serpentine-bearing rocks, and the intrusion may be divided longitudinally into three zones on the basis of the distribution of these minerals. In the central part of the intrusion, from section 28+00W to section 44+00W, pentlandite is the dominant phase but it is usually accompanied by a small amount of awaruite. Heazlewoodite is the most common mineral in the eastern part of the intrusion where it occurs either alone or together with pentlandite. A variety of sulphide-alloy assemblages occur in the western part of the

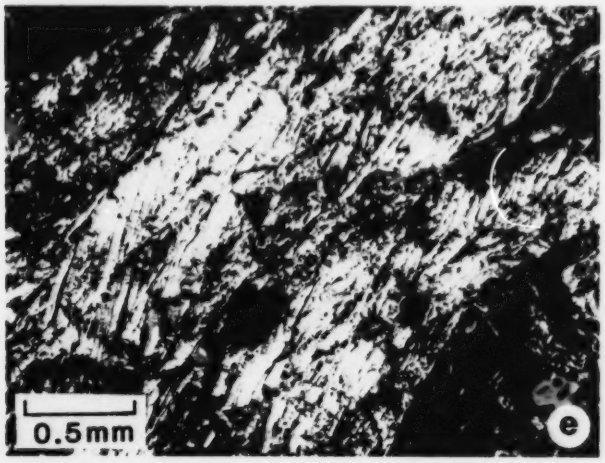

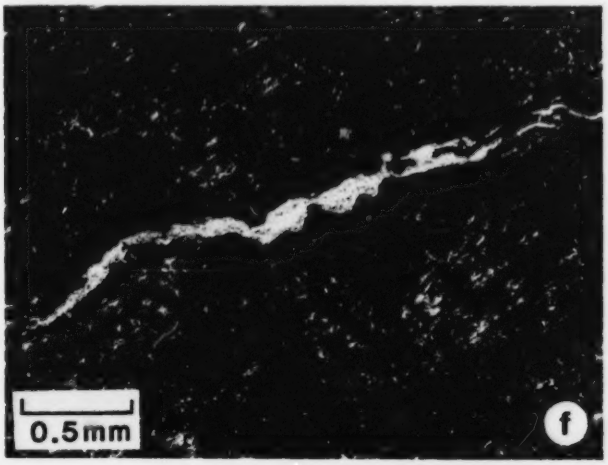

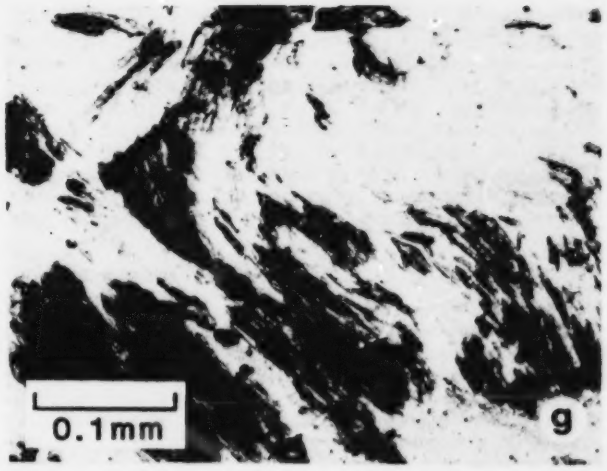

Figure 10. Textures related to serpentinization of the Ultramafic Zone.

(a) Incipient serpentinization with development of lizardite along grain boundaries and fractures within olivine and "apparent fibres" of chrysotile at right angles to grain boundaries. Sample E16-1670, transmitted polarized light.

(b) Pseudomorphic mesh texture with lizardite mesh cores and rims. Although olivine is completely serpentinized, relict clinopyroxene persists (upper right). Sample E9-1165, transmitted polarized light.

(c) Lizardite hourglass texture with numerous veins of brucite + magnetite. Sample E16-725, transmitted polarized light.

(d) Pseudomorphic mesh texture with lizardite mesh centres and antigorite apparently replacing lizardite in mesh rims. This photomicrograph is a good illustration of the contrasting polishing characteristics of lizardite and antigorite with the latter standing out in relief. Sample E21-1200, reflected plane light.

(e) Nonpseudomorphic ribbon texture with lizardite "ribbons" apparently developed along subparallel fractures. The opaque grains are primary chromite. Sample W7-255, transmitted polarized light.

(f) Nonpseudomorphic interpenetrating texture developed with blades or plumes of antigorite. The vein is composed of carbonate. Sample W12-1840, transmitted polarized light.

(g) Poorly crystallized secondary diopside (high relief) intergrown with serpentine and chlorite. Sample W7-255, transmitted plane light.

intrusion including pentlandite, heazlewoodite, awaruite, pentlandite+heazlewoodite, and pentlandite+heazlewoodite+awaruite. Native copper has been observed in several samples from both the central and western zones but not in the presence of awaruite. Millerite is the sulphide phase in the talc-carbonate rocks at the basal contact of the intrusion. The assemblage pyrrhotite+pentlandite+chalcopyrite occurs in some serpentinite samples adjacent to the basal contact, notably in the sulphide-rich zone in section 4+00E described above. The assemblage pyrrhotite+pentlandite+mackinawite+valleriite was observed in two samples from the sulphide-rich layers in the central part of the intrusion (Chamberlain, unpublished notes).

The distribution of sulphide and alloy minerals is broadly consistent with the model proposed by Eckstrand (1975) whereby rocks containing relict olivine are characterized by the assemblage pentlandite+awaruite, completely serpentinized rocks commonly contain heazlewoodite with or without pentlandite and/or awaruite, and talc-carbonate rocks typically contain millerite. However, there are some apparent deviations from the model in that some completely serpentinized samples contain the assemblage pentlandite+awaruite and a few relict olivine-bearing specimens have pentlandite+heazlewoodite. Eckstrand (1975, Fig. 6) suggested an idealized footwall to hangingwall distribution of opaque mineral assemblages, but I have not found this to be strictly applicable in the Ultramafic Zone.

The textures observed in the serpentinized rocks fall into the five categories: incipient serpentinization (Fig. 10a), pseudomorphic mesh texture (Fig. 10b,d), pseudomorphic hourglass texture (Fig. 10c), nonpseudomorphic ribbon texture (Fig. 10e), and nonpseudomorphic interpenetrating texture (Fig. 10f). In the pseudomorphic textures, the outlines of primary olivine and pyroxene crystals may be discerned and some relict magmatic grains may even be present. Little or no trace of primary magmatic texture is found in the nonpseudomorphic textural types. The pseudomorphic mesh texture is by far the most frequently observed type among the samples studied. Nonpseudomorphic textures are developed only locally.

Lizardite is the most common serpentine mineral in the Dumont intrusion, particularly in the partly serpentinized peridotites and pseudomorphic-textured serpentinites where it usually constitutes the mesh rims, mesh centres, and hourglass textures. Chrysotile occurs in some samples as mesh rims, as fibres bordering, and oriented perpendicular to, fractures that cut across the pseudomorphic texture, and as cross- or slip-fibres filling crosscutting fractures. Chrysotile also seems to be the most common serpentine in the nonpseudomorphic ribbon textures. In most cases, chrysotile appears to have grown at the expense of lizardite and only rarely can it be argued that it has formed directly from olivine. Antigorite most commonly occurs as rims replacing lizardite along original olivine grain margins and internal fractures (Fig. 10d). A few examples of antigorite rosettes replacing lizardite were also observed. Brucite and magnetite have similar textural relationships. Both are typically localized along original olivine grain boundaries and, less commonly, along intragranular cracks in the pseudomorphic-textured samples. They also occur sparsely intergrown with serpentine within pseudomorphs. Brucite, magnetite, and chrysotile are intergrown in veins (Fig. 10c). Magmatic chromite grains in the serpentinized rocks virtually always have rims of magnetite which are in sharp contact with the chromite but have ragged contacts with the silicate matrix. This type of rim is considered to be an overgrowth and contrasts with the ferritchromite reaction rims commonly observed on chromite in regionally metamorphosed rocks (e.g., Bliss and MacLean, 1975). Such rims indicate that the surface of the chromite grains provided a favourable nucleation site for magnetite. Chlorite and diopside form intergrowths with serpentine that pseudomorphically replace primary clinopyroxene (Fig. 10g). The diopside in these

Table 2. Representative olivine analyses – arranged in order of increasing stratigraphic height

Sample no.	E8-1160	E21-3079	E16-2185	E16-1670	E21-2150	E21-1837	W13-520	E21-1200	W7-300
Subzone	LP	LP	LP	D	D	D	UP	UP	UP
SiO_2	39.4	40.1	39.6	40.1	40.7	40.0	39.9	39.0	39.7
FeO	13.0	11.2	10.7	9.80	7.35	7.82	7.17	14.6	14.7
MnO	0.25	0.31	0.14	0.14	0.11	0.07	0.08	0.22	0.26
MgO	47.7	47.8	49.8	49.0	51.4	50.5	52.4	45.6	44.7
CaO	nd	0.04	nd	0.10	0.10	0.08	0.09	0.13	0.08
NiO	0.25	0.31	0.27	0.35	0.37	0.32	0.33	0.17	na
Total	100.6	99.8	100.6	99.5	100.0	98.8	100.0	99.8	99.4
Cations/4 oxygen									
Si	0.978	0.994	0.974	0.991	0.989	0.986	0.971	0.983	1.00
Fe	0.270	0.232	0.220	0.203	0.149	0.161	0.146	0.308	0.310
Mn	0.005	0.006	0.003	0.003	0.002	0.001	0.002	0.005	0.006
Mg	1.767	1.765	1.825	1.804	1.861	1.856	1.901	1.714	1.680
Ca	-	0.001	-	0.003	0.003	0.002	0.002	0.004	0.002
Ni	0.005	0.006	0.005	0.007	0.007	0.006	0.006	0.003	-
Fo (mole %)	86.8	88.4	89.3	89.9	92.6	92.0	92.9	84.8	84.4

nd - not detected; na - not analyzed

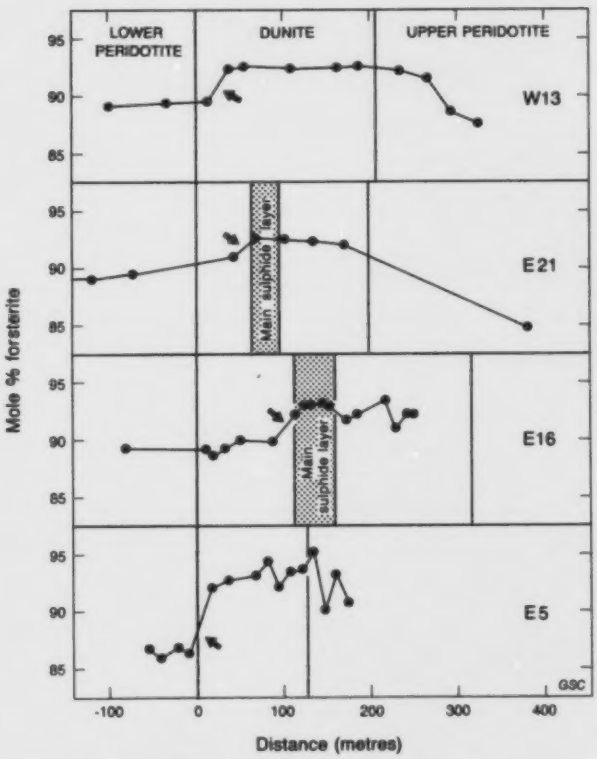

Figure 11. Variation of the forsterite content of olivine in drillholes E5 (section 17+30E), E16 (section 36+00W), E21 (section 36+00W) and W13 (section 108+00W). The horizontal scale gives the distance above (+) or below (-) the base of the Dunite subzone and thus stratigraphic top is to the right. The data for drillhole E5 are inferred from whole-rock analyses whereas those for the other drillholes are microprobe analyses of olivine. The abrupt increase in forsterite content in the lower part of the Dunite Subzone is indicated by arrows.

pseudomorphs tends to form minute crystals (>50 microns) whereas some coarser secondary diopside (about 0.5 mm) has been observed in nonpseudomorphic serpentinite.

The olivines in partly serpentinized samples host a variety of inclusions of presumed secondary origin. These include planar arrays of minute fluid inclusions, acicular grains, possibly of serpentine, and tiny opaque dendrites, similar in appearance to the dendritic magnetite inclusions in olivine from the Gardiner intrusion, East Greenland, described by Frisch and Keusen (1977).

The distribution of secondary minerals and textures in cross-section 36 + 00W is depicted in Figure 9. There is a systematic progression from mesh texture with relict olivine mesh centres in the zone of least altered rocks, through mesh textures with lizardite mesh centres, pseudomorphic hourglass textures, and , near the upper contact of the Ultramafic Zone, mesh textures with lizardite cores and antigorite rims. The occurrence of antigorite within a few tens of metres of the upper contact is characteristic.

Mafic Zone

The essential secondary minerals in the Mafic Zone include actinolite, epidote and minor chlorite. Quartz, pyrite, calcite and leucoxene are accessories. As noted above, the texture preserves many features of the igneous precursor. The epidote occurs as very fine grained, opaque masses replacing plagioclase, and is intergrown with quartz in some pseudomorphs. Actinolite replaces both clinopyroxene and orthopyroxene and takes on a variety of habits. It most commonly forms anhedral blades after clinopyroxene which are 1 to 2 mm in size, have frayed or hackly terminations, have interlocking grain boundaries and are frequently twinned. Masses of subparallel acicular actinolite grains, 0.05 mm long, make up generally square pseudomorphs after orthopyroxene. Pale green, felted patches of very fine grained interlocking and radiating actinolite occur in areas once filled by intercumulus material. Chlorite occurs mainly as very fine grains making up irregular patches which bear no particular relationship to the primary texture. Magmatic quartz has recrystallized in some places to a finer grain size.

MINERAL COMPOSITIONS

Analytical method

The chemical compositions of the various minerals were determined using a Materials Analysis Company electron microprobe. The concentrations of Si, Ti, Al, Cr, Fe, Mn, Mg, Ca, Na, and K in the silicate minerals were measured simultaneously with the instrument operated in the energy dispersive mode with an accelerating potential of 15 kilovolts. The concentrations of Cr, Ti, Al, Fe, Mn, and Mg in the oxide minerals, and of Ni, Co, Cu, Fe, and S in the sulphide and alloy minerals were determined with the instrument operated in the wavelength dispersive mode with an accelerating potential of 15 kilovolts. Nickel in the silicate and oxide minerals was determined using wavelength dispersive analysis with an accelerating potential of 25 kilovolts.

In each case, analytical standards for the principal constituents were chosen to match the composition and structure of the mineral being analyzed as closely as possible. Thus, the following standards were used as appropriate: synthetic olivine, synthetic diopside, synthetic Al-bearing enstatite, synthetic magnetite, natural chromite, natural serpentine, natural kaersutite, synthetic FeS_2, NiS, CoAs, nickel metal and copper metal. Minor elements in the silicate minerals were determined using kaersutite as a standard for Ti, Al, Ca, Na, and K, chromite for Cr, and biotite for Mn. The concentration of Ni in silicate and oxide minerals was determined using a synthetic magnetite standard containing 2% Ni.

Primary minerals

Olivine: Representative analyses of olivine are included in Table 2. No significant variation of olivine composition within individual samples was observed but it should be noted that since the olivine has been serpentinized along grain boundaries in even the least altered specimens, it is possible that thin zoned crystal margins would not be detected. The cryptic variation of olivine composition across the Ultramafic Zone is considerable and systematic as illustrated in Figure 11. It was found that the Mg/Mg+Fe ratio of the bulk rock was nearly equal to that of the contained olivine in almost all samples, and so the forsterite content of olivine may usually be inferred from the whole-rock analysis. The forsterite content of olivine is

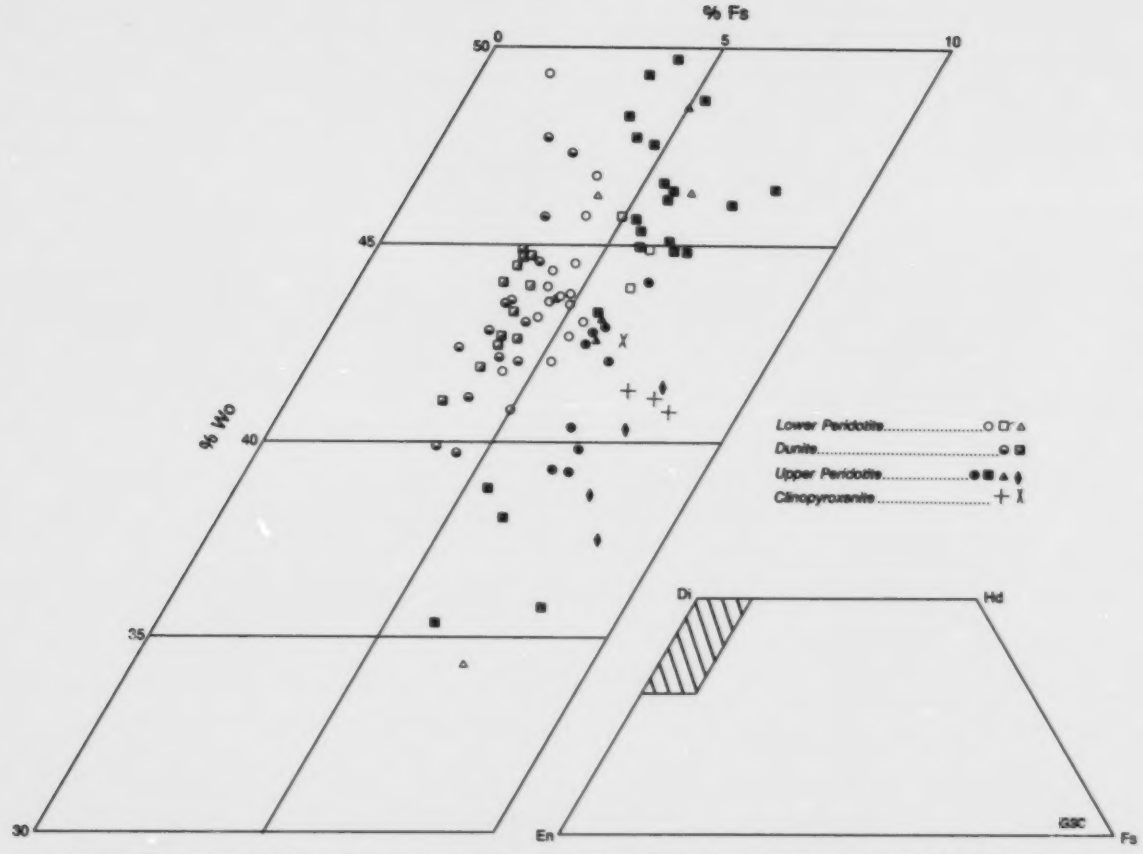

Figure 12. Compositions of Dumont clinopyroxenes plotted in the pyroxene quadrilateral. Each symbol type represents analyses from a single sample to indicate degree of inhomogeneity.

85 ± 2 mole per cent in the basal, orthocumulus part of the Lower Peridotite Subzone and increases gradually upwards to about 90% in the lower part of the Dunite Subzone. The forsterite content then increases abruptly to about 92.5 ± 1% and remains essentially constant across the upper part of the Dunite and into the lowermost Upper Peridotite Subzone. The forsterite content decreases upwards across the Upper Peridotite to about 84 to 85% at the top of the Ultramafic Zone. (The Mg/Mg+Fe ratio in the whole-rock at the top of the zone averages 0.82 which is lower than that of the contained olivine, and presumably reflects the relatively high proportion of retained intercumulus liquid.) The olivines were also analyzed for the minor elements Ni, Mn and Ca (Table 2). The concentrations of Ca and Mn approach the lower limits of detection of the analytical method but the data indicate that the concentrations of the latter element is significantly lower in the Dunite than in either the Lower Peridotite or Upper Peridotite subzones. The cryptic variation of the nickel content of olivine from unmineralized specimens correlates generally with the forsterite content. The concentration increases from about 0.2% at the base of the Ultramafic Zone to about 0.35% in the lower part of the Dunite Subzone, is essentially constant across the Dunite, and then decreases upwards across the Upper Peridotite to about 0.1% at the top of the Ultramafic Zone. The concentration of nickel in olivine from magmatic sulphide-bearing samples is extremely variable and essentially independent of forsterite content: this phenomenon will be discussed in some detail below.

Clinopyroxene: The clinopyroxenes in the Ultramafic Zone are chrome-rich diopsides and endiopsides (Fig. 12). They contain up to 3% Al_2O_3 and 1.3% Cr_2O_3 but have very low concentrations of TiO_2, MnO, and Na_2O (Table 3). The clinopyroxene crystals in any given sample from the Ultramafic Zone are compositionally zoned such that the cores are richer in MgO, FeO, Cr_2O_3, and Al_2O_3, but poorer in CaO than the margins (Fig. 13). In addition the Al/Al+Cr and Mg/Mg+Fe ratios are higher in the margins than in the cores of the crystals. The good correlation of Al_2O_3 and Cr_2O_3 contents of the clinopyroxenes (Fig. 14) reflects the fact that the altervalent substitution of Cr^{3+} for a divalent cation is balanced by a coupled substitution of the Tschermak ($Al^{3+} \rightleftharpoons Si^{4+}$) rather than the kosmochlor ($Na^{+} \rightleftharpoons Ca^{2+}$) type. The cryptic variation of the average Mg/Mg+Fe ratio of clinopyroxene across the zone parallels that in olivine although in any given sample the ratio is slightly lower in the latter mineral. There is no significant variation of the average CaO, Cr_2O_3, or Al_2O_3 contents of clinopyroxene across the Ultramafic Zone, although the variation within

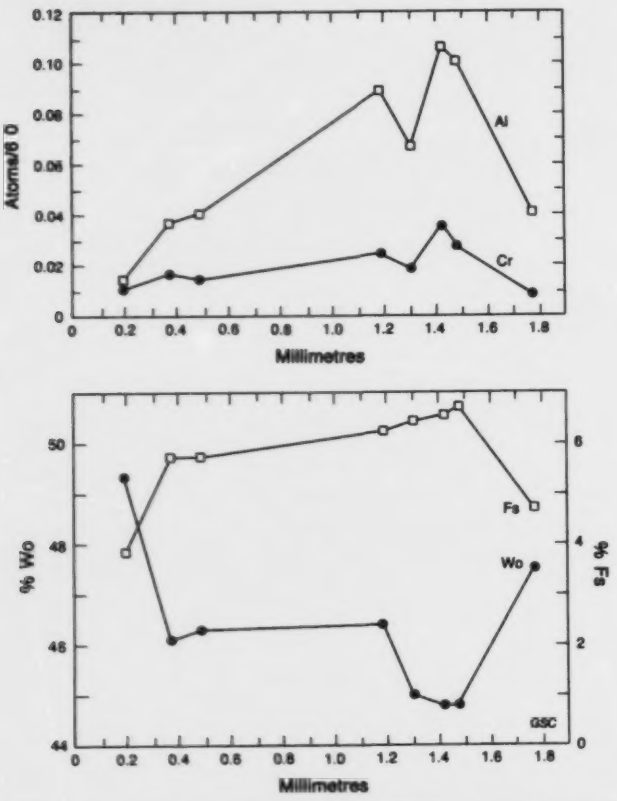

Figure 13. Analyses across a single clinopyroxene oikocryst illustrating crystal zoning with chromium, aluminum and iron enrichment in the cores and calcium enriched rims. Sample E21-1200 (Upper Peridotite Subzone).

individual samples is large. The zoning of clinopyroxene supports the conclusion that it represents orthocumulate as opposed to heteradcumulate crystallization.

Clinopyroxene has been preserved in only two samples from the Mafic Zone and these are from the Clinopyroxenite Subzone. Their compositions overlap with those from the immediately underlying Upper Peridotite Subzone but differ in that the crystals within each sample are homogeneous. The cryptic variation of clinopyroxene composition in the Mafic Zone must be inferred from whole-rock analyses owing to the pervasive alteration. Accordingly, there is a slight increase in the Mg/Mg+Fe ratio across the Clinopyroxenite from 0.86 at the base to 0.89, followed by a steady and precipitous decrease upwards across the Gabbro Subzone to 0.71 at the top of the unit (Fig. 5). The rocks in the Quartz Gabbro are thought to represent mixtures of cumulus crystals and intercumulus liquid in variable proportions and so the cryptic decrease of the whole-rock Mg/Mg+Fe ratio is not strictly representative of the contained clinopyroxene.

Chromite: The chromites display a range of chemical compositions, both as zoning within individual crystals and as cryptic variation across the Ultramafic Zone. The concentrations of the principal oxide constituents are illustrated in Figure 15, and representative analyses are given in Table 4. On average the chromites from the Dunite are richer in Cr_2O_3, Al_2O_3, and MgO, but poorer in FeO, Fe_2O_3, and TiO_2 than those from either the Lower Peridotite or Upper Peridotite subzones. The crystal cores are richer in Cr_2O_3 and MgO, but poorer in FeO, Fe_2O_3, Al_2O_3, and TiO_2 than the rims. Some of the chromite rims, particularly in samples from the orthocumulate rocks at the base of the Lower Peridotite, are extremely rich in TiO_2 in comparison with published analyses of chromites from other environments which rarely exceed 1.5% (e.g., Table 4, sample E8-1160). Crystal zoning is most pronounced in the chromites from near the top of the Upper Peridotite (Table 4, sample W13-245), and is indicative of the reaction of cumulus chromite with intercumulus liquid.

Table 3. Representative average clinopyroxene compositions – arranged in order of increasing stratigraphic height

Sample no.	E8-1160	E21-3079	W13-1530	W13-1060	E16-1245	W13-245	E21-1200	W7-300	E21-1135	E21-1100
Subzone	LP	LP	LP	D	D	UP	UP	UP	C	C
n	4	3	15	12	14	9	23	4	5	1
SiO_2	52.9	52.7	53.2	53.3	53.4	52.8	53.4	53.4	52.8	53.8
TiO_2	0.11	0.34	0.12	0.17	0.20	0.21	0.10	0.15	0.12	0.11
Al_2O_3	1.83	1.96	2.21	2.19	1.69	2.67	1.36	2.47	1.83	1.72
Cr_2O_3	0.84	1.06	1.05	0.89	0.86	0.91	0.65	0.90	0.65	0.54
FeO	3.54	3.44	2.96	2.31	2.35	4.01	3.83	5.09	4.96	4.15
MnO	0.13	0.27	0.05	0.06	nd	0.10	0.11	0.12	0.12	0.17
MgO	18.0	17.08	18.6	18.9	19.1	18.3	18.0	18.6	17.9	18.5
CaO	21.5	21.6	21.7	21.6	21.6	20.2	22.3	19.6	20.4	21.3
Na_2O	0.34	0.55	0.11	0.14	nd	0.15	0.22	0.08	0.02	nd
Total	99.2	99.0	100.0	99.6	99.2	99.4	100.0	100.4	98.8	100.6
Cations / 6 oxygen										
Si	1.942	1.941	1.931	1.936	1.946	1.929	1.949	1.935	1.948	1.951
Ti	0.003	0.009	0.003	0.005	0.005	0.006	0.003	0.004	0.003	0.003
Al	0.079	0.085	0.095	0.094	0.073	0.115	0.059	0.106	0.080	0.074
Cr	0.024	0.031	0.030	0.026	0.025	0.026	0.019	0.026	0.019	0.015
Fe	0.109	0.106	0.090	0.070	0.072	0.123	0.117	0.154	0.153	0.126
Mn	0.004	0.008	0.002	0.002	-	0.003	0.003	0.004	0.004	0.005
Mg	0.985	0.938	1.006	1.023	1.037	0.997	0.979	1.004	0.985	1.000
Ca	0.843	0.852	0.844	0.840	0.843	0.791	0.872	0.761	0.806	0.827
Na	0.024	0.039	0.008	0.009	-	0.011	0.016	0.006	0.001	-
Mg/Mg + Fe	0.900	0.898	0.918	0.936	0.935	0.890	0.893	0.867	0.866	0.888
Wo	43.6	44.9	43.5	43.5	43.2	41.4	44.3	39.7	41.4	42.3
En	50.8	49.5	51.9	52.9	53.1	52.2	49.7	52.3	50.7	51.2
Fs	5.6	5.6	4.6	3.6	3.7	6.4	6.0	8.0	7.9	6.5

n - number of analyses used in computing average; nd - not detected

The composition of chrome spinel is to some extent indicative of the petrological-tectonic setting of the rock in which it occurs (Irvine, 1965, 1967; Thayer, 1970) with chromites from stratiform intrusions, ophiolitic peridotites, and peridotite nodules in basalts having distinctive compositions. The Dumont chromites have compositions generally similar to those from other stratiform intrusions, although some have relatively high Mg/Mg+Fe ratios.

Secondary minerals

Serpentine: Representative analyses and structural formulae of the serpentine minerals from the Ultramafic Zone are given in Table 5. Antigorite contains more silicon and aluminum than do either lizardite or chrysotile. In the structural formula on the basis of 14 oxygen [i.e., 10 O^{2-} + 8 $(OH)^{-}$], silicon and aluminum sum to 4 or slightly greater in antigorite but have a distinctly lower total in lizardite and chrysotile. The chemical analyses of antigorite have higher summations, implying a lower concentration of hydroxyl, and consistent with its slightly different stoichiometry. Where two or more serpentines occur in the same specimen, lizardite mesh cores tend to have the highest Mg/Mg+Fe ratios, lizardite mesh rims and chrysotile have similar but lower ratios, and antigorite has a significantly lower ratio. There is a rough inverse correlation between the amount of Si and Fe in the structural formulae for any particular serpentine polytype (Fig. 16). This may reflect the substitution of Fe^{3+} for Si in tetrahedral sites or possibly the charge balancing of Fe^{3+} in octahedral sites by the substitution of Al for Si in tetrahedral sites. The Mg/Mg+Fe ratios of all the serpentine minerals, however, are very much higher than those of the precursor olivine or bulk rock. Chrysotile tends to contain more chromium than coexisting lizardite and antigorite. Bastite pseudomorphs after clinopyroxene are notable for their high concentrations of aluminum and chromium, and also contain small amounts of calcium. Rucklidge (1972) found chlorine contents as high as 0.8% in serpentine mesh rims in partially serpentinized dunite from the Dumont Sill. Rucklidge and Patterson (1977) suggested the chlorine is present in the form of the compound $Fe_2(OH)_3Cl$ rather than in solid solution in serpentine. This conclusion was subsequently shown to be incorrect by Muira et al. (1981) who confirmed the chlorine-rich nature of fine grained serpentine in mesh rims adjacent to relict olivine. I have determined whole-rock chlorine concentrations (Fig. 17) and found the mean of 28 samples to be 0.28 ± 0.11%. The five antigorite-bearing samples which were analyzed contained significantly less than the average of chlorine (0.12 ± 0.06%), and thus support the view of Muira et al. (1981) that recrystallization of fine grained serpentine is accompanied by expulsion of chlorine. However, the fact that completely serpentinized samples,

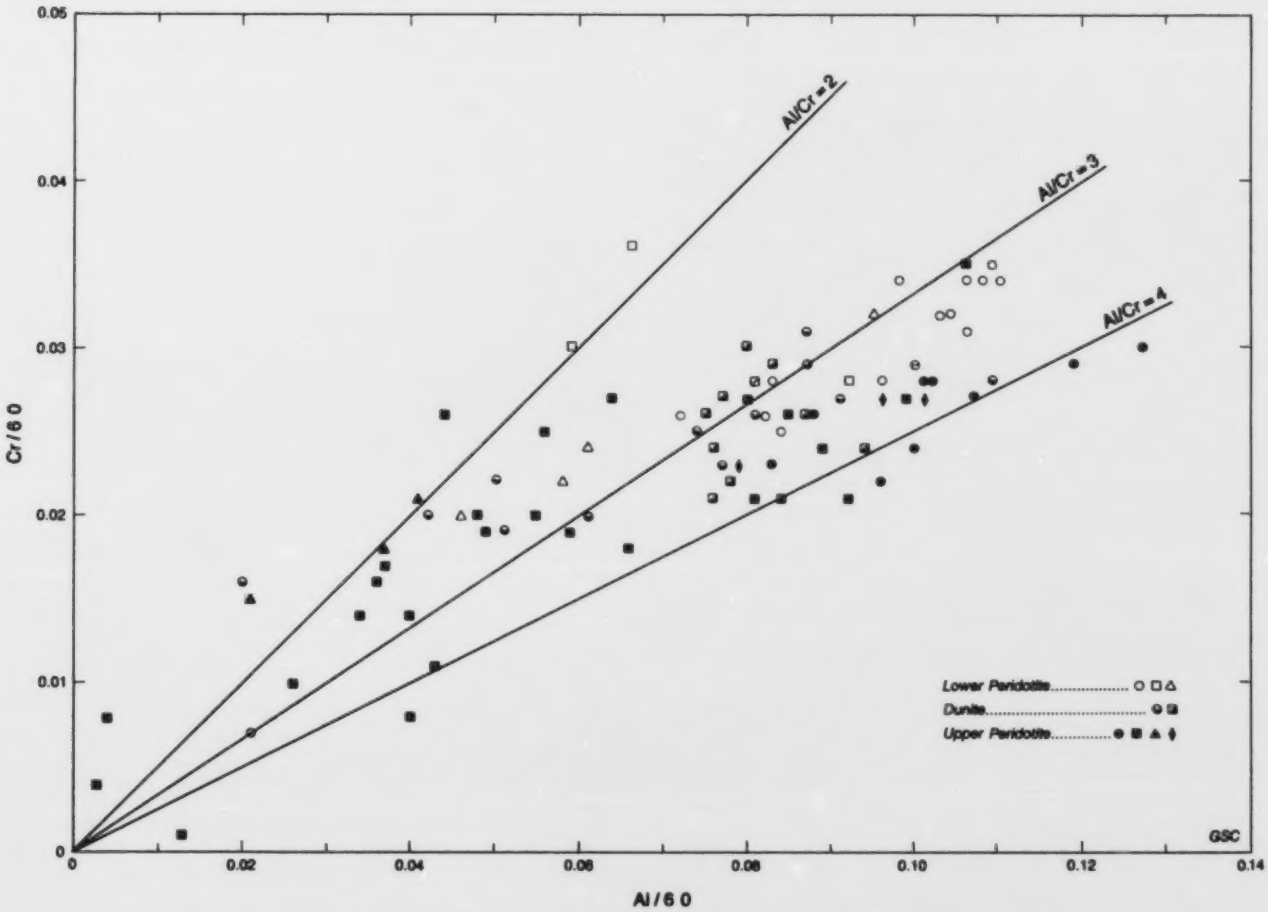

Figure 14. Correlation between chromium and aluminum contents of Dumont clinopyroxenes. Symbolism the same as Figure 12.

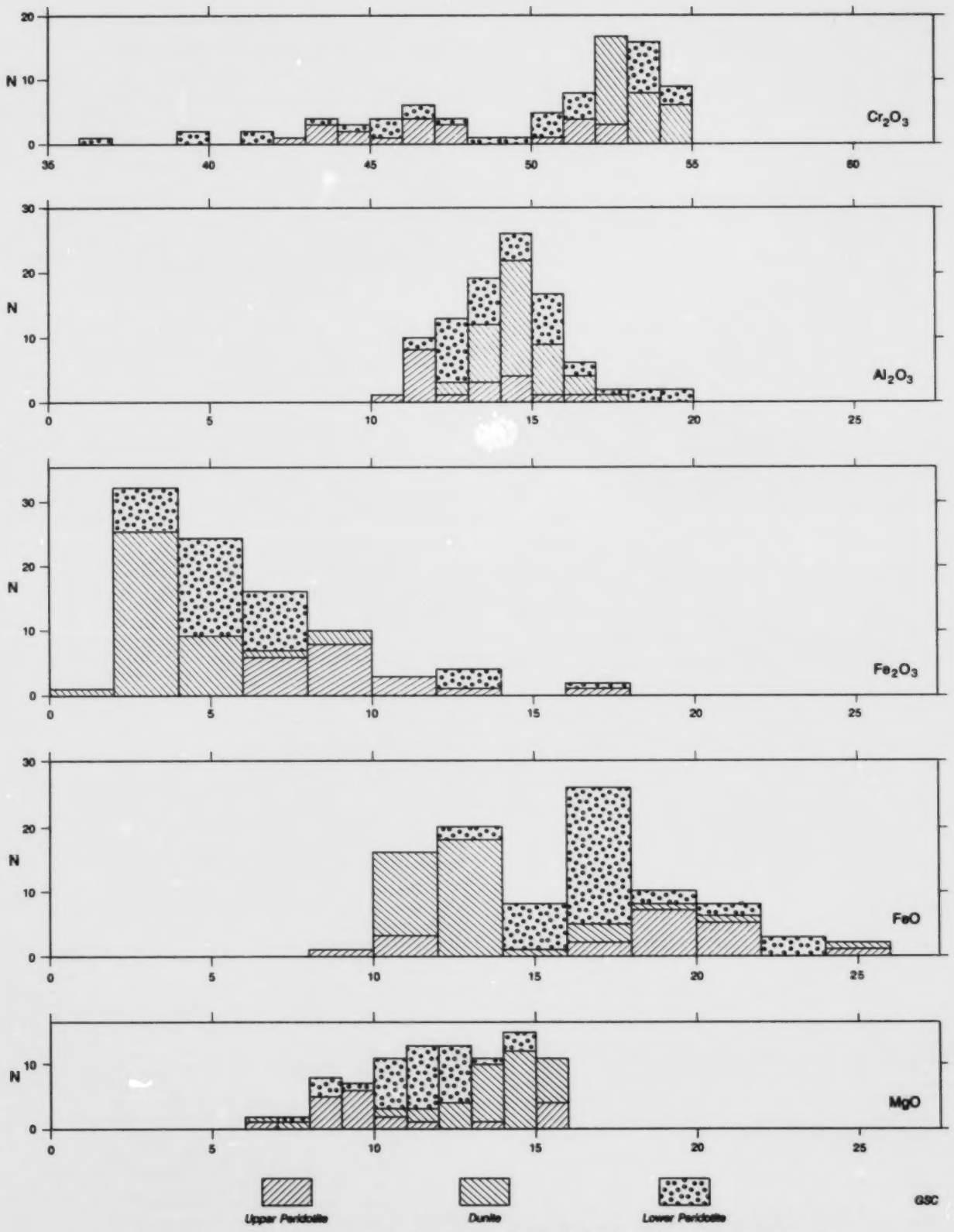

Figure 15. Histograms showing frequency distribution of oxide concentrations in analyzed chromites.

Table 4. Representative chromite analyses – arranged in order of increasing stratigraphic height

Sample no.	E8-1160 LP		E21-3079 LP		E16 2185 LP		E21 2150 D		E21 1837 D		W13 245 UP		E21 1200 UP	
Subzone	A	B	A	B	A	B	A	B	A	B	A	B	A	B
TiO_2	1.72	3.91	0.60	0.72	0.39	0.41	0.20	0.23	0.21	0.23	0.33	2.43	0.54	1.19
Al_2O_3	12.8	11.3	15.7	18.2	14.4	15.4	14.8	13.5	15.7	16.5	11.5	11.4	12.4	14.0
Cr_2O_3	41.1	39.6	49.4	43.4	52.5	50.7	54.9	52.0	55.5	54.0	52.1	42.1	47.7	46.2
Fe_2O_3	13.3	13.0	7.29	7.37	5.4	5.4	4.5	8.1	2.63	3.00	7.12	12.0	11.7	9.7
FeO	21.9	20.9	15.1	17.9	16.3	16.3	11.6	10.9	10.8	10.6	18.0	22.0	17.5	19.5
MgO	8.73	10.3	13.2	11.2	12.2	12.1	15.2	15.3	15.7	15.8	10.2	8.64	11.2	10.5
Total	99.7	99.7	101.3	98.8	101.2	100.3	101.0	100.0	100.6	100.2	99.3	98.6	101.0	101.1
Cations / 4 oxygens														
Ti	0.043	0.098	0.014	0.017	0.009	0.010	0.005	0.005	0.005	0.005	0.008	0.062	0.013	0.029
Al	0.502	0.440	0.578	0.687	0.538	0.577	0.539	0.500	0.573	0.600	0.448	0.452	0.472	0.533
Cr	1.079	1.040	1.223	1.101	1.315	1.275	1.347	1.296	1.356	1.320	1.359	1.120	1.218	1.176
Fe^3	0.333	0.325	0.171	0.178	0.129	0.129	0.104	0.193	0.061	0.069	0.177	0.305	0.283	0.234
Fe^2	0.609	0.581	0.396	0.481	0.432	0.435	0.301	0.287	0.280	0.275	0.498	0.619	0.472	0.525
Mg	0.432	0.511	0.617	0.535	0.576	0.575	0.703	0.717	0.724	0.730	0.503	0.434	0.541	0.503

A and B represent extreme compositions of several analyses from each sample; A is usually a crystal core and B a crystal rim. Total iron analyzed as FeO, proportions of FeO and Fe_2O_3 recalculated on basis of charge balance.

even those in which lizardite is partially recrystallized to antigorite, contain appreciable concentrations of chlorine suggests that serpentine retains some chlorine.

Diopside: Secondary diopside within any given serpentinite sample is nearly homogeneous. Average compositions of primary and secondary clinopyroxene from any given sample are similar with respect to the major constituents CaO, MgO, and FeO but the secondary grains are very much poorer in Al_2O_3 and Cr_2O_3 (Fig. 18). For example, compare column 7 in Table 3 to column 6 in Table 6.

Chlorite: The analyzed chlorites from the Ultramafic Zone have about 6 silicon and 1.5 iron atoms per 28 oxygens and therefore may be characterized as clinochlore (Table 6). Chlorite has the lowest Mg/Mg+Fe ratio of the nonmetallic secondary minerals, and the concentrations of Cr_2O_3 approach the analytical detection limit. The chlorites from the Mafic Zone rocks have 5.7 silicon and from 2.7 to 4.5 iron atoms per 28 oxygens and are thus classified as pycnochlorite.

Amphibole: All the amphiboles analyzed are calcic, low in aluminum and may be described as tremolite or actinolite depending upon their Mg/Mg+Fe ratio (Table 6). There is some compositional variation within individual samples, particularly in respect to Al_2O_3 content, but this variation does not seem to correlate with the different textural habits present. The low TiO_2 and Al_2O_3 concentrations of the amphiboles support their secondary as opposed to igneous origin.

Other secondary minerals: Some of the other secondary minerals were analyzed on a reconnaissance basis. Brucite was difficult to analyze owing to its very fine grain size and instability under the electron beam, but semiquantitative results indicate that it has a lower Mg/Mg+Fe ratio than the coexisting serpentine. Similarly, magnesite is more iron-rich than the coexisting talc.

Sulphides and alloys

Two textural modes of occurrence of sulphide and alloy minerals have been described above: minute monomineralic grains which were generated during alteration of the intrusion and larger polymineralic grains having textures indicative of magmatic origin. The minerals occurring in the magmatic grains appear to be essentially homogeneous within any given sample. The secondary grains are typically too small to allow detection of zoning but the grains in any given sample display a range of composition.

Pentlandite is the most common of these minerals and also shows the greatest range of composition (Table 7). The Ni/Fe ratio is distinctly higher in pentlandite that coexists with heazlewoodite than in that which coexists with awaruite, as would be expected from the work of Harris and Nickel (1972). Perhaps the most striking feature of the pentlandite compositions is the extreme range in cobalt concentration, from 0.5 to 37 weight per cent. In those samples in which pentlandite in both magmatic and secondary grains was analyzed, the latter have significantly higher cobalt content. In general, the cobalt content of pentlandite varies directly as the degree of serpentinization and inversely as the amount of sulphide in the rock. It would appear that the incorporation of cobalt into pentlandite occurs more at the expense of iron than of nickel. The cobalt-rich nature of many of the pentlandites is of interest in view of the fact that the rocks contain on average only about 0.01% cobalt. It is likely that the cobalt resided mainly in olivine prior to serpentinization but that it is extremely incompatible with respect to serpentine and the other nonmetallic secondary minerals.

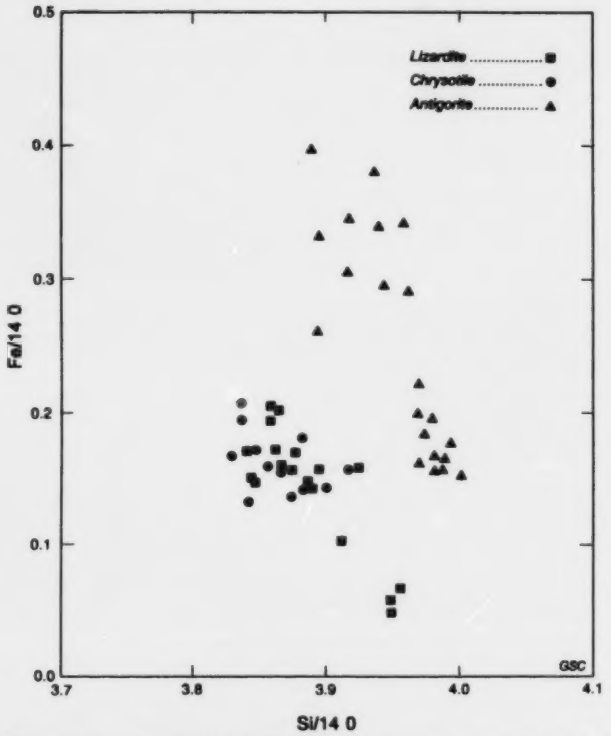

Figure 16. Composition of serpentine minerals in terms of the number of Si and Fe atoms in the structural formula. Note that for each of the polytypes there is a rough inverse correlation between Fe and Si (see text).

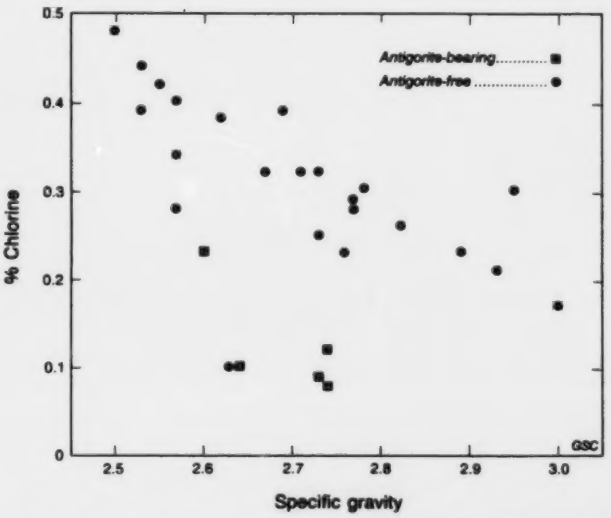

Figure 17. Variation of the chlorine concentration and specific gravity of whole-rock samples from the Ultramafic Zone. The chlorine concentration of antigorite-free samples varies inversely with specific gravity and thus directly with the degree of serpentinization.

Table 5. Representative serpentine analyses

Sample no.	E21-2378				E21-2150			E21-1200			
Subzone	LP				D			UP			
Mineral	Liz(c)	Liz (r)	Chrys	Ant	Liz(r)	Chrys	Ant	Liz(c)	Liz(r)	Ant	Bast
n	4	2	3	6	3	3	5	7	2	6	4
SiO_2	42.9	41.0	41.0	43.3	40.2	41.1	43.4	41.6	41.5	43.9	38.5
Al_2O_3	0.24	0.38	0.34	0.32	0.33	0.82	0.30	0.58	0.34	1.02	3.03
Cr_2O_3	0.04	0.35	0.37	0.10	0.18	0.24	nd	0.10	0.06	0.04	0.73
FeO	0.77	2.18	1.92	2.11	2.44	2.48	2.52	1.97	3.16	4.62	3.48
MgO	43.6	42.6	41.9	42.3	41.9	42.7	42.5	43.1	42.3	42.3	39.6
Total	87.6	86.5	85.5	88.1	88.7	87.3	88.7	87.4	87.4	91.9	85.6
Cations / 14 oxygen											
Si	3.957	3.867	3.902	3.985	3.864	3.844	3.976	3.875	3.887	3.927	3.707
Al	0.026	0.042	0.038	0.035	0.037	0.090	0.033	0.064	0.038	0.108	0.344
Cr	0.003	0.026	0.028	0.007	0.014	0.018	-	0.007	0.004	0.003	0.056
Fe	0.059	0.172	0.153	0.162	0.196	0.194	0.193	0.153	0.248	0.346	0.280
Mg	5.984	5.991	5.945	5.804	6.000	5.956	5.807	5.990	5.915	5.634	5.678

Liz(c) – lizardite mesh centre, Liz(r) – lizardite mesh rim, Chrys – chrysotile, Ant – antigorite, Bast – bastite after clinopyroxene; Total iron analyzed as FeO; n - number of analyses used in computing average; nd - not detected

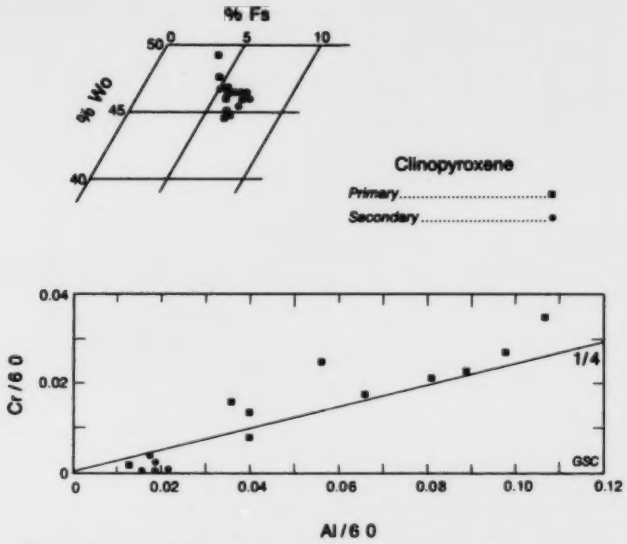

Figure 18. Compositions of primary and secondary clinopyroxenes in sample W13-1530 (Lower Peridotite Subzone).

The heazlewoodite specimens that were analyzed contained about 1% iron but no detectable cobalt or copper. The metal/sulphur ratio is close to the stoichiometric value of 1.5 [i.e. $(Ni, Fe)_3S_2$]. The awaruite compositions consistently yield formulae of about $Ni_{2.95}Fe_{1.05}$ and are thus slightly more iron-rich than the Ni_3Fe stoichiometry. The limited number of secondary awaruite grains analyzed are apparently even more iron-rich but this may simply reflect fluorescence of the silicate matrix because many awaruite grains are of the same order of size as the electron beam of the microprobe. An important observation is that the awaruite typically contains on the order of 0.5 weight per cent copper and thus is the main copper-bearing mineral other than native copper. The awaruite also contains between 0.2 and 2.6 weight per cent cobalt.

ECONOMIC GEOLOGY

Introduction

The potential economic significance of the Dumont intrusion derives from the presence of disseminated, nickel-rich sulphide and alloy minerals within the ultramafic rocks. Two textural modes of occurrence of such minerals have been described. The secondary type comprises minute and generally monomineralic grains that were generated during alteration of the body. These grains are present in such small quantities that they make a negligible contribution to the nickel content of the rock. In any event, their very fine grain size would militate against their recovery by conventional mineral dressing techniques. The magmatic type comprises relatively coarse polymineralic grains which have textures

Table 6. Representative analyses of secondary chlorite, diopside and actinolite

	Chlorite				Diopside			Actinolite		
Sample no.	E21-1295	E21-1200	E21-1100	E21-830	E21-1275	E21-1200	W7-255	E21-1135	E21-830	E21-290
Subzone	UP	UP	C	G	UP	UP	UP	C	G	QG
SiO_2	32.9	30.9	29.1	28.1	53.9	53.0	53.1	56.0	54.3	52.7
TiO_2	nd	nd	0.09	nd	nd	nd	nd	0.07	nd	0.12
Al_2O_3	12.1	14.7	19.0	18.6	0.34	0.43	0.30	0.82	2.17	2.65
Cr_2O_3	0.19	0.05	nd	nd	0.07	0.08	0.09	0.18	0.08	nd
FeO	4.56	9.44	8.20	16.3	0.94	4.67	2.37	6.23	8.82	16.9
MnO	nd	nd	0.17	0.22	nd	0.16	0.16	0.11	0.14	0.27
MgO	34.4	32.5	29.7	23.0	17.8	17.7	17.0	21.0	18.6	13.8
CaO	nd	nd	nd	nd	26.2	24.0	26.0	12.4	12.7	12.0
Total	84.7	87.6	86.2	86.2	99.3	99.8	98.9	96.9	97.0	98.4
Formula										
Si	6.464	6.000	5.689	5.734	1.974	2.074	1.964	7.870	7.735	7.669
Ti	-	-	0.013	-	-	-	-	0.007	-	0.013
Al	2.805	3.368	4.385	4.479	0.015	0.020	0.013	0.136	0.365	0.455
Cr	0.030	0.008	-		0.002	0.002	0.003	0.020	0.009	
Fe	0.749	1.533	1.341	2.782	0.029	0.153	0.073	0.732	1.053	2.057
Ma	-	-	0.028	0.038	-	0.005	0.005	0.013	0.017	0.033
Mg	10.074	9.406	8.655	6.996	0.971	0.742	0.938	4.399	3.957	2.993
Ca	-	-	-	-	1.028	1.820	1.031	1.867	1.942	1.871
O	28	28	28	28	6	6	6	23	23	23

Total iron analyzed as FeO; nd - not detected

Table 7. Representative analyses of sulphides and alloys

Sample no.	E21-2048				W13-1330		W4-690			W4-220		E5-860	W13-1530
Texture	M	M	S	S	M	M	S	S	S	S	S	S	S
Mineral	PN	AW	PN	AW	PN	HZ	PN	AW	PN	HZ	AW	ML	CU
Ni	28.5	73.2	27.8	67.7	31.8	73.1	24.2	71.8	31.8	71.9	71.7	62.9	0.33
Fe	35.5	27.2	30.4	30.3	32.1	1.22	14.7	24.1	22.7	0.80	24.6	0.20	2.91
Co	1.96	0.50	5.56	0.50	2.12	nd	28.5	2.39	12.8	nd	0.66	0.10	nd
Cu	nd	0.50	nd	0.57	nd	nd	nd	na	nd	na	na		98.0
S	33.7	na	33.2	na	32.6	25.8	32.7	na	32.6	26.1	na	35.6	na
Total	99.7	101.4	97.0	99.3	98.6	100.1	100.1	98.3	99.9	98.8	97.0	99.3	101.2
Formula													
Ni	3.70	0.712	3.66	0.594	4.27	3.10	3.24	0.721	4.27	3.10	3.24	0.721	
Fe	4.85	0.278	4.21	0.393	4.53	0.05	2.07	0.255	3.20	0.04	0.263	0.003	0.033
Co	0.25	0.005	0.73	0.006	0.28	-	3.80	0.024	1.71	-	0.006	0.001	-
Cu	-	0.004	-	0.006	-	-	-		-	-	-	-	0.964
S	8	-	8	-	8	2	8	-	8	2	-	1	-

Texture: M – relict magmatic grains, S – secondary grains, nd – not detected, na – not analyzed;
Mineral: PN - pentlandite, AW - awaruite, HZ - heazlewoodite, ML - millerite, Cu - native copper

suggesting they originated as droplets of molten sulphide that were immiscible in the parent magma. It is this latter type that hosts the bulk of the nickel which would be recoverable by conventional methods. Magmatic sulphides are restricted to the Dunite and Lower Peridotite subzones of the intrusion with the most extensive sulphide-enriched layers occurring in the former unit. As noted above, two widely separated zones of magmatic sulphide enrichment are known to occur in the Lower Peridotite and, given that this unit has not been explored in any detail, I do not believe that one should discount the possibility that an undiscovered zone of sulphide enrichment might occur at the basal contact of the intrusion.

Intermineral distribution of nickel

The nickel contained in the ultramafic rocks is distributed among a variety of primary and secondary silicate, oxide, hydroxide, sulphide, and metallic minerals. Knowledge of the distribution of nickel among these constituent minerals is a prerequisite to the rational evaluation of the assay data presented below. In particular, the potential recoverability of the nickel will depend upon its partitioning between the sulphide/alloy and non-sulphide/alloy fractions.

Consider first the distribution of nickel prior to alteration. Except at its margins, the Ultramafic Zone was generally made up of at least 95% olivine. Given the very low concentrations in clinopyroxene and chromite, it follows that almost all of the nickel in the sulphide-free rocks resides in olivine. This is illustrated in Figure 19a where the microprobe analyses of nickel in olivine are plotted against the assay values for the corresponding rocks. For this purpose the assays have been recalculated on a volatile-free basis. The two quantities are essentially equivalent for the unmineralized specimens. This also indicates that nickel has been immobile during serpentinization, at least for those samples in which the olivine has not been completely destroyed. Moreover, the regularity of the cryptic variation of nickel content of olivine allows prediction of its concentration at given stratigraphic levels in the Ultramafic Zone, and comparison of the assays of completely serpentinized rocks suggest that nickel has been immobile in these as well. A further implication is that the nickel content of olivine has not changed during alteration. The nickel contents of olivines in the magmatic sulphide-bearing samples are significantly lower than the corrected assay values and the differences reflect the nickel content and modal proportion of the magmatic sulphide grains prior to serpentinization (Fig. 20).

The concentrations of nickel in serpentine and magnetite are compared to that in the precursor olivine in Figure 19b. In the sulphide-free samples, the magnetite contains more nickel than the olivine whereas the serpentine contains less. The serpentine and magnetite together may account for almost all of the nickel released upon breakdown of the olivine but the inhomogeneous nature of the secondary minerals precludes a precise statement to this effect. The serpentine and magnetite in the mineralized samples each contain much less nickel than the precursor olivine and their nickel contents in many samples approach the analytical detection limit. An implication of these data is that much of the nickel released from the olivine during serpentinization is taken up by the magmatic sulphide grains. This means that serpentinization may have increased the nickel tenor of the sulphide/alloy fraction and therefore greater recovery of nickel might be expected from the more altered rocks.

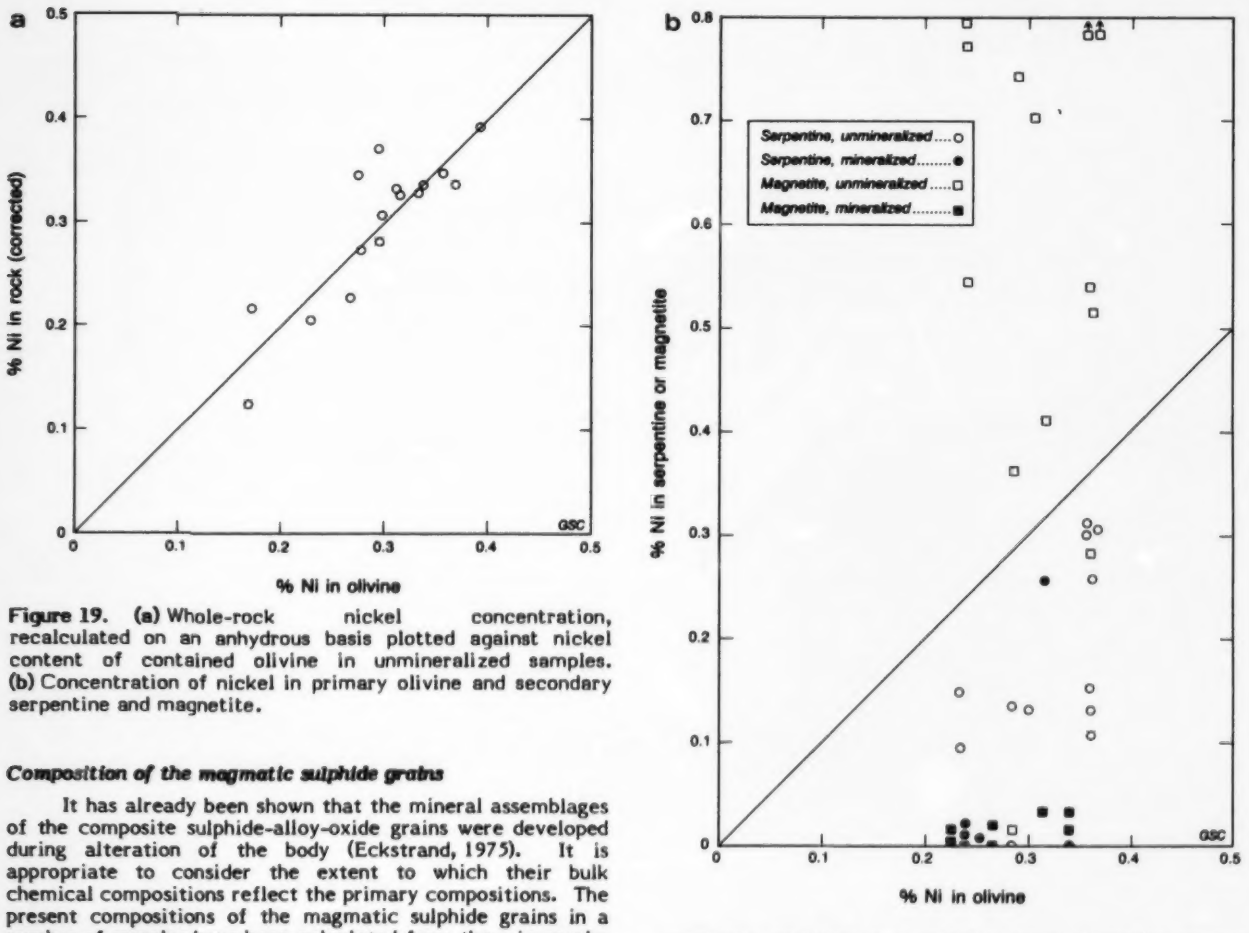

Figure 19. (a) Whole-rock nickel concentration, recalculated on an anhydrous basis plotted against nickel content of contained olivine in unmineralized samples. (b) Concentration of nickel in primary olivine and secondary serpentine and magnetite.

Composition of the magmatic sulphide grains

It has already been shown that the mineral assemblages of the composite sulphide-alloy-oxide grains were developed during alteration of the body (Eckstrand, 1975). It is appropriate to consider the extent to which their bulk chemical compositions reflect the primary compositions. The present compositions of the magmatic sulphide grains in a number of samples have been calculated from the microprobe analyses of the constituent minerals together with their modal proportions determined with the aid of a quantitative image analyzer, and the results are given in Table 8.

The sulphur and oxygen contents of magmatic sulphide liquids are determined by the fugacities of the two species which, in the case of sulphide droplets dispersed in a silicate magma, will likely be buffered by the latter (Naldrett, 1969). Consequently, the concentrations of sulphur and oxygen in unaltered magmatic sulphides tend to fall within a rather narrow range: about 38 to 40 weight per cent sulphur, and 0 to 4 weight per cent oxygen. Moreover, where the sulphides remain dispersed in the silicate matrix during crystallization and cooling, as would have been the case at Dumont, it is likely that any oxygen initially contained in the sulphide would be lost to the silicate host which effectively buffers the oxygen fugacity (Naldrett, 1969). The present sulphur and oxygen contents of the magmatic sulphide grains are therefore too low and too high, respectively, for them to represent primary concentrations, and it is clear that the two constituents have been exchanged with either the solid matrix or the migrating fluid phase during serpentinization. The total sulphur plus oxygen content of the grains averages only about 28 weight per cent and, as there is no evidence to suggest that the volume of the grains has changed significantly during alteration, it follows that the apparent increase in total metal content is an absolute as well as a relative change. The primary total metal content of the magmatic sulphides was probably about 61 weight per cent. The mean metal concentrations normalized to this total are 40.4% Fe, 18.9% Ni, 1.0% Cu and 0.7% Co. These normalized values would reflect the primary compositions if the only effect of alteration on the grains had been the loss of sulphur and gain of oxygen. However, it was suggested above that nickel and cobalt were added to the sulphide/alloy fraction during serpentinization.

An indication of the relative importance of primary and secondary contributions to the sulphide compositions is given by the distribution coefficient

$$K_{D(Ni\text{-}Fe)}^{sulphide/olivine} = \left(\frac{Ni}{Fe}\right)^{sulphide} \left(\frac{Fe}{Ni}\right)^{olivine}$$

Although the value of this coefficient has been debated recently (Fleet et al., 1977; Naldrett, 1979, 1981), there is a growing body of evidence to indicate that values in the range of 5 to 10 are typical of magmatic conditions (Thompson et al., 1984). I have calculated the apparent $K_{D(Ni\text{-}Fe)}^{sulphide/olivine}$ for the samples containing relict olivines (Table 8). Note that these are not actual distribution coefficients because the primary olivine compositions are combined with the present sulphide values. It is interesting in this regard that there is a general inverse relationship

between the apparent distribution coefficient and the specific gravity of the sample. The distribution coefficient is 10 or less in the least altered samples having specific gravities of greater than 2.7, whereas coefficients of 11 or higher are characteristic of more altered samples with specific gravities of less than 2.7. Because the composition of relict olivine is primary, the increase of the distribution coefficient due to serpentinization implies a proportional increase in the Ni/Fe ratio of the sulphide fraction.

There are insufficient data to allow a quantitative treatment of the possible changes in the cobalt and copper tenors of the magmatic sulphides. Naldrett (1981) has reported that the cobalt contents of sulphides from most deposits of komatiitic affinity fall in the range of 0.22 to 0.34 weight per cent. All but one of the Dumont samples have significantly higher cobalt contents than this and it seems clear that cobalt has been greatly enriched in the sulphide fraction during alteration. Concentrations of 0.5 to 1.5 per cent copper are typical of komatiitic sulphides (Naldrett, 1981) and thus most of the Dumont sulphides appear depleted in copper whilst a few are abnormally rich. However, the overall average is in the middle of the komatiite range. The analytical data coupled with textural observations suggest considerable mobility of copper during serpentinization.

Assay data and resource estimation

An assay profile across the Upper Peridotite, Dunite, and part of the Lower Peridotite subzones in drillhole E16 is depicted in Figure 20. The variation in the nickel and forsterite contents of olivine are also shown. The positions of the three conformable nickel-enriched layers are indicated by distinct peaks in the assay values, and the area between the assay and olivine nickel curves reflects the amount of nickel resident in the sulphide fraction prior to serpentinization. The variability of the nickel content of olivine among samples means that it would be very difficult to infer the proportion of nickel residing in the sulphide/alloy fraction from the assay value alone. By contrast, the nickel content of olivine from sulphide-free samples of the Dunite is apparently much less variable. For example, the mean of 265 assays of variably serpentinized Dunite containing no significant magmatic sulphides is 0.292% nickel with a standard deviation of 0.0165%. From these data I would conclude that material assaying greater than about 0.35% nickel (i.e. mean plus 3 standard deviations) probably contains conspicuous amounts of magmatic sulphides. However, as illustrated by Figure 20, the converse is not necessarily true; some samples that do contain significant magmatic sulphides have assay values less than the "threshold" level.

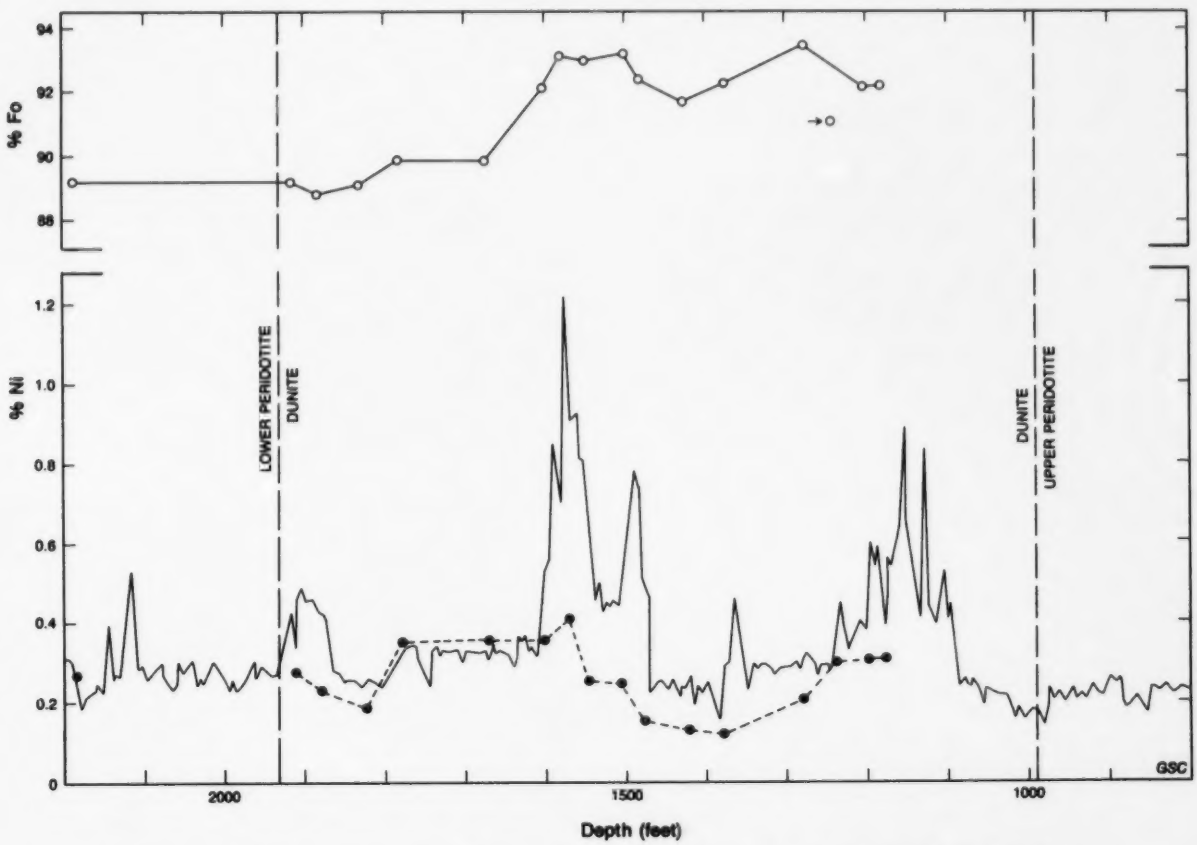

Figure 20. Nickel content of whole-rock (solid line) and contained olivine (filled circles), and forsterite content (open circles) of olivine in drillhole E16. The sample marked by the arrow contains an abnormally large amount of intercumulus material which accounts for the low forsterite content.

Table 8. Magmatic sulphide grains: grain size, modal and chemical composition, and distribution coefficient

Sample no.	Mean grain size mm	Modal % sulphide	Mode PN	Mode MT	Mode AW	Mode CU	Calculated concentrations (wt %) Fe	Ni	Cu	Co	S	Olivine O	Olivine Fo (mole %)	Olivine Ni (ppm)	K_D	G
E16-1180	0.25	0.24	58	26	16	–	44.18	28.23	0.09	0.94	19.37	7.19	92.3	3070	12.2	2.55
E16-1380	0.26	0.10	73	22	5	–	43.88	24.49	0.03	1.13	24.39	6.08	92.3	1380	23.8	2.55
E16-1425	0.45	1.82	44	56	–	tr	56.59	12.56	–	0.67	14.70	15.48	91.8	1225	11.6	2.62
E16-1480	0.70	2.03	68	28	–	4	45.09	19.42	4.00	1.04	22.71	7.74	92.6	1570	15.4	2.64
E16-1500	0.70	1.68	77	15	–	8	38.96	21.99	8.00	1.18	25.72	4.15	93.2	2585	11.4	2.63
E16-1550	0.70	1.85	57	36	7	–	48.69	21.38	0.04	0.90	19.04	9.95	93.0	2500	9.4	2.73
E16-1575	0.55	2.29	55	17	26	–	39.99	35.37	0.15	0.95	18.74	4.80	93.1	4140	11.3	–
E16-1600	0.35	0.83	55	38	7	–	49.41	20.81	0.04	0.87	18.37	10.51	92.2	3550	7.0	2.77
E16-1670	0.28	0.66	16	57	27	–	54.16	24.25	0.16	0.34	5.34	15.76	90.0	3473	9.9	2.84
E16-1910	0.63	1.21	52	48	–	–	53.72	14.85	–	0.80	17.37	13.27	89.2	2356	8.8	2.95
Mean	0.49	1.27	56	34	9	1	47.5	22.3	1.2	0.88	18.6	9.5	92.0	2585	12.1	2.70
(Std. dev.)	(0.19)	(0.78)	(17)	(15)	(1)	(3)	(6.0)	(6.5)	(2.7)	(0.24)	(5.7)	(4.2)	(1.3)	(978)	(4.7)	(0.14)

Mineral: PN - pentlandite, MT - magnetite, AW - awaruite, CU - native copper. G - specific gravity; K_D - distribution coefficient (see text)

Figure 20 also illustrates the position of the sulphide-enriched layers in relation to the primary layering of the sill. The base of the lower layer corresponds to that of the Dunite Subzone in this intersection although it locally trangresses this boundary (Fig. 4). The base of the middle layer corresponds to the discontinuity in the forsterite content of olivine and the base of the uppermost layer is approximately three-quarters of the way through the Dunite Subzone.

Assay profiles from a series of drillholes along the length of the intrusion are shown in Figure 21, and these give an indication of the apparent thickness, lateral extent and nickel content of the three nickel-enriched layers. The average grades, calculated on the basis of the 0.35% "cut-off", and true thicknesses in each cross-section are given in Table 9. These data may be used to make an order of magnitude estimation of the nickel resources contained in the intrusion. For this purpose, it has been assumed that the nickel-enriched layers extend to a vertical depth of 500 m below the bedrock surface, and that the average specific gravity of the rock is 2.6. The middle layer extends from section 36+00W to 84+00W, a strike length of 2430 m, with an average true thickness of 24 m and a weighted average grade of 0.50% nickel. The calculated mass is 82 million tonnes. The upper layer has the same apparent strike length as the middle layer, although it not present in one cross-section, and its average true thickness is also 24 m. It contains 80 million tonnes with an average grade of 0.45% nickel. The lower nickel-enriched layer extends from section 36+00W to 44+00W, and has a strike length of about 350 m. This layer was not intersected in sections 38+00W and 42+00W because drilling did not penetrate the lowermost Dunite Subzone. Its average true thickness is 26 m, its average grade is 0.41%, and its mass is 13 million tonnes. It is apparent from the assay profiles that a higher grade zone occurs in the lower part of the middle layer at its eastern end. This zone has a strike length of 730 m and an average true thickness of 14 m, and contains 14 million tonnes with a weighted average grade of 0.71% nickel.

PETROGENESIS

Nature of the parent and derivative magmas

With the exception of some rocks described from the Quartz Gabbro Subzone, all of the available samples from the Dumont Sill are cumulates and the nature of the magma from which they crystallized is known only by inference. The composition of olivine is very useful in this regard inasmuch as the distribution coefficient

$$K_{D(Mg\text{-}Fe)}^{Ol/L} = \left(\frac{Fe}{Mg}\right)^{Ol} \left(\frac{Mg}{Fe}\right)^{L}$$

is relatively insensitive to temperature, pressure and composition, and has a mean value of 0.30 (σ = 0.03) in experimental studies of basaltic systems (Roeder and Emslie, 1970). The most primitive rocks within the intrusion occur in the Dunite Subzone where the maximum forsterite content of olivine is about 93 mole per cent. This suggests a Mg/Mg+Fe ratio of 0.799 in the magma from which it crystallized. This is somewhat higher than the ratios typical of basaltic magmas but is within the range observed in peridotitic komatiite liquids. An average value of the distribution coefficient of 0.33 is preferred for such ultramafic magmas (Bickle et al., 1977; Arndt, personal communication, 1978) in which case a Mg/Mg+Fe ratio of 0.814 is indicated for the liquid in equilibrium with olivine of Fo_{93} composition. I have compiled analyses of spinifex-textured peridotites having Mg/Mg+Fe ratios close to 0.814 and from these have derived the model magma composition given in Table 10. Thus, I am proposing that the parent magma of the Dumont Sill was a peridotitic komatiite containing about 27.5 weight per cent MgO.

The komatiitic affinity of the parent magma is supported by certain compositional characteristics described below. This conclusion differs from earlier workers who had postulated that the parent magma was a tholeiitic picrite (Besson and Capitant, 1976; Bonneau, 1977; Besson, 1979).

The compositions of the few samples of noncumulate rocks from the Quartz Gabbro (Table 11) are probably equivalent to those of the more evolved liquids of the intrusion. The feasibility of deriving such liquids by fractional crystallization of the postulated parent magma is demonstrated by calculations presented subsequently. It is significant that gabbros of virtually identical composition (Table 11) to that of the least primitive of the noncumulate Quartz Gabbro samples occur as sills about a kilometre to the north and stratigraphically above the Dumont body. Not only does this support the existence of a mobile, highly differentiated komatiite magma but also suggests that late magmatic liquids were tapped-off from the main magma chamber.

The average composition of the sill will be equivalent to that of the parent magma if the intrusion crystallized as a closed system. The average composition of the body cannot be precisely calculated owing to the uncertainty in the relative proportions of its various subdivisions, but the exercise is nevertheless instructive. The average compositions of the individual subzones of the sill have been weighted according to their mapped area (Fig. 3) and mean densities to yield the bulk composition of the sill given in Table 12. This average composition contains 32.2% MgO and is significantly more primitive than the model parent liquid. If the preceding calculations are not greatly in error, there are two reasonable explanations for the apparent discrepancy. Firstly, as discussed above, the gabbroic sills overlying the intrusion indicate that an unknown quantity of differentiated magma was tapped-off from the main body and, secondly, it is probable that the parent magma would have carried olivine phenocrysts in suspension at the time of intrusion. I will argue below that these intratelluric phenocrysts amounted to about 12.5% of the mass of the main body of the intrusion, and the bulk composition of the sill has been recalculated to show the effect of the removal of this amount of olivine. The resultant composition is still more magnesian than the model parent magma but a reasonable match is achieved if 10% gabbroic liquid is added (Table 12).

The most magnesian spinifex-textured peridotites normally found in komatiitic sequences contain in the order of 32 to 34% MgO. It is interesting that the bulk composition of the sill, including that component considered to represent intratelluric phenocrysts, is very similar to those of such lavas. A possible interpretation is that the bulk intrusion does represent a liquid composition but that the liquid partly crystallized prior to or during emplacement with little or no fractional crystallization (i.e., equilibrium crystallization).

Emplacement and differentiation of the intrusion

The cumulus textures, macroscale phase layering, cryptic variation of mineral compositions, and geological setting leave little doubt that the Dumont intrusion was emplaced as a virtually horizontal sill that fractionally crystallized in situ. The apparent rarity of features such as rhythmic and graded layering, cross-stratification, and scour channels may indicate that magmatic currents did not play an important role in crystal accumulation and, moreover, most other aspects of the sill are consistent with its emplacement as a single pulse of magma. Experimental and petrographic studies (Arndt, 1976; Arndt et al., 1979) indicate that olivine and minor chromite are the liquidus phases for komatiitic magmas containing more than about 15% MgO, whereas olivine and subordinate clinopyroxene are on the liquidus of magmas having between 12 and 15%, and clinopyroxene and plagioclase are liquidus phases for melts with 9 to 12% MgO. The sequence of rock types and cryptic variation upward from the base of the Dunite Subzone is generally consistent with these crystallization relations inasmuch as there is an olivine cumulate overlain in turn by an olivine-chromite cumulate, a clinopyroxene cumulate, a clinopyroxene-plagioclase cumulate, and a quartz gabbro. However, the nature of the Lower Peridotite Subzone is problematical in this context. The forsterite content of olivine increases upward across this unit which is the reverse of the normal cryptic trend produced by fractional crystallization, and the olivine is everywhere less magnesian than in the Dunite Subzone. Moreover, the rock is an olivine-chromite cumulate whereas chromite is not a cumulus mineral in the Dunite. On the latter two accounts, the Lower Peridotite would appear to have crystallized from a less primitive magma than did the overlying Dunite Subzone. These anomalous features may be

Table 9. Average grades and true thicknesses of upper, middle and lower nickel-enriched layers

Cross-section	Upper layer*		Middle layer*		Middle layer**		Lower layer*	
	Grade	True thickness	Grade	True thickness	Grade	True thickness	Grade	True thickness
36+00W	0.45	26	0.57	24	0.84	11	0.41	26
38+00W	0.46	30	0.62	24	0.75	16	–	–
40+00W	0.59	22	0.61	32	0.76	18	0.41	26
42+00W	0.40	17	0.66	32	0.75	20	–	–
44+00W	–	–	0.52	32	0.64	20	0.40	27
46+00W	0.43	13	0.56	38	0.68	21	–	–
48+00W	0.47	22	0.48	39	0.66	8	–	–
52+00W	0.52	25	0.48	25	0.64	8	–	–
60+00W	0.47	20	0.47	17	–	–	–	–
68+00W	0.44	19	0.38	14	–	–	–	–
76+00W	0.41	16	0.50	33	–	–	–	–
84+00W	0.38	23	0.50	19	–	–	–	–
Weighted Average	0.45	24	0.50	24	0.71	14	0.41	26

* Calculated on the basis of a 0.35% Ni cut-off grade
** Calculated on the basis of a 0.60% Ni cut-off grade

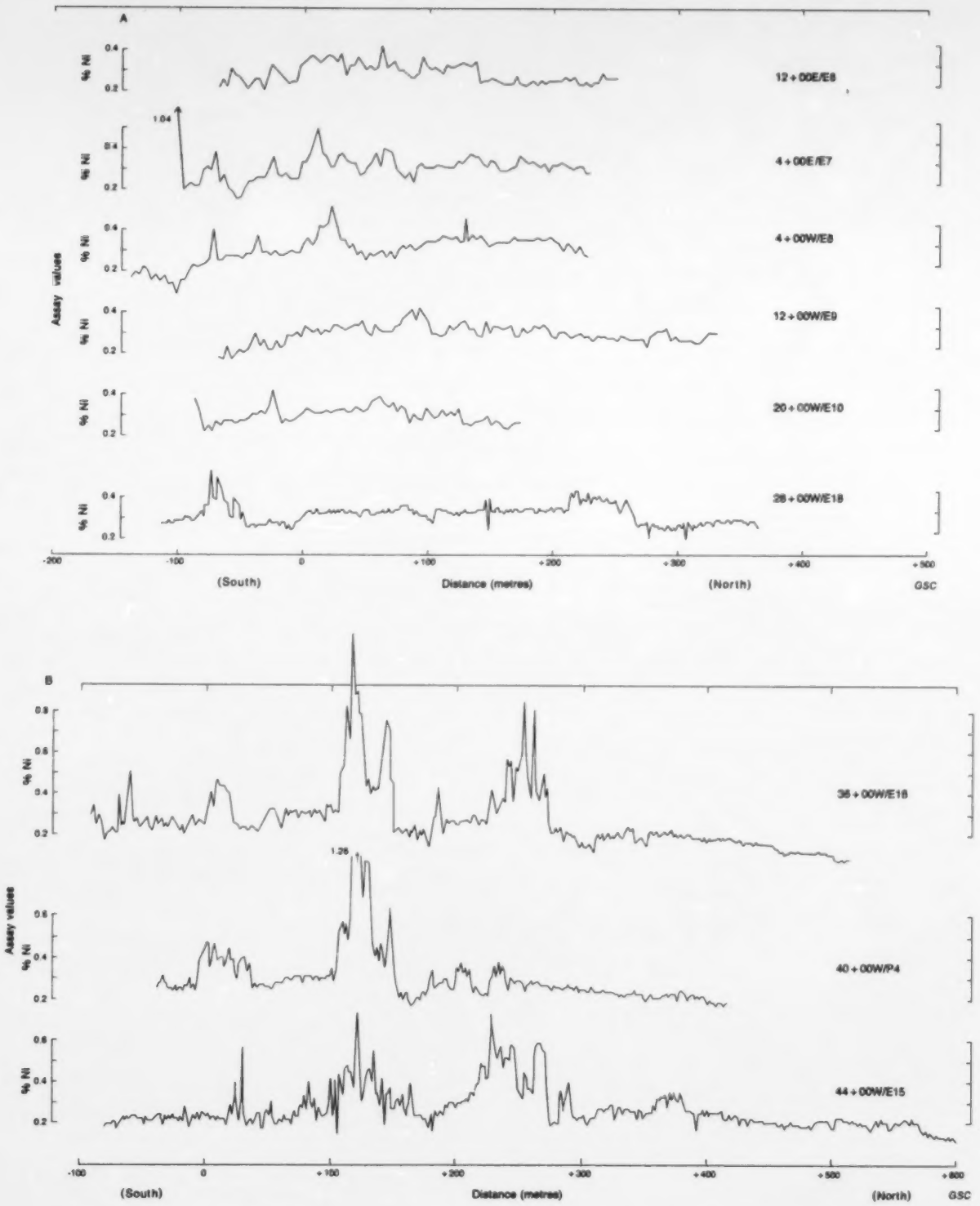

Figure 21. Nickel assay profiles of sections along the length of the sill compiled from data provided by Dumont Nickel Corporation. The profiles are labelled in terms of cross-section/drillhole number. The horizontal scale gives the distance above (+) or below (-) the base of the Dunite Subzone and thus stratigraphic top is to the right.

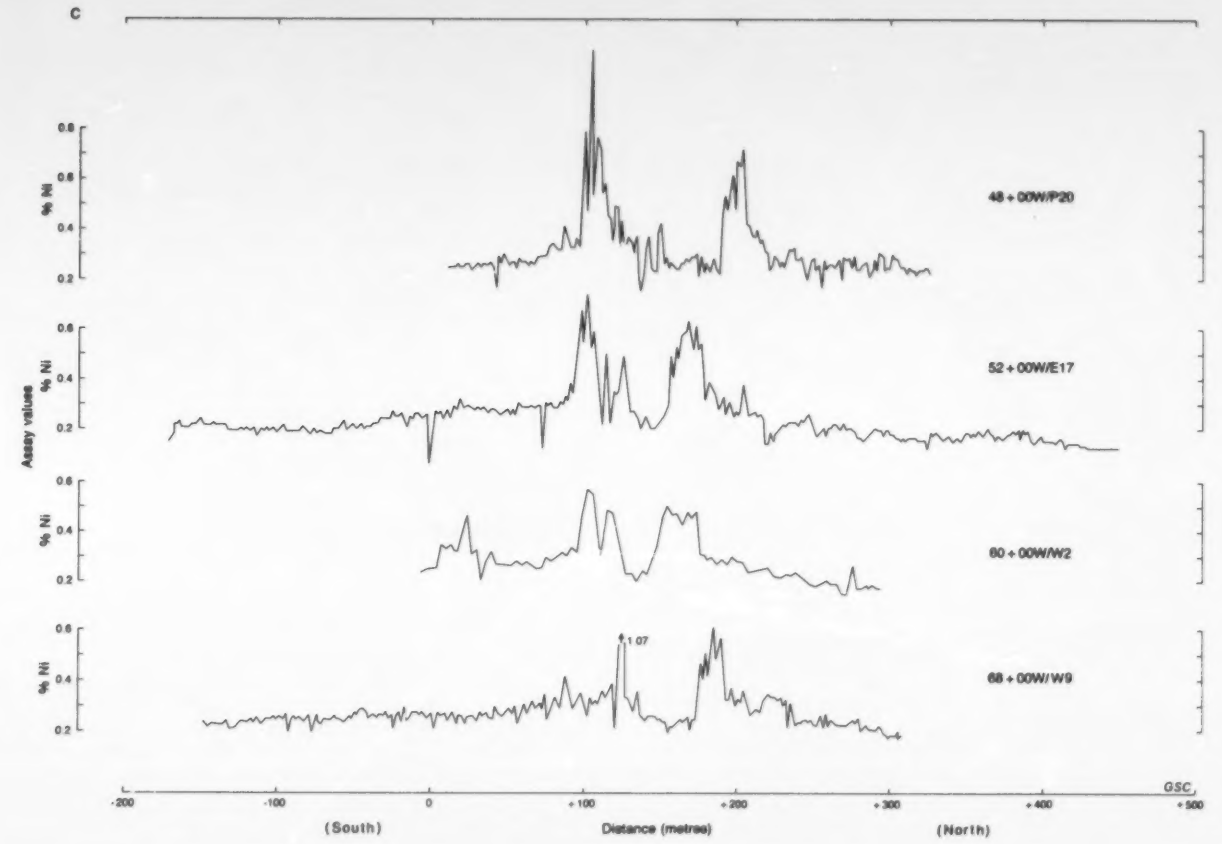
C
% Ni
Assay values
48 + 00W/P20
52 + 00W/E17
60 + 00W/W2
68 + 00W/W9
1.07
-200
-100
0
+100
+200
+300
+400
+500
(South)
Distance (metres)
(North)
GSC

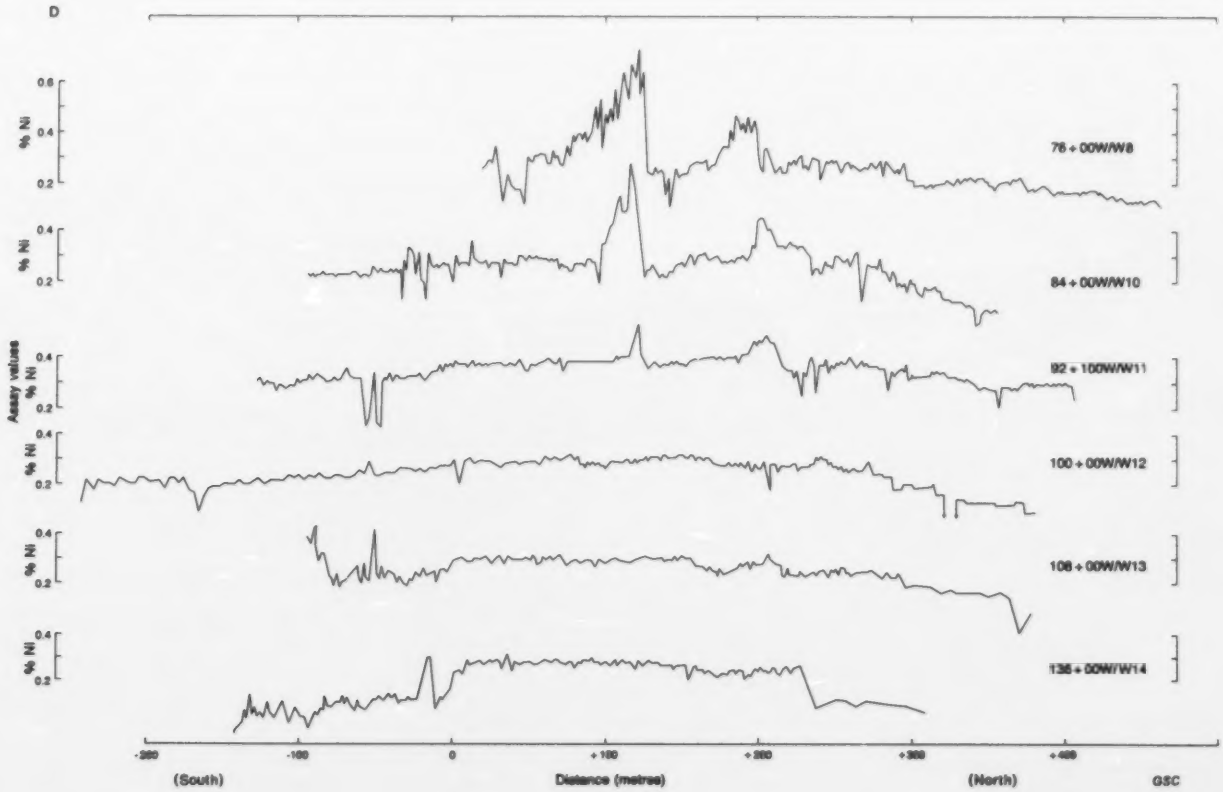
D
% Ni
Assay values
76 + 00W/W8
84 + 00W/W10
92 + 100W/W11
100 + 00W/W12
108 + 00W/W13
136 + 00W/W14
-200
-100
0
+100
+200
+300
+400
(South)
Distance (metres)
(North)
GSC

Table 10. Compositions of spinifex-textured peridotites and model parent magma of Dumont Sill

	1	2	3	4	5	6	7	8	9	10	11	12	13	Model composition
SiO_2	46.7	45.6	46.7	45.8	46.6	47.8	47.4	48.6	45.2	47.6	47.7	47.2	45.6	47.5
TiO_2	0.30	0.30	0.28	0.3	0.29	0.30	0.32	0.32	0.29	0.34	0.32	0.32	0.27	0.32
Al_2O_3	5.65	6.34	6.00	7.06	6.25	6.50	6.49	6.28	6.17	6.37	6.37	6.56	7.35	6.50
Cr_2O_3	0.37	0.50	0.38	0.33	0.38	0.40	0.33	0.20	0.45	0.40	0.46	0.37	0.41	0.30
FeO	10.8	10.7	10.9	10.8	10.8	10.7	11.1	11.0	11.5	11.2	11.0	11.1	11.7	11.1
MnO	0.25	0.23	0.24	0.14	0.23	0.17	0.16	0.17	0.21	0.19	0.17	0.18	0.21	0.18
MgO	29.4	29.1	29.4	28.2	28.1	27.8	27.9	27.7	28.6	27.7	27.3	27.4	25.9	27.5
CaO	5.58	6.10	5.22	6.75	5.79	5.86	5.96	6.01	5.89	5.75	6.19	5.92	7.62	6.00
Na_2O	0.11	0.58	0.22	0.19	0.22	0.02	0.22	0.06	0.60	0.18	0.14	0.18	0.80	0.15
K_2O	-	0.03	0.25	0.02	0.45	0.69	0.53	0.03	0.04	0.62	0.46	0.66	0.06	-
P_2O_5	-	0.02	0.01	0.02					0.02					
Co	-	0.010	-	0.008	-	0.012	0.012	0.008	0.011	0.012	0.013	0.012	-	0.0110
Cu	-	-	-	0.005	-		0.003	0.008		-	-	-	-	0.0050
Ni	-	0.141	0.156	0.150	0.139	0.145	0.141	0.110	0.149	0.163	0.140	0.132	0.134	0.1400
V	-	0.014	0.011	0.013	0.012	-	0.013	-	0.013			-	-	0.0125
Zr	-	0.0017	0.0021	0.0011	0.0012	-	-	-	0.0016			-	-	0.0020
Mg/Mg+Fe	.829	.829	.828	.824	0.822	0.822	0.817	0.817	0.816	0.815	0.815	0.814	0.800	0.813

Analyses recalculated to 100% on volatile-free basis and total iron reported as FeO. Data sources: 1 – Naldrett and Turner (1977), Yakabindie, Western Australia; 2, 9 – Nesbitt and Sun (1976), Mt. Burges, western Australia; 3, 5 – Nisbet et al. (1979), Belingwe, Zimbabwe; 4 – Duke (unpublished), Malartic, Quebec; 6, 10, 11, 12 – Nisbet et al. (1977), Belingwe, Zimbabwe; 7, 8 – Williams (1978), Belingwe and Lonely Mine, Zimbabwe; 13 – Arndt et al. (1977), Munro, Ontario.

largely explained if the Lower Peridotite Subzone formed by the accumulation of intratelluric phenocrysts carried in the magma at the time of intrusion.

Suppose that the Dumont Sill was emplaced instantaneously as a uniform suspension of olivine (Fo_{93}) and chromite in a liquid of the model composition (Fig. 22a). The initial grain sizes of the olivine and chromite phenocrysts would be close to those observed in the basal orthocumulate rocks, that is, about 0.5 and 0.05 mm respectively. Using the methods of Bottinga and Weill (1970, 1972), I calculate the density of the model liquid to be 2.77 gm/cm^3 and the viscosity to be 9 poises at 1550°C, the estimated liquidus temperature at low pressure. The densities of olivine and chrome spinel at this temperature are 3.11 gm/cm^3 and 4.64 gm/cm^3, respectively, applying the thermal expansion factors tabulated by Skinner (1966). The Stokes' Law settling velocities derived from these data are 5.4×10^{-3} cm/sec for olivine and 3.2×10^{-4} cm/sec for chromite[1]. Even allowing for the reduction of velocities in a suspension, the settling velocities are rapid by comparison, for example, with those calculated for basaltic magmas, and application of the equations of Gray and Crain (1969) indicates that the intratelluric phenocrysts would accumulate rather quickly on the floor of the magma chamber (Fig. 22b). Recent studies have suggested that mafic magmas are non-Newtonian fluids which have finite yield strengths, and therefore suspended crystals must exceed a minimum critical radius if they are to settle or rise through the magma (McBirney and Noyes, 1979). The yield strengths of peridotitic magmas have not been determined but the occurrence of komatiitic lavas as thin, extensive flows is indicative of rather low yield strengths. Moreover, crystal settling is well exemplified by the classic spinifex-bearing peridotitic komatiite flows (Pyke et al., 1973), and I believe that the Lower Peridotite is analogous to the B-zone in such lavas. The large difference between the settling velocities of olivine and chromite is a feature which has been documented in olivine-chromite cumulates in other intrusions (Jackson, 1961; Campbell, 1978) and, when viewed in conjunction with the homogeneous distribution of the two minerals in the Lower Peridotite, may suggest that the chromite did not settle as individual grains but aggregated with other cumulus crystals.

If the magma was intruded carrying a uniform suspension of olivine and chromite, it is not clear why chromite was not also a cumulus phase during accumulation of the Dunite. One explanation is that chromite was not part of the initial suspension but that crystal growth of olivine during accumulation of the crystal mush brought the liquid composition onto the olivine-chromite cotectic.

The rocks within 30 to 50 m of the base of the intrusion are regarded as orthocumulates. They contain about 70 weight per cent olivine (Fo_{84-87}) but a proportion of this presumably grew from the trapped intercumulus liquid. The amount of intercumulus liquid retained in an orthocumulate rock is given by the ratio of the concentration in the rock of an element excluded from the cumulus minerals to its concentration in the initial liquid. Among the elements for which analytical data are available, Al, Ti, V, Zr and Ca may be considered to be virtually incompatible with respect to olivine crystallization, and although the first three elements do enter chromite, the proportion of this phase is sufficently small so as not to invalidate the following argument. Thus, comparison of the average orthocumulate composition in Table 13 with the model parent liquid in Table 10 indicates that the average rock contains about 50% trapped intercumulus liquid (i.e., TiO_2: 0.14/0.32 = 0.44, Al_2O_3: 2.7/6.5 = 0.42, V: 0.0076/0.013 = 0.58, Zr: 0.0009/0.0018 = 0.5, CaO: 3.7/6.0 = 0.62). This is very similar to the

[1] The velocity (v) of an isolated sphere of low particle Reynolds' number, radius r and density ρ_s moving in response to gravity in an infinite medium of density ρ_f and viscosity η is given by $v = 2gr^2 (\rho_s - \rho_f)/9\eta$ where g is the gravitational acceleration constant and downwards is the positive direction. Velocities are reduced in a suspension and experimental studies suggest a reduction by a factor of 65% in a 20% suspension and a factor of 96% in a 50% suspension (Shaw, 1965). The velocities will be further reduced where the particles deviate from spherical shape.

proportions of retained intercumulus liquid observed in recent experimental and field studies of basaltic magmas (Campbell et al., 1978; Irvine, 1980, p. 351). The average Mg/Mg+Fe ratio of the basal rocks is 0.856 which is lower but similar to the weighted average of the Mg/Mg+Fe ratios of the initial olivine and model liquid (0.872). The model liquid contains about 40 normative per cent olivine which, when added to the initial proportion of cumulus olivine gives almost the same quantity of olivine as is observed in the rocks (i.e., (0.40 x 50) + 47 = 67%, as compared to 70 modal per cent).

The basal orthocumulate rocks grade upwards into meso- and adcumulates, and the proportion of trapped liquid indicated by the incompatible element concentrations decreases to about 4% at the top of the subzone. (At these levels, the quantities of incompatible elements in cumulus chromite become significant and have been accounted for.) The olivine composition changes to $Fo_{89.5}$ over the same interval, and is thus much less magnesian than would have resulted simply from equilibration between cumulus olivine (Fo_{93}) and the small indicated amount of trapped liquid. According to one widely invoked mechanism, adcumulus growth is considered to occur at or just below the surface of the accumulating pile of crystals by downward diffusion of the components of the cumulus mineral(s) to the site of crystallization and mechanical displacement of intercumulus liquid upwards. When developed to the extreme, the resulting rock consists virtually entirely of cumulus minerals having the same composition as the initial crystals, and any postcumulus material would have the bulk composition of the initial trapped liquid (Wager and Brown, 1968, p. 64). Hess (1972) argued that such a mechanism of adcumulus growth was unlikely on the basis of heat flow calculations

Table 11. Composition of noncumulate rocks from the Dumont intrusion and overlying sills

	Dumont Sill			Overlying sills			Average	
Sample no.	E21-160	E21-335	E21-570	NIX-6	NIX-14B	NIX-16	$\bar{x}$	σ
SiO_2	52.6	51.7	52.5	50.1	52.0	52.2	51.8	0.9
TiO_2	0.65	0.89	0.92	1.02	1.30	1.17	0.99	0.23
Al_2O_3	12.8	15.0	14.4	14.3	13.4	12.8	13.8	0.9
Cr_2O_3	0.004	0.006	0.004	nd	nd	nd		
Fe_2O_3	0.72	2.18	1.56	5.97	4.35	7.06		
FeO	10.8	12.4	16.2	9.40	12.6	9.51	15.1	2.2
MnO	0.24	0.21	0.25	0.20	0.23	0.25	0.23	0.02
MgO	9.49	7.87	5.40	5.55	5.41	5.69	6.57	1.7
CaO	11.85	10.9	8.30	11.4	8.59	7.21	9.7	1.9
Na_2O	1.13	1.35	1.29	1.96	1.88	3.61	1.87	0.91
K_2O	0.23	0.17	0.10	0.06	0.15	0.47	0.20	0.15
Co	0.0061	0.0056	0.0077	na	na	na	0.0065	-
Cu	0.0026	0.0027	0.0012	na	na	na	0.0022	-
Ni	0.0088	0.0064	0.0055	na	na	na	0.0069	-
V	0.0280	0.0320	0.0295	na	na	na	0.030	-
Zr	0.0042	0.0060	0.0078	na	na	na	0.0060	-

Analyses of overlying sills are from Vogel (1979); nd - not detected; na - not analyzed

Table 12. Bulk composition of the Dumont Sill calculated from average compositions of subzones

	Lower Peridotite	Dunite	Upper Peridotite	Clino-pyroxenite	Gabbro	Quartz Gabbro	Intrusion	Intrusion less phenocrysts*	Plus differentiated liquid**
SiO_2	40.6	40.3	42.1	51.2	51.0	52.2	45.2	45.8	46.4
TiO_2	0.07	0.004	0.04	0.11	0.20	0.40	0.15	0.17	0.25
Al_2O_3	1.50	0.24	1.10	9.02	13.9	14.9	6.23	7.12	7.80
Cr_2O_3	0.99	0.20	0.89	0.42	0.05	0.02	0.46	0.52	0.47
FeO	10.1	7.80	10.2	4.67	7.51	10.3	9.25	9.59	10.1
MnO	0.12	0.12	0.13	0.15	0.18	0.19	0.15	0.16	0.17
MgO	44.8	49.5	47.9	17.2	13.2	8.2	32.2	29.5	27.2
CaO	1.22	0.30	0.60	17.4	13.6	12.2	5.63	6.42	6.8
Na_2O	0.00	0.00	0.00	0.65	1.13	1.31	0.50	0.56	0.69
K_2O	0.00	0.00	0.02	0.02	0.09	0.18	0.06	0.06	0.07
Ni	0.26	0.32	0.24	0.016	0.010	0.0080	0.165	0.141	0.128
V	0.0041	0.001	0.0023	0.012	0.016	0.020	0.0087	0.010	0.012
W.F.	0.236	0.172	0.192	0.029	0.127	0.244	1.000		

Total iron calculated as FeO; W.F. - weight fraction of total intrusion represented by subzone
*Bulk composition less 12.5% olivine (Fo_{93}). **Bulk composition of intrusion less 12.5% olivine plus 10% average noncumulate rock composition (see text).

which showed that the rate of diffusion of mass was much too slow relative to the rate of diffusion of heat and of crystal accumulation. This objection would be particularly relevant in the case of the Lower Peridotite if the model of its formation by the rapid accumulation of intratelluric phenocrysts is correct. Irvine (1980) concurred with Hess' (1972) conclusion and suggested that adcumulus growth occurs at significant depths below the surface of the accumulating pile by a process of infiltration metasomatism whereby compaction of the pile under its own weight causes an upward flow of intercumulus liquid which reacts with cumulus crystals along its path. I believe a similar "auto filter pressing" process was important in the formation of the Lower Peridotite.

During the initial stage of accumulation of intratelluric phenocrysts following intrusion, the magma would have been essentially stagnant and cooling would have been by conductive heat transfer across both the upper and lower contacts. Although some undercooling might have occurred

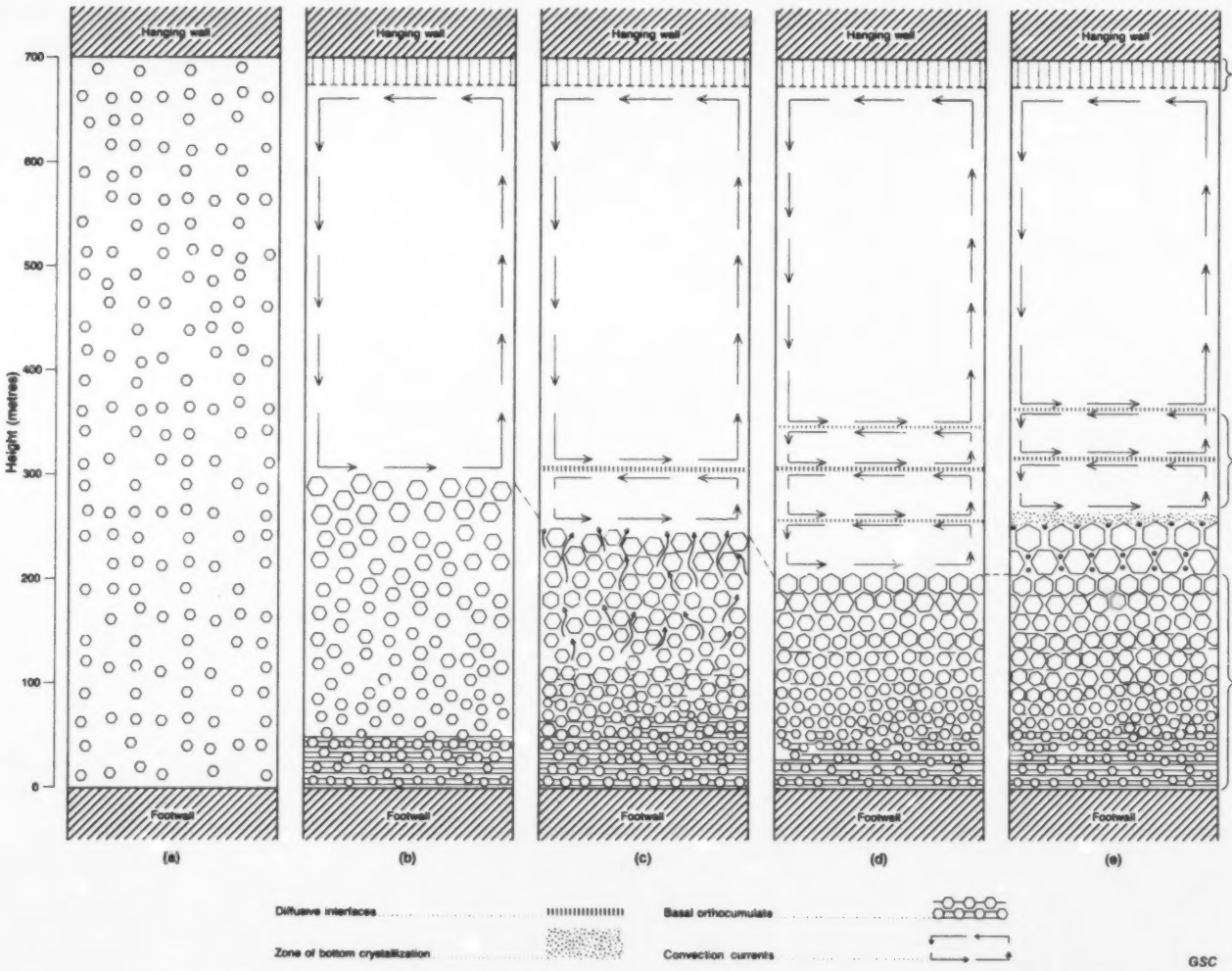

Figure 22. Schematic depiction of the proposed model for the accumulation of the Lower Peridotite and Dunite Subzones. **(a)** Intrusion of a peridotitic komatiite magma carrying 10% olivine and possibly minor chromite in suspension. **(b)** Rapid settling of the intratelluric phenocrysts which accumulate as a crystal mush (50% crystals – 50% liquid) in the lower part of the chamber. The supernatant magma begins to convect and heat loss through the roof of the chamber may have caused crystallization of an upper chilled margin. Heat loss through the floor of the intrusion caused orthocumulate crystallization of the lowermost crystal mush. **(c)** The crystal mush compacts under its own weight, causing the somewhat fractionated pore liquid to percolate upwards towards the main body of primitive magma. The introduction of this pore liquid at the floor of the main chamber leads to a compositional stratification of the magma whereby heat and matter are transferred by convection within liquid layers and by diffusion between layers. **(d)** The mixing of the fractionated pore liquid with primitive magma would depress the liquidus of olivine and the onset of crystallization at the floor of the chamber would be delayed. **(e)** In addition to depressing the liquidus of olivine, the mixing process would raise the solvus of sulphide. The magma cooled and became simultaneously saturated in olivine and sulphide which segregated from the magma at the floor of the chamber in their "cotectic" proportions to form the Dunite Subzone.

Table 13. Average composition of orthocumulate rocks from the basal Lower Peridotite Subzone

	Mean*	σ
SiO_2	41.5	2.0
TiO_2	0.14	0.05
Al_2O_3	2.72	0.91
Cr_2O_3	1.06	0.07
FeO	11.5	1.1
MnO	0.21	0.06
MgO	38.3	3.2
CaO	3.89	2.5
Na_2O	0.23	0.24
Ni	0.22	0.03
Co	0.012	0.003
V	0.0076	0.0023
Zr	0.0009	0.0003
Total	99.8	
Mg/Mg+Fe	0.856	0.016

* Mean and standard deviation of analyses of 10 samples: E5-860, E5-900, E5-960, E5-1000, E8-1160, E9-1165, E9-1215, E9-1255, E9-1275, E9-1285 (Appendix 2).

at the margins, the main body of the crystal-liquid suspension would have been at the liquidus temperature. As a crystal mush built up on the floor of the magma chamber, a thermal gradient would have been established across the partially consolidated pile (for example, see Irvine, 1970a, Fig. 17). Cooling would promote crystallization of the trapped pore liquid, and reaction with the liquid would cause the cumulus olivine to become less forsteritic. The degree of reaction would reflect the temperature gradient, and so at any point in time the forsterite content of olivine would be expected to decrease with depth in the pile. Of course, if this process were to go to completion, a perfect orthocumulate rock would be produced. However, the pile would probably undergo compaction both during and after accumulation, and the resultant upward filter pressing of the residual pore liquid would prevent complete orthocumulus growth. Reaction with the migrating liquid would tend to reduce the forsterite content of the cumulus olivine but the effect would be slight within the Lower Peridotite. The marked increase of grain size upwards across the Lower Peridotite may reflect a greater degree of compaction at depth in the pile. Alternatively, it could have arisen in part from crystal growth during settling, inasmuch as the crystals at the top of the pile would have settled the greatest distance if the initial distribution of phenocrysts in the suspension was uniform. If the initial porosities of the meso-and adcumulates were similar to that inferred for the basal orthocumulate rocks (i.e., about 50% pore liquid by weight), then crystallization of about 68% of the intercumulus liquid is indicated to yield the average final olivine composition (Fo_{89}). This amount of crystallization would increase the concentration of incompatible elements in the residual pore liquid by a factor of 3.2 and the estimates of the final amount of trapped liquid given above should be reduced accordingly. Therefore, I am proposing that the rock ultimately contained about 4% residual liquid and that an amount of liquid equivalent to 12% of the initial crystal mush was expelled from the pile. This would mean that the intratelluric olivine phenocrysts made up about 12.5% of the magma at the time of intrusion.

The contact between the Lower Peridotite and Dunite subzones has been defined by the disappearance of chromite as a cumulus phase, but it is also marked by a sharp increase in the grain size of olivine and a decrease in the proportion of intercumulus material (Fig. 5). This contact very probably reflects a change in the thermal regime of the intrusion and a different mechanism of accumulation of olivine. Once accumulation of the intratelluric phenocrysts had progressed to a certain point, the essentially crystal-free supernatant liquid would have begun to convect, thereby establishing an adiabatic temperature gradient across the magma (Fig. 22b). An important property of convecting magmas is that the liquidus temperature gradient is expected to be greater than the adiabatic gradient, and crystallization is therefore likely to occur in a stable, nonconvecting layer adjacent to the floor of the magma chamber rather than at the upper contact where the maximum heat loss takes place. Lucid explanations of this phenomenon have been offered by Jackson (1961, p. 93-99) and Irvine (1970a, p. 1034-1036). Alternatively, bottom crystallization might have resulted from a compositionally controlled liquidus temperature gradient as described by Irvine (1980). This would have required a compositional gradient in the magma which could have resulted from an influx of primitive magma at the floor of the chamber, from melting of roof rocks, or from fractional crystallization at the roof of the chamber.

The Dunite Subzone is an extreme olivine adcumulate with only a fraction of a per cent intercumulus material in all but a few samples. It is unlikely that rocks with virtually no residual porosity (e.g., Fig. 6c) could have developed by the infiltration mechanism adopted for the Lower Peridotite. Indeed, Irvine (1980, p. 371) notes that there is probably a lower limit of a few per cent below which compaction cannot reduce the amount of intercumulus liquid. Therefore, I believe that the Dunite Subzone accumulated by in situ crystallization at the floor of the magma chamber. As noted above, the development of such an adcumulate texture at or near the top of the crystal pile implies a relatively slow rate of crystal accumulation.

The upward displacement of the abrupt increase in the forsterite content of olivine from the base of the Dunite Subzone is an important clue to the mechanism of cumulate formation and to the origin of the magmatic sulphide layers in the Dunite. The displacement is similar to the "uncoupling" of phase layering and cryptic variation resulting from the infiltration metasomatism process modelled by Irvine (1980). Irvine predicted that reaction between cumulus crystals at the base of one layer and fractionated liquid percolating upward from the underlying layers would cause an upward displacement of the discontinuity in cryptic variation.

The observation that the amount of upward displacement of the abrupt increase of forsterite content reflects the thickness of meso- and adcumulate rocks in the underlying Lower Peridotite supports the notion that the displacement is related to such a filter-pressing mechanism. At the eastern end of the intrusion, where the Lower Peridotite is thin and is an orthocumulate through its entire thickness, the increase in forsterite content corresponds to the base of the Dunite Subzone (Fig. 11, DDH E5). In the thick central part of the sill, the displacement is about one-third the thickness of the Dunite (Fig. 11, DDH E16 & DDH E21), whereas at the western end, where the Lower Peridotite is of intermediate thickness, there is a small upward displacement (Fig. 11, DDH W13).

It is significant that the magmatic sulphide mineralization occurs in that part of the Dunite Subzone where the evidence suggests the greatest amount of filter-pressing of the underlying Lower Peridotite. Irvine (1980) proposed that

infiltration metasomatism led to the formation of magmatic sulphides in the Muskox Intrusion. Specifically, he suggested that intercumulus liquid became sulphide-saturated as it migrated upward and "precipitated" a relatively large proportion of sulphide as it crossed the compositional discontinuity marking the boundary between two layers. A striking feature of the olivine compositions plotted in Figure 20 is the decrease in the nickel content upward across the sulphide layers with a much smaller corresponding change in forsterite content. This type of depletion in nickel was predicted by the calculations of Duke and Naldrett (1978) for the fractionation of olivine and molten sulphide from a sulphide-saturated peridotitic komatiite magma. This observation, together with the conclusion reached below that olivine and sulphide are present in their "cotectic" proportions, is compelling evidence for the simultaneous accumulation of sulphide and olivine. Therefore, I am proposing a model that differs from that of Irvine (1980) in one fundamental respect. Rather than the discontinuity in cryptic variation and occurrence of magmatic sulphides reflecting reaction of migrating pore liquid with cumulus crystals, I believe that these features result from the mixing of this liquid with more primitive liquid at the floor of the magma chamber.

Compaction of the crystal mush that formed the Lower Peridotite would have expelled fractionated liquid from the top of the pile which, upon mixing with the overlying primitive magma, would have resulted in compositional gradients in the magma perpendicular to the floor of the magma chamber. The diffusivity of heat is greater than that of matter in magmas, and such mixing would probably have led to stratification of the magma whereby composition and temperature changed in a stepwise rather than in a continuous fashion, with heat and mass transfer occurring by convection within the layers and by diffusion between the layers (Fig. 22c, d). This phenomenon has been discussed in a number of recent papers including those by Turner and Gustafson (1978), McBirney and Noyes (1979), Irvine (1980), and Rice (1981). Addition of fractionated liquid to the primitive magma would have lowered the olivine liquidus temperature (Fig. 23b), prolonging the pause in olivine accumulation, and would have produced a stepwise trend of

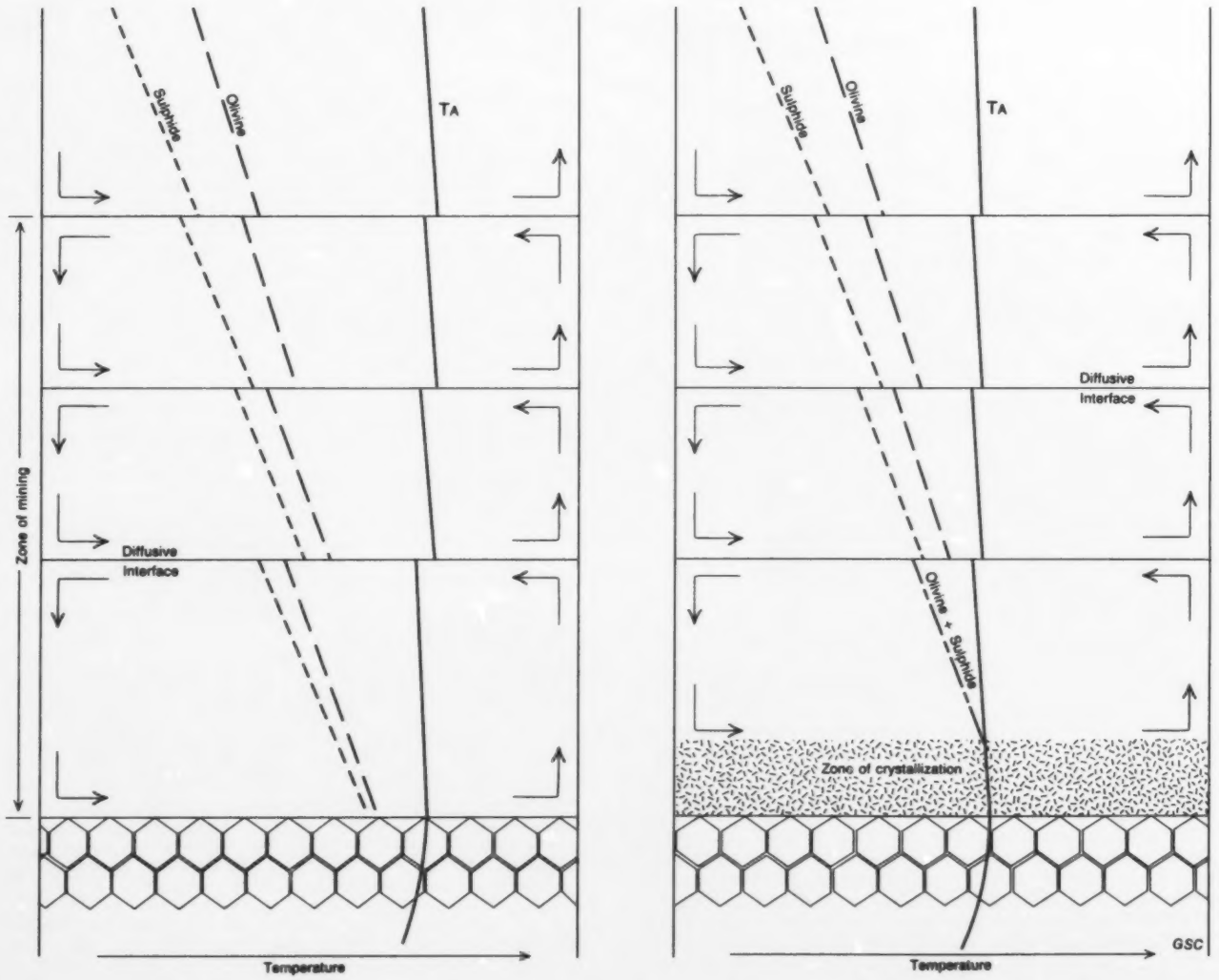

Figure 23. Possible thermal regimes in the zone of mixing at the onset of the accumulation of the Dunite Subzone. The left and right diagrams correspond to stages (d) and (e) in Figure 22.

increasing Mg/Mg+Fe ratio in the magma upward from the floor of the chamber. The evolution of the filter-pressed liquid to more fractionated composition with time, coupled with the slow rate of mass transfer, would mean that the compositional gradient would be greatest near the floor. Accumulation of the Dunite Subzone would have commenced with the onset of crystallization in a thin zone at the floor of the chamber (Fig. 22e, 23), and the gradient in magma composition would have promoted a "reverse" cryptic trend in olivine composition. A characteristic of stratified convecting systems is a sudden mixing of adjacent layers, or "rollover", for any one of a number of reasons (Rice, 1981). Extraction of a dense component and release of latent heat attending the crystallization of olivine at the floor would have decreased the density of the lowermost liquid layer and could have promoted rollover due to gravitational instability. The abrupt increase in the forsterite content of olivine may well reflect such a rollover in the stratified liquid.

Infusion of fractionated liquid from the underlying cumulates would have had the effect of bringing the magma closer to sulphide saturation since the fractionated liquid is expected to have had a lower sulphide solubility and a higher sulphur content than the primitive magma. The possibility that magma mixing might induce sulphide saturation was discussed by Irvine (1977). Magmatic sulphides occur erratically in the Lower Peridotite Subzone, but their generally very fine grain size and low abundance indicates that they formed after accumulation when crystallization of the trapped pore liquid had raised the sulphur concentration in the residual liquid to the saturation point. These observations suggest that the magma was somewhat undersaturated in sulphide at the time of emplacement but that sufficient filter pressing occurred in the thick, central part of the intrusion to cause the blended magma to be sulphide-saturated when the Dunite Subzone began to accumulate. That the magma was mutually saturated with olivine and sulphide is indicated not only by the marked decrease in the nickel content upward across the sulphide-rich layers, as described above, but also by the relative proportions of olivine and sulphide present in the rocks.

The relative proportion of sulphide that separates from a crystallizing magma is related to the sulphide solubility and the rate of change of solubility as crystallization proceeds. If the solubility (S) is essentially constant, the olivine/sulphide ratio is given by

$$R = \frac{(1-S)}{S}$$

The average modal proportion of magmatic sulphide in the Dunite in the drill intersection depicted in Figure 20 is 1.3 volume per cent (Table 8), which suggests that the olivine and sulphide exsolved from the magma in a 60:1 ratio by weight. This in turn would indicate that the maximum sulphide solubility was about 1.6 weight per cent (= 0.64 weight per cent sulphur). Shima and Naldrett (1975) reported that the experimentally determined solubility in a peridotitic komatiite containing 23 weight per cent MgO was between 0.33 and 0.47 weight per cent sulphur at 1450°C and $10^{-9 \cdot 2}$ bars oxygen pressure. The proposed parent magma for the Dumont Sill is significantly more magnesian than the experimental liquid and would have a liquidus temperature of about 1550°C. Therefore, the sulphide solubility inferred for the Dumont magma from the modal proportion of sulphide is in qualitative agreement with the limited experimental data. It seems reasonable to conclude that the mineralized Dunite represents accumulation of olivine and sulphide in the proportions required by a liquid fractionation path that followed the intersection of the olivine liquidus and the sulphide-silicate liquid solvus in a peridotitic komatiite system.

Although olivine crystallization and sulphide liquation are believed to have occurred in a very narrow zone at the floor of the magma chamber, it is interesting that the two phases appear to be close to hydraulic equivalence. The average grain sizes of olivine and sulphide in the Dunite are 1.7 and 0.48 mm respectively. Taking the density of molten sulphide to be 4.0 gm/cm^3 (Barrett et al., 1977) and the other parameters as above, the Stokes' Law settling velocities are 6.5×10^{-2}cm/s for olivine and 1.9×10^{-2} cm/s for sulphide. Unlike the olivine crystals, the sulphide droplets were probably very nearly spherical initially and therefore the actual settling velocities of the phases could have been quite similar.

The degree of nickel depletion in olivine across the middle sulphide-rich layer evident in Figure 20 suggests that the olivine and sulphide fractionated from a volume of magma much smaller than the total available. For example, from the calculations of Duke and Naldrett (1978) and those outlined below, the amount of depletion observed would require fractionation of a mass of olivine and sulphide equivalent to about one-quarter that of the magma. An implication of this observation is that the nickel-depletion cycle represents fractionation within a layer of magma which was about four times the thickness of the cycle and which did not exchange constituents rapidly with the overlying layer. Thus the occurrence of three nickel-enriched layers in the central part of the intrusion may indicate three successive rollover events.

The base of the Upper Peridotite Subzone is marked by the appearance of cumulus chromite. The relative proportions of olivine and chromite in the Upper Peridotite Subzone are in agreement with those produced by cotectic crystallization in the MgO-Cr_2O_3-SiO_2 system, and the decrease in the relative proportion of chromite upwards may reflect a curved olivine-chromite cotectic as suggested by Irvine (1975). Although the Upper Peridotite is coarser grained than the Lower Peridotite, the ratios between the sizes of olivine and chromite are similar, indicating that the two minerals are not hydraulically equivalent in either unit. In the case of the Lower Peridotite, it was suggested that the chromite settling velocities were increased due to aggregation or chain formation. An alternative explanation is available in the case of the Upper Peridotite inasmuch as crystallization occurred at or near the rising floor of the magma chamber and relative settling velocities were not important.

The transition between the Upper Peridotite and Clinopyroxenite subzones would appear to mark a reaction relationship of the type

olivine + chromite + liquid = clinopyroxene + liquid

This precise reaction relationship has not been demonstrated experimentally and the data for related systems are ambiguous. Schairer and Yoder (1962) found that part of the clinopyroxene-olivine boundary curve in the system forsterite-diopside-silica was a reaction (forsterite + liquid = diopside). Kushiro and Schairer (1963) tended to discount this reaction but observed that clinopyroxene and orthopyroxene could be produced simultaneously by reaction of forsterite with the liquid. Kushiro (1969) reported that this latter reaction occurs only at pressures less than about 6 to 7 kilobars. Dickey et al. (1971) found that chrome diopside melts incongruently in the system CaO-MgO-Cr_2O_3-Al_2O_3-SiO_2 at 1 bar but not at 10 kilobars. Irvine (1970b) observed that reaction of olivine with liquid to form clinopyroxene seems to have occurred in certain ultramafic bodies in the Abitibi belt described by Naldrett and Mason (1968) and MacRae (1969).

It is argued below that the top of the Upper Peridotite represents the point at which approximately 42% of the original body of magma had crystallized, and therefore the concentrations of incompatible elements would have been 1.7 times those in the parent magma. Three analyzed samples from the uppermost Upper Peridotite average 3.0% CaO, 3.4% Al_2O_3, 0.15% TiO_2, 0.0063% V, and 0.0008% Zr. Dividing these by 1.7 times their concentrations in the model parent liquid (Table 10) gives consistent estimates of the amount of intercumulus liquid trapped in the rock of from 23 to 30%. This relatively high proportion may reflect a lack of compaction of the pile owing to a hiatus in crystallization because of the reaction relationship described above, and also the fact that clinopyroxene is close to the liquidus.

The discontinuity in the variation of the Mg/Mg+Fe ratio at the Upper Peridotite-Clinopyroxenite contact probably reflects the fact that the distribution coefficient $K_{D(Mg-Fe)}^{Cpx/L}$ is lower than the corresponding coefficient for olivine, that is, about 0.23 as compared with 0.30 (Grove, 1978; Roeder and Emslie, 1970), and therefore clinopyroxene is more magnesian than olivine that crystallizes from a given liquid. The lowermost Clinopyroxenite Subzone is virtually monomineralic but it is apparent that clinopyroxene (possibly accompanied by orthopyroxene) was not alone on the liquidus for very long before being joined by plagioclase. The cryptic variation of Mg/Mg+Fe and TiO_2 in the cumulate rocks upwards through the Gabbro Subzone and into the Quartz Gabbro Subzone form continuous trends (Fig. 5) that presumably reflect relatively simple fractional crystallization. The noncumulate rocks are more differentiated than the cumulates, but little is known about their field relationships. For example, the noncumulates may occur as dykes or may represent pockets of late liquid. The noncumulate material that occurs at the base of the Quartz Gabbro is instructive in this respect. The Mg/Mg+Fe ratio in this rock is 0.35 whereas that in the underlying cumulate is 0.71. If the ratio in the cumulate rock is essentially equivalent to that in the contained clinopyroxene and that in the noncumulate represents a liquid, then a distribution coefficient of 0.22 is indicated. This is close to experimentally determined values of $K_{D(Mg-Fe)}^{Cpx/L}$ (Grove, 1978; Duke, 1976) and therefore it is possible that the noncumulate rock at the base of the Quartz Gabbro represents the liquid from which the cumulates at the top of the Gabbro Subzone crystallized. This "liquid" composition was compared in Table 11 to those of gabbroic sills overlying the Dumont intrusion, and it was argued that a mobile magma of this extremely differentiated composition was produced by fractional crystallization. Applying similar logic, it might be concluded that the cumulate rocks of the Quartz Gabbro imply the existence of an even more evolved liquid. However, the cumulates of the Quartz Gabbro tend to contain a greater proportion of intercumulus material than those of the Gabbro Subzone and, inasmuch as the compositions plotted in Figure 5 are whole-rock values which represent the average of cumulus and intercumulus material, the degree of differentiation in the Quartz Gabbro may be somewhat exaggerated.

It is unfortunate that the top of the Dumont Sill has not been observed. I believe that I have demonstrated that liquids containing as little as 5.5% MgO have been derived from a peridotitic parent magma having at least 27.5% MgO by a relatively simple fractional crystallization process. However, the final stages of this differentiation process remain obscure due to a lack of exposure and limited sampling.

Computer simulation of the differentiation of the intrusion

Certain aspects of the differentiation process outlined above may be tested and augmented with the aid of the computer model of fractional crystallization developed by Duke and Naldrett (1978) and Duke (1979). Given a specified initial magma composition and the relative proportions of olivine, clinopyroxene, orthopyroxene, plagioclase and sulphide removed from the magma, the program calculates the compositions of the residual liquid and the subtracted phases as a function of the amount of fractional crystallization. It has been proposed that the Lower Peridotite formed by the accumulation of intratelluric phenocrysts and I have therefore attempted to model the differentiation of the intrusion upward from the base of the Dunite Subzone. The shortcomings of the computer model in this context are that it does not simulate the fractional crystallization of chromite and that no allowance is made for the trapping or migration of intercumulus liquid. However, I do not believe that these limitations substantially affect the results discussed below. The initial magma composition used was that of the model peridotitic komatiite parent liquid in Table 10, and the differentiation was simulated in the following stages corresponding to the subdivisions of the sill:

1. Dunite Subzone: olivine and sulphide were removed from the liquid in a 60:1 ratio until an amount equivalent to 20% of the initial mass of the magma had been removed.
2. Upper Peridotite Subzone: olivine alone was removed from the liquid until 42% of the initial mass of the magma had been removed.
3. Clinopyroxenite Subzone: clinopyroxene and orthopyroxene were removed from the remaining liquid in a 2:1 ratio until the cumulative amount removed was equivalent to 45% of the initial mass of the magma.
4. Gabbro Subzone: clinopyroxene, orthopyroxene and plagioclase were removed from the remaining liquid in a 4:4:2 ratio; these proportions were established after some experimentation with the model and are consistent with the normative composition of the Gabbro once adjustments are made for the estimated amount of trapped intercumulus liquid.

The computer model appears to provide a reasonable simulation of the differentiation of the Dumont Sill. However, it is emphasized that these calculations do not prove that the process of differentiation which I have suggested did in fact occur, but simply that it is a viable explanation. Moreover, the computations deal with the composition, proportions and sequence in which phases are removed from the magma, but the actual physical process by which removal occurs is not stipulated.

The calculations indicate that the MgO content of the liquid decreased from 27.5% at the onset of crystallization to 22.2% at the top of the Dunite Subzone and to 12.3% at the top of the Upper Peridotite Subzone; that is, the points where chromite and clinopyroxene, respectively, became liquidus phases (Table 14). Arndt (1976) found in melting studies of a peridotitic komatiite having a bulk MgO content of 25.1% that these minerals appeared on the liquidus when the MgO content of the liquid had decreased to about 15% and 9%, respectively, at 1 atmosphere pressure. The late appearance of chromite in Arndt's experiments is probably attributable to the relatively low partial pressure of oxygen in his runs (i.e., within the stability field of wustite). Arndt noted that variation diagrams of natural spinifex-textured rocks indicate that the fractional crystallization of clinopyroxene becomes apparent when the MgO content of the liquid had decreased to about 14%, which is significantly

more magnesian than the level he observed in his experiments, and he suggested that the rock used as a starting material in his experiments had been depleted in calcium during alteration. The MgO content of the magma upon the cumulus appearance of clinopyroxene suggested by the computer model is thus intermediate to the extremes indicated by Arndt's field and experimental data. I believe that the differences in the timing of the cumulus appearance of clinopyroxene could also reflect the influence of total pressure, inasmuch as the liquidus of pyroxene increases more rapidly with increasing pressure than that of olivine. Thus the differentiation trends typical of basaltic komatiite suites would represent fractional crystallization in magma chambers at deeper levels than the Dumont body, whereas the 1 atmosphere experiments were at rather lower pressures than would have prevailed in the Dumont magma.

According to the computer model, fractional segregation of an amount of material equivalent to 42% of the initial mass of the liquid would reduce the forsterite content of the precipitating olivine to 84.6%, corresponding to its composition at the top of the Ultramafic Zone. The calculated composition of the liquid remaining after 72% fractionation of the initial mass of the melt (Table 14) matches the composition of the most evolved noncumulate rocks (Table 11) reasonably well. The calculation of the bulk composition of the intrusion suggested that the sequence from the base of the Dunite to the top of the Gabbro Subzone should account for 60% of the mass of the magma implying that these most evolved liquids, including the overlying sills, were generated during accumulation of the Quartz Gabbro Subzone. The calculated composition of the liquid remaining after 60% fractionation is similar to that of two of the noncumulate rocks from the Quartz Gabbro (Table 11).

The Al_2O_3 vs. FeO/FeO+MgO variation diagram has been widely used since Arndt et al. (1977) demonstrated that the komatiitic and iron-rich tholeiitic rocks from Munro Township, Ontario defined distinctive fields on the diagram. Unfortunately, some other workers have used this diagram as a universal discriminator of komatiitic rocks, a purpose for which it was never intended. The model trend and analyses of the Dumont rocks have been plotted in this diagram in Figure 24. The model liquid trend parallels the line dividing the tholeiite and komatiite fields for much of its length and thus mimics the trend defined by spinifex-textured rocks from many localities. However, as a consequence of plagioclase separation, the liquid trend bends and crosses into the tholeiite field at a point where its MgO content has been reduced to about 9%. The noncumulate rocks from the Dumont Sill as well as the overlying sills plot very close to the model liquid trend. These noncumulate rocks contain slightly less Al_2O_3 for a given FeO/FeO+MgO ratio than most "typical" basaltic komatiite lavas that have been described and the extreme iron enrichment observed in the Dumont rocks contrasts with most basaltic komatiites.

The olivine cumulates from the Ultramafic Zone plot in the appropriate part of the diagram; that is, on lines joining points on the liquid trend to the olivine compositions which fall on the abscissa. It is interesting to note that because olivine containing less than about 91 mole per cent forsterite plots in the tholeiite field of the Al_2O_3 vs. FeO/FeO+MgO diagram, extreme olivine adcumulates that crystallized from a komatiitic magma may also plot as tholeiites, depending upon the relative amount of retained intercumulus liquid. The samples from the Gabbro Subzone define a large field in the diagram indicative of variable proportions of cumulus pyroxene and plagioclase and intercumulus liquid.

Table 14. Compositions of silicate liquid, olivine and sulphide calculated using computer model

	Silicate liquid				
F	1	20	42	60	72
SiO_2	47.7	49.3	52.6	52.7	53.1
TiO_2	0.32	0.40	0.56	0.75	0.98
Al_2O_3	6.58	8.10	11.2	13.0	14.8
FeO	11.2	11.76	12.0	14.4	16.3
MnO	0.18	0.19	0.20	0.23	0.25
MgO	27.4	22.2	12.3	8.83	5.64
CaO	6.07	7.41	10.1	8.87	7.26
Na_2O	0.15	0.19	0.26	0.38	0.53
Zr	0.0020	0.0025	0.0034	0.0051	0.0071
V	0.0126	0.0156	0.0218	0.0274	0.0340
Ni	0.1365	0.0631	0.0177	0.0150	0.0097
Co	0.0109	0.0082	0.0060	0.0064	0.0634
Cu	0.0049	0.0031	0.0043	0.0062	0.0088

	Sulphide			Olivine		
F	1	20		1	20	42
Fe	44.2	50.6	SiO_2	41.3	41.0	39.8
Ni	15.2	8.6	FeO	6.88	8.68	14.5
Co	0.62	0.49	MnO	0.12	0.19	0.2
Cu	0.99	0.65	MgO	51.1	49.6	44.9
S	38.9	39.7	CaO	0.24	0.30	0.4
			Ni	0.33	0.20	0.13
			Fo (mole %)	93.0	91.1	84.6

F = Per cent of initial mass of magma fractionally segregated.

The Quartz Gabbro analyses are more tightly clustered and fall closer to the liquid trend, supporting the conclusion that a greater proportion of intercumulus liquid has been retained.

The noncumulate rocks of the Quartz Gabbro and the overlying sills are compositionally similar in many respects to the iron-rich tholeiite host rocks of the intrusion and would indeed plot in overlapping fields on the Al_2O_3 vs. FeO/MgO+FeO variation diagram. However, there are subtle but significant differences in chemistry which demonstrate to my satisfaction that the two groups of rocks are not comagmatic. In particular, the tholeiite lavas have distinctly higher concentrations of TiO_2, Zr and V for a given MgO content than the Dumont rocks. Variation diagrams involving these three components are quite instructive (Fig. 25, 26). Zirconium may be regarded as an incompatible element throughout the crystallization of the Dumont magma and therefore is a useful index of the degree of fractional crystallization required to yield a given liquid composition, provided that an accurate estimate of its concentration in the parent liquid can be made. Titanium and vanadium are incompatible with respect to olivine crystallization and, although they are incorporated to a certain extent in the pyroxenes, they are nevertheless concentrated in the residual liquid (Duke, 1976). Moreover, since they are accepted to different degrees by the pyroxenes, pyroxene fractionation will produce a different slope than olivine fractionation on a TiO_2 vs. V variation diagram.

There is reasonable agreement between the model trend and the measured concentrations of Ti and Zr in the Dumont rocks (Fig. 25). The olivine cumulates from the Ultramafic Zone plot as expected between the origin and the liquid trend; the scatter in the data largely reflect the uncertainty in the analysis of Zr at such low levels. The rocks with cumulus pyroxene would be expected to plot slightly to the TiO_2-rich side of the olivine cumulate trend owing to the small amount of Ti taken up by the pyroxenes, and most of the samples of the Clinopyroxenite and Gabbro subzones conform to this prediction. The Quartz Gabbro samples appear to be somewhat depleted in TiO_2.

The Ti and V concentrations of the rocks also agree well with those predicted by the computer program (Fig. 26). The olivine ± chromite cumulates are depleted in these elements but have similar Ti/V ratios as the postulated parent magma. Some of these cumulates have lower Ti/V ratios than the modal liquid which may reflect preferential partitioning of V into cumulus chromite or may merely result from analytical error at low concentrations. Rocks from the Clinopyroxenite and Gabbro subzones plot along lines joining the clinopyroxene trend to plagioclase (i.e., the origin). The cumulates from the Quartz Gabbro plot in a field limited by lines joining points on the model clinopyroxene and liquid trends with plagioclase, and these results support my contention that the Quartz Gabbro cumulates contain a large proportion of retained pore liquid. The noncumulate rocks from the Quartz Gabbro plot close to the model liquid trend. It is significant that none of the rocks have Ti/V ratios in excess of 20, a feature which distinguishes them from most tholeiitic rocks.

The variation of nickel content in the intrusion is of particular interest since it is sensitive to the amount and nature of sulphide segregation. This is illustrated by the calculated variation of olivine composition for the fractional crystallization of olivine alone as compared to the removal of both olivine and sulphide in Figure 27. Although the analytical data for the Dumont olivines are scattered with respect to the Dumont model trend, the majority of olivines are unquestionably significantly depleted in nickel in comparison with the olivine fractionation trend. Much of the scatter in the compositions of the olivines from the Dunite Subzone may reflect the uneveness of sulphide distribution in the unit described above. Separation of a greater proportion of sulphide at any point would lead to greater nickel depletion in the coprecipitating olivine. Moreover, nickel is expected to be redistributed during subsolidus cooling, partitioning preferentially into the sulphide fraction: hence the samples with the greatest proportion of sulphide would exhibit the most additional depletion of nickel in the olivine. With a few exceptions, the olivines from the Upper Peridotite

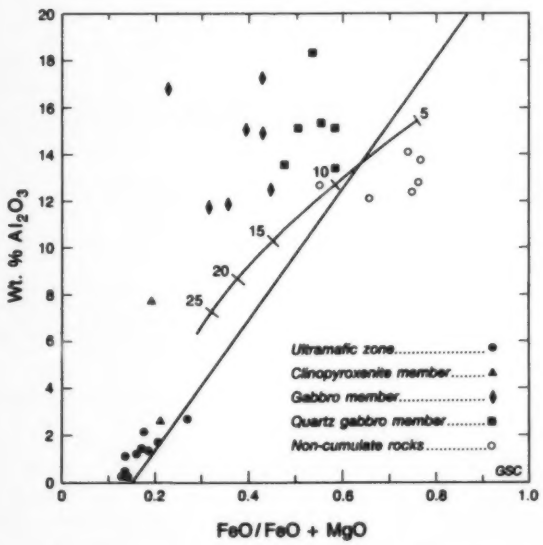

Figure 24. Variation of Al_2O_3 and FeO/FeO+MgO in the Dumont rocks (FeO is total iron expressed as FeO). The solid line separates the upper komatiite field from the lower iron-rich tholeiite field of Arndt et al. (1977). The hatched line is the calculated liquid differentiation trend with the liquid's MgO content marked at points along the trend.

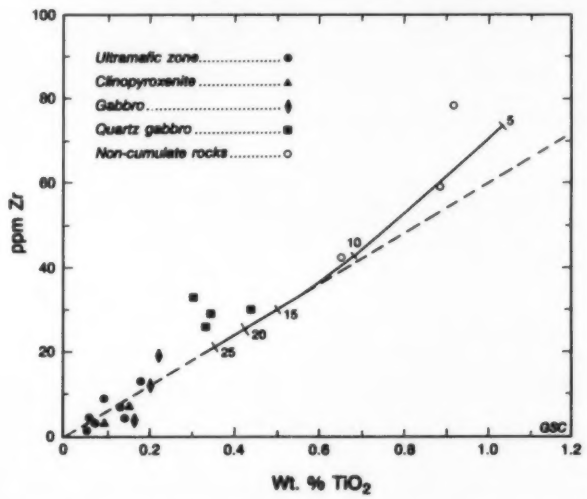

Figure 25. Variation of Zr and TiO_2 in the Dumont rocks. The dashed line indicates the chondritic ratio. The solid line is the calculated liquid differentiation trend with the MgO content of the liquid marked at points along the trend.

have similar compositions to the model trend. The compositions of the rocks from the Lower Peridotite Subzone are thought to have been modified by reaction with migrating intercumulus liquid and therefore their olivines are not necessarily expected to match the model trend. It is significant that the fractionation of sulphide during the earliest stages of fractional crystallization of the magma is manifested in the depleted nickel concentrations in subsequent rocks in the intrusion, even in the most evolved samples.

Nature of the alteration processes

The textures and mineral assemblages of the rocks of the Ultramafic Zone are for the most part typical of what Wicks and Whittaker (1977) termed Type 3 serpentinization; that is, the process took place in a regime of falling or constant temperature without significant shearing or the nucleation of antigorite. It is likely that the main episode of serpentinization took place during or immediately following cooling of the intrusion after its crystallization from the magma. I have argued that the sill was emplaced into submarine lavas at a relatively high level in the crust, and the elevated concentrations of chlorine and boron (up to 0.5 and 0.01%, respectively) may indicate that seawater, either connate or circulating, was the serpentinizing fluid. The retrograde serpentinization of iron-bearing olivine may be represented by the reaction

$$10(Mg_{1.86}Fe_{0.14})SiO_4 + 14.2H_2O = 5Mg_3Si_2O_5(OH)_4 + 3.8(Mg_{0.95}Fe_{0.05})(OH)_2 + 0.4Fe_3O_4 + 0.4H_2$$

which was reversed by Moody (1976) at temperatures in the range of 330 to 360°C at pressures of 0.5 to 2.0 kilobars. This defines the maximum temperature at which the retrograde serpentinization of the Ultramafic Zone is likely to have taken place, inasmuch as such alteration may be expected to proceed by nonequilibrium processes at temperatures well below the minimum stability of olivine (Nesbitt and Bricker, 1978). The inhomogeneity of the nickel contents of secondary minerals within any given sample is indicative of disequilibrium.

Antigorite is virtually restricted to the upper margin of the Ultramafic Zone where it appears to have formed by the recrystallization of lizardite. Although the phase relations among the serpentine minerals are not yet entirely understood, it is widely agreed that antigorite is stable with respect to lizardite and chrysotile at higher temperatures (e.g., Evans, 1977), except possibly where the lizardite is aluminous (Caruso and Chernosky, 1979). It seems reasonable to conclude that the antigorite in the Dumont Sill was a product of incipient regional metamorphism, presumably during the Kenoran Orogeny. The fact that there has not been reaction between the relict chromite grains and their magnetite rims also suggests that the effects of regional metamorphism were limited. Evans and Frost (1975, p. 959) reported that "the stable spinel in antigorite-serpentinites is Al-poor magnetite, Cr-magnetite, or ferrit-chromite, depending on the local Cr/Fe^{3+} ratio in the rock."

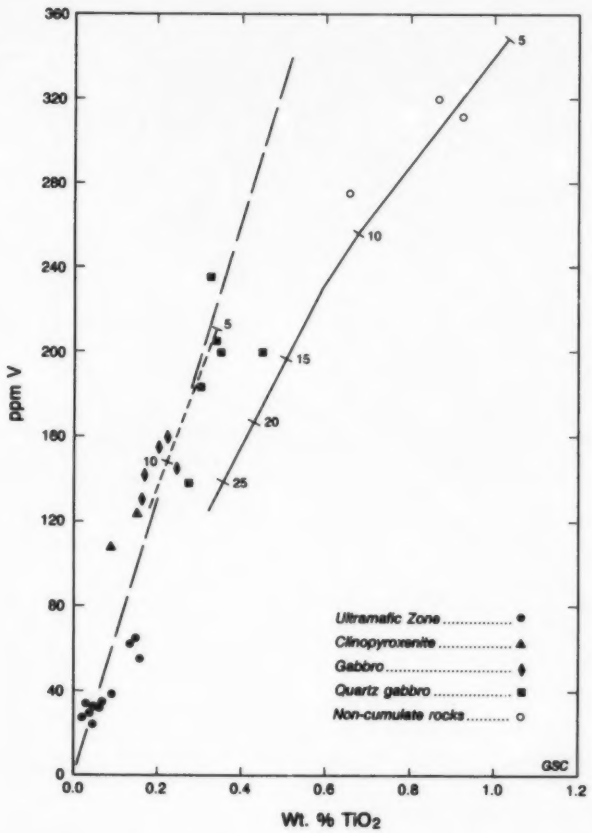

Figure 26. Variation of V and TiO_2 in the Dumont rocks. The long-dashed line is the chondritic ratio. The solid and short-dashed lines are the calculated liquid and clinopyroxene trends respectively, with the MgO content of the liquid marked at points along the trends.

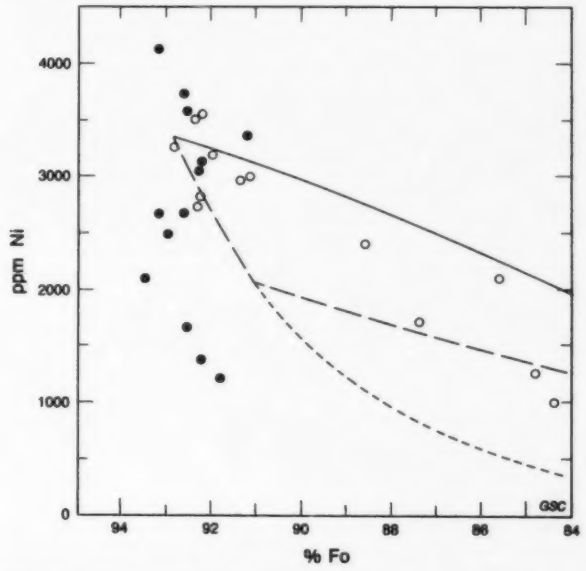

Figure 27. Variation of nickel and forsterite contents of olivines from the Dunite and Upper Peridotite Subzones. The solid and short-dashed lines are the sulphide-undersaturated and sulphide-saturated trends respectively (Duke and Naldrett, 1978). The long-dashed line is the Dumont model trend. Filled circles represent samples containing magmatic sulphides, open circles are sulphide-free samples.

The compositions of the ultramafic rocks are plotted in the CaO-(MgO+FeO)-SiO_2 ternary system in Figure 28. The rocks plot close to the olivine-calcic pyroxene tie line as would be expected if their alteration involved essentially an addition of volatile constituents. The secondary mineral assemblages in serpentinites corresponding to the lower greenschist and subgreenschist facies of metamorphism are also depicted. The most commonly observed assemblage, that is, lizardite+brucite+magnetite+diopside+chlorite ± chrysotile, would be consistent with the lowest grades of metamorphsim.

The alteration of the Mafic Zone rocks is also considered to have occurred during or shortly after the initial cooling of the body, rather than during regional metamorphism. The evidence for this is the pseudomorphic nature of the secondary mineral textures and the fact that albite, an expected phase in low grade regional metamorphic assemblages in such rocks, is absent.

Composition – volume relationships during serpentinization

Serpentinization of the dunitic rocks was accompanied by reduction of their densities by as much as 25% (Fig. 8). This implies that either the volume of the rocks increased or their mass decreased. The problem of conservation of volume as opposed to conservation of mass during serpentinization has been the subject of much discussion in the literature (e.g. Thayer, 1966; Hostetler et al., 1966). The Dumont serpentinites typify the apparent dilemma very well. On the one hand, there is excellent preservation of magmatic textures with, for example, completely serpentinized olivine grains enclosed in pristine oikocrysts of chromite or clinopyroxene, which seems to preclude a substantial volume increase. On the other hand,the fact that ratios among the major elements (Si/Mg+Fe, Mg/Fe, Mg/Ni, etc.) can be shown to be equivalent to those in the unaltered precursor indicates that the only changes in composition involved the addition of volatile components such as water, carbon dioxide, and chlorine.

I believe the rationalization of this problem by Wicks and Whittaker (1977) is applicable in the case of the Dumont body. That is, that the serpentinization proceeds by essentially isovolumetric replacement on a grain-for-grain basis, but that the excess matter may only migrate a very short distance before precipitation in one of the ubiquitous serpentine ± brucite ± magnetite veins. Thus, in practical terms, the process may appear isovolumetric on the scale of a thin section but mass is preserved on the scale of the hand specimen used for chemical analysis.

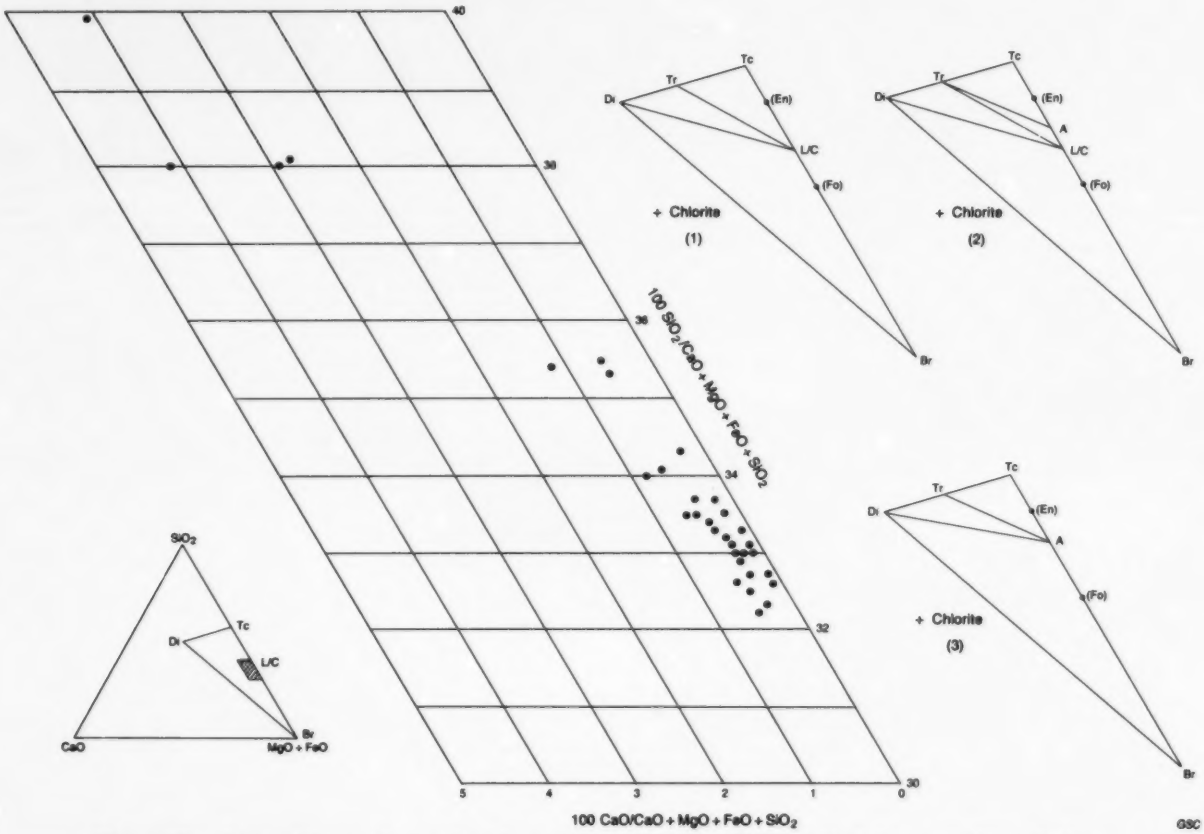

Figure 28. Compositions of samples from the Ultramafic Zone plotted in a portion of the CaO-MgO-SiO_2 system. The sequence of assemblages in this system generated during progressive subgreenschist to lower greenschist metamorphism is represented in parts 1 through 3 (after Evans, 1977). Abbreviations: A – antigorite, Br – brucite, Di – diopside, En – enstatite, Fo – forsterite, L/C – lizardite/chrysotile, Tc – talc, Tr – tremolite.

Gresens (1967) outlined a quantitative approach to the analysis of metasomatic changes which has been incorporated in a series of computer programs by Appleyard (1980). The Gresens equation relating changes in the mass of the individual components and in the volume of the rock is

$$\Delta C_i = M \left[F_v C_i^b \frac{\rho^b}{\rho a} - C_i^a \right]$$

where C_i^a and C_i^b are the concentrations of the subscript component in the initial and final rocks, respectively, ΔC_i is the change in the mass of the subscript component in producing the final rock from the initial rock, F_v is the ratio of the final to the initial volumes, M is the initial mass of the rock, and ρ^a and ρ^b are the initial and final specific gravities. Given the compositions and specific gravities of the initial and final rocks, one arrives at a series of linear equations describing all possible combinations of changes in mass and volume.

Although there are no completely unaltered rocks in the Ultramafic Zone, a calculation may be carried out using a number of the least altered samples as the initial compositions. This has been done with a group of samples from that part of the Dunite Subzone where the initial olivine composition was $Fo_{92.5 \pm 0.5}$. Sample E21-1837, which is about 90% serpentinized, and sample W13-520, which is 99% serpentinized, were each compared to four less altered samples. These included samples E16-1550, E16-1600 and W13-905, which are each about 60% altered and sample W13-1060 which is about 50% altered. Synoptic histograms of the values of F_V where $\Delta C_i = 0$ ("zero change volume factors") are given in Figure 29. In each case there is a distinct peak including the factors for Si, Mg, total Fe, Mn and O, indicating that these elements have been essentially immobile and that their volume factors reflect the actual change in volume during serpentinization. The average volume factor for sample E21-1837 is 1.13, indicating a 13% increase in volume in going from about 57 to 90% alteration. The average factor for sample W13-905 is 1.21, which indicates a 21% volume increase in going from 57% to virtually complete serpentinization. The volume factors for H, Cl, Fe^{3+} fall to the left of the main peak indicating that these elements have been added to the rock during serpentinization, whereas those for Fe^{2+} and Ca fall to the right indicating their removal. Of course the apparent addition of Fe^{3+} and removal of Fe^{2+} is simply an oxidation effect; the total amount of iron in the rock is unchanged. The loss of calcium is not surprising given its well known mobility in a variety of alteration processes. However, it was not apparent from a casual inspection of the analytical data and was only brought to light by means of the Gresens' calculations.

It is interesting that serpentinization resulted in an addition of hydrogen but not oxygen. Thus, although the reaction given above to describe serpentinization is one of hydration, it would appear that the process is actually a hydrogenation reaction. This is consistent with the observation by Barnes and O'Neil (1969) that waters emanating from modern serpentinites have very high pH values (>10). Thus extraction of hydrogen ions from the aqueous serpentinization fluid would enrich it in $(OH)^-$, thereby increasing the pH.

DISCUSSION

Comparison with other layered komatiitic intrusions

Layered intrusions of probable komatiitic affinity have been described from other localities and it is interesting to compare some of these to the Dumont Sill. A number of such bodies occur within the Abitibi greenstone belt. I have already noted that at least four other ultramafic-mafic bodies occur at approximately the same stratigraphic level as the Dumont intrusion in the area to the east of Amos (Weber and Latulippe, 1964) and it is likely that the five intrusions are part of a comagmatic suite. I have examined one of the other bodies, the Landrienne (Amos) sill, and have found the textures and compositions to be very similar to those of the corresponding Dumont rocks. The sequence, which is repeated, possibly by faulting, is peridotite (poikilitic wehrlite) overlain in turn by clinopyroxenite and gabbro. The exposed part of the Landrienne sill is much less magnesian than the most primitive rocks of the Dumont body with Mg/Mg+Fe ratios averaging about 0.84 in the peridotite, and thus resembles the upper part of the Dumont Sill.

Several ultramafic-mafic complexes occur in Ontario to the south and west of Lake Abitibi (Naldrett and Mason, 1968; MacRae, 1969), and Arndt et al. (1977) have pointed out that these include intrusions of both tholeiitic affinity (e.g., Dundonald sill, Centre Hill complex, Munro-Warden sill) and komatiitic affinity (e.g., Munro-Beatty sill, Ghost Range intrusion). Like the Dumont Sill, the layered komatiitic intrusions and thick, differentiated flows are characterized by rather thin clinopyroxenite units overlying the peridotites, whereas the tholeiitic bodies have a greater proportion of clinopyroxene cumulates relative to olivine cumulates (Arndt et al., 1977; Arndt, 1977). The komatiitic Munro-Beatty sill has associated basal nickel sulphide mineralization.

Nisbet et al. (1977) have described a differentiated sill from the base of the Reliance Formation in the circa 2.7 Ga old Bulawayan Group of Zimbabwe. The body has a similar lithological sequence to the Dumont Sill, with a basal dunite overlain in turn by poikilitic wehrlite, a thin clinopyroxenite layer, and quartz gabbro. The sill is smaller than the Dumont intrusion, measuring only about 70 m thick and 5 km in strike length. The Mashaba Ultramafic Suite of Zimbabwe includes numerous intrusions that are considered to be time equivalents of the ultramafic lavas in the Bulawayan Group (Wilson, 1979). The Mashaba igneous complex itself (Wilson, 1968) is a very large, irregular intrusion including both sheeted and dyke portions that outcrop over an area of about 75 by 30 km. It is believed to have been emplaced in at least four distinct pulses of peridotitic magma that differentiated to give dunite, chromitite, poikilitic and lesser granular harzburgite, orthopyroxenite, gabbro and norite. Thus the Mashaba complex may have crystallized from a similar parent magma to that of the Dumont Sill, but it differs considerably in lithology, size and complexity.

The Kaapmuiden bodies in the Barberton Mountainland of South Africa intrude tholeiitic basalts of the Komati Formation (Viljoen and Viljoen, 1970). They comprise a basal peridotite chill zone overlain in turn by a main dunite-peridotite zone, an orthopyroxenite zone, a websterite zone, an anorthositic gabbro zone, and an upper dunite-peridotite zone. Numerous intrusive pods of gabbroic pegmatoid occur, particularly in the latter zone. The Kaapmuiden bodies are sills ranging from 5 to 9 km in length and from 0.8 to 1.5 km in width, and thus are similar in size to the Dumont intrusion. However, like the Mashaba complex, they contrast with the Dumont Sill in the prominence of orthopyroxene. The late-stage gabbroic pegmatoids are an interesting parallel to the coarse grained, noncumulate rocks and pegmatitic schlieren that I have described from the Quartz Gabbro Subzone at Dumont.

Numerous intrusions of komatiitic affinity occur in the Archean Yilgarn Block in Western Australia. Few detailed studies have been published but these bodies are described as typically comprising a central core of dunite within an envelope of peridotite (Naldrett and Turner, 1977). In this respect they are at least superficially similar to the Dumont Ultramafic Zone but differ in that they generally lack

significant amounts of gabbroic differentiates. Rhythmic cryptic layering, which is not observed at Dumont, is well developed in the upper peridotitic part of the Six Mile Well intrusion (Naldrett and Turner, 1977). Several of the Australian bodies contain centrally disposed zones of disseminated magmatic sulphides, a parallel with the Dumont Sill which will be examined in more detail below.

Layered sills of komatiitic affinity also occur in Proterozoic terranes. However, their parent magmas probably contained no more than about 20% MgO and they are thus somewhat less magnesian than their Archean analogues. The prime Canadian examples occur in the Ungava region of Quebec and in the Thompson nickel belt of Manitoba. Francis and Hynes (1979) have described sills from the Chukotat Group in Ungava which display an upward sequence of layering beginning with a melanogabbro basal chilled margin, overlain in turn by pyroxene peridotite, oikocrystic peridotite, an upper pyroxene-rich unit, a main gabbro unit, a heterogeneous gabbro unit, and a dark, fine grained gabbroic to quartz dioritic chilled margin. The sills

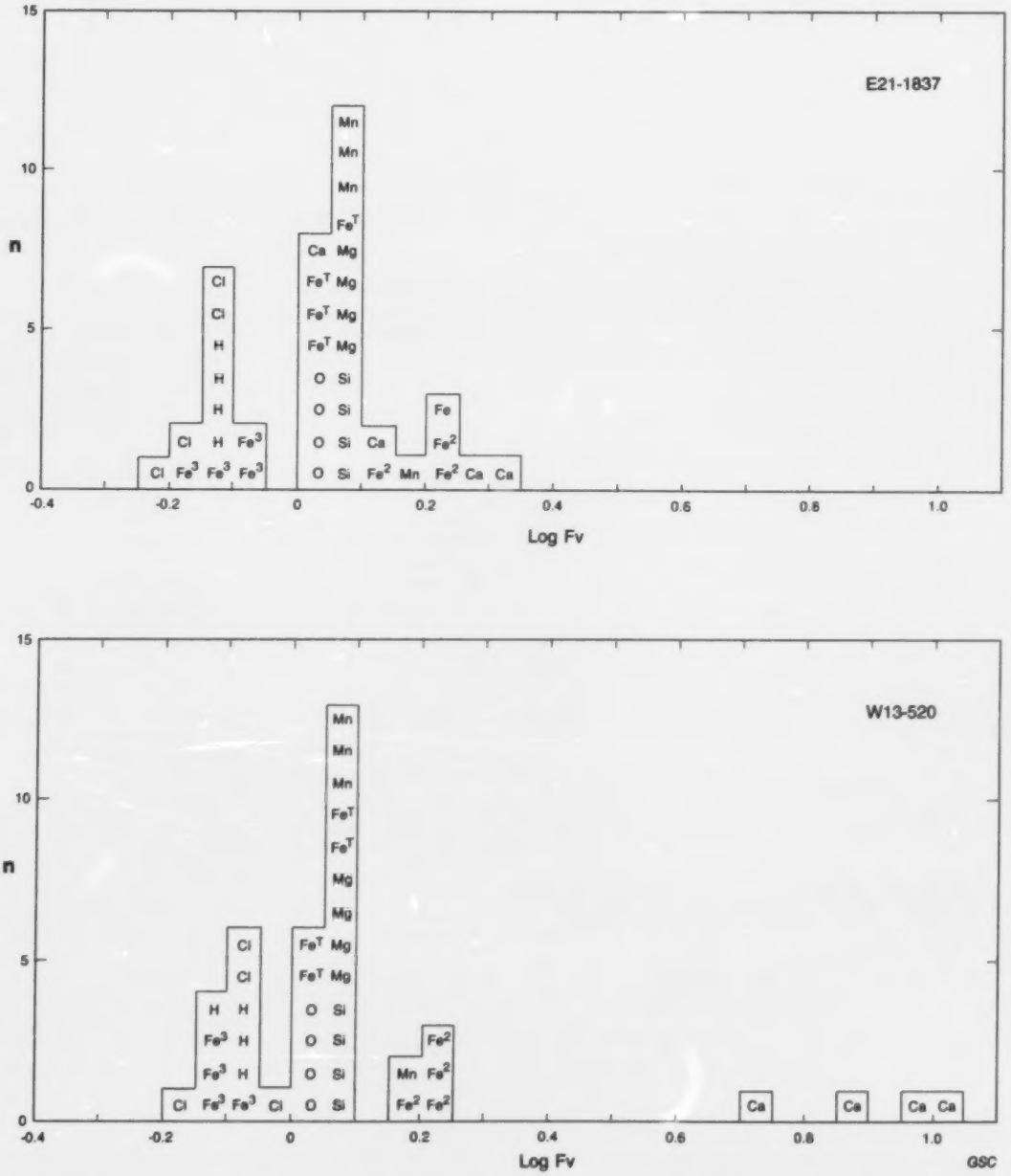

Figure 29. Changes in volume and major element concentrations during serpentinization of dunite as indicated by the Gresens metasomatic equation. Synoptic histograms of zero change volume factors for each of two dunites. Sample E21-1837 is about 90% serpentinized whereas sample W13-520 is about 99% serpentinized. The histograms are derived by comparison of each of these samples to four less altered dunites (i.e., about 60% serpentinized). See text for details.

which host the rich nickel-copper sulphide ores are relatively thin (100 to 200 m) and consist of a dunite or wehrlite core that grades outward through poikilitic wehrlite to clinopyroxenite margins at both the top and bottom of the intrusions (Miller, 1977; Barnes, 1980). These ore-bearing sills do not have gabbroic differentiates and their differentiation has been attributed to segregation of phenocrysts during flow of the magma. The ultramafic bodies in the Thompson belt are for the most part concordant and in some cases have pyroxenite zones at their upper margin (Peredery, 1979). The dominance of orthopyroxene over calcic clinopyroxene in the Thompson bodies is a notable difference from the Ungava sills and also from Dumont. A layered sill of late Precambrian age occurs at Gebel Dahanib in southeastern Egypt (Dixon, 1981). It grades upward from dunite and harzburgite at the base through orthopyroxenite to gabbro and anorthosite.

The predominance of clinopyroxene in some komatiitic intrusions and orthopyroxene in others probably reflects differences in either depth of crystallization or bulk composition. There have been only a few experimental studies of the crystallization of komatiitic liquids, but it would appear that the primary liquidus field of orthopyroxene expands with increasing pressure at the expense of those of olivine and clinopyroxene. For a peridotitic komatiite composition with about 33% MgO, Green et al. (1975) found that the olivine liquidus was between 1680 and 1700°C at 10 kilobars and that olivine crystallized alone down to 1450°C at which point it was joined by orthopyroxene. However, at 2 kilobars pressure, the olivine liquidus was about 1650°C and it was the only liquidus phase until it was joined by clinopyroxene at 1300 ± 40°C. Arndt (1976), using a komatiite with 25.1% MgO, observed that calcic pyroxene crystallized in experiments at 1 bar and 10 kilobars but that pyroxene was calcium-poor at pressures of 15 kilobars and above. Arndt also found that while plagioclase crystallized at 1 bar, it did not occur in runs at 10 kilobars or above.

An interesting characteristic of most of the komatiitic intrusions that I have listed here is that they tend to occur as groups of bodies localized at a particular stratigraphic horizon within each terrane.

Nickel sulphide deposits associated with komatiitic rocks

Three principal types of magmatic nickel sulphide deposits are found in association with ultramafic rocks of komatiitic affinity. Most numerous are small (about 10^6 tonnes) but high grade (1 to 5% Ni) deposits occurring as basal accumulations in peridotitic lava flows or in the feeders to such flows. The Kambalda ores of Western Australia are the most important of this type but significant examples are known in Canada (e.g., the Marbridge and Langmuir deposits in the Abitibi belt) and in Zimbabwe (e.g., Damba). Much larger (about 10^7 tonnes) high grade deposits form as basal accumulations in intrusive komatiite bodies. The Agnew deposit in Western Australia is the prime example from an Archean terrane, but the Proterozoic deposits of the Thompson and Ungava belts in Canada probably belong in this category. The third type is the one of interest here and includes deposits consisting of extensive zones of disseminated magmatic sulphides within the central portions of synvolcanic dunite-peridotite bodies which represent shallow level intrusive members of the komatiite suite. The prototype of this group is the Mt. Keith deposit, which is one of a number of similar occurrences within a series of ultramafic lenses that lie along a 200 km belt between Wiluna and Leonora in the Yilgarn Block in Western Australia. The individual lenses are as much as 20 km in length and 1 km in width, and are characterized by virtually monomineralic dunite cores that grade outward to more pyroxene-rich peridotite margins (Binns et al., 1977; Naldrett and Turner, 1977). Disseminated sulphides make up 2 to 3% of the rock in crudely conformable zones within the dunite core. The Mt. Keith deposit is reported to contain about 290 million tonnes grading 0.6% nickel (Burt and Sheppy, 1975), while the deposit at Six Mile Well, about 20 km to the south, contains about 54 million tonnes of 0.6% nickel (Naldrett and Turner, 1977). A number of similar deposits also occur in the Forrestania area of Western Australia (Porter and McKay, 1981).

The Dumont deposit may be considered to be a variant of the Mt. Keith type: the Ultramafic Zone at Dumont is dimensionally and petrographically similar to the bodies that host the Australian deposits, and the primary characteristics and grade of mineralization are essentially identical. The presence of a significant proportion of mafic differentiates in the Dumont Sill is the principal contrasting feature. The Epoch deposit in Zimbabwe (Clutten et al., 1981), which contains 5 million tonnes grading 0.64% nickel, is similar in this respect. I have argued that the Dumont mineralization represents the accumulation of olivine and molten sulphide in the proportions required by a fractionation path that followed the intersection of the olivine liquidus with the sulphide-silicate liquid solvus in a peridotitic komatiite magma. The relatively large proportion of olivine which precipitates under such conditions would have impeded the coalescense of the sulphide droplets and militated against their accumulation in high grade pools. It follows that the rather restricted range of grades of deposits of the Mt. Keith type is not accidental but is a direct consequence of the particular process of sulphide segregation and largely reflects the composition of the parent magmas and the solubility of sulphide. Insufficient data are available on the other deposits to allow me to conclude whether the filter-pressing/magma-mixing model proposed to explain the disposition of magmatic sulphides in the Dumont intrusion is generally applicable to deposits of this type.

Exploration guidelines

The geological setting of the nickel sulphide mineralization associated with the Dumont Sill, and the model proposed for its origin, suggest a number of exploration guidelines for deposits of the Dumont or Mt. Keith type.

1. The first stage in the exploration for such deposits should be the identification of ultramafic, synvolcanic, sill-like intrusions of komatiitic affinity. The average composition of these bodies is ultramafic, there is an abundance of olivine cumulates, and mafic differentiates may or may not be present. Although the bulk composition of an intrusion is usually difficult to determine with any certainty, the composition of the most magnesian olivine is generally indicative of the nature of the parent magma. There are a variety of geochemical and mineralogical indicators of komatiitic affinity.
2. Evidence of sulphide-saturation should be sought in any intrusions which satisfy the criteria outlined in (1). The presence of even trace amounts of magmatic sulphides may be significant. Sparse, erratically distributed and mainly postcumulus sulphides occur in the Lower Peridotite in the Dumont intrusion, indicating that although the magma was not saturated when emplaced, its sulphur content was not negligible. The depletion of nickel in olivine documented in the Dumont rocks is also considered to be diagnostic of sulphide segregation. Olivine in the Dunite Subzone immediately overlying the main sulphide layer is strongly depleted in nickel. What is of more interest in the context of exploration is the moderate depletion apparent in olivine at some distance from the mineralization, both in the Dunite Subzone and in the overlying Upper Peridotite. It will seldom be possible to carry out microprobe analyses of olivine as a routine exploration technique, however, I have

demonstrated that whole-rock analyses of olivine-rich rocks give a reasonable approximation of the composition of the contained olivine.

3. The sulphide-enriched zones which comprise these deposits are centrally disposed within their ultramafic host rocks, and the filter-pressing/magma-mixing hypothesis suggests a reason why this is the case. In any event, both empirical and theoretical considerations indicate that the thick, central portions of the intrusions are most likely to host disseminated magmatic sulphides of the Dumont type. At a more detailed level of examination, evidence of circumstances that favour filter pressing should be sought. In the case of the Dumont deposit, the sulphide layers overlie the thickest part of a unit that is believed to represent an accumulation of intratelluric phenocrysts. An "uncoupling" of phase layering and cryptic layering may be indicative of filter pressing as suggested by Irvine (1980). In the Dumont intrusion, the zone of sulphide enrichment overlies the greatest upward displacement of the discontinuity in the cryptic variation of Mg/Mg+Fe in olivine from the modal discontinuity marking the base of the Dunite Subzone.

4. Finally, the possibility that intrusions that host centrally disposed zones of disseminated magmatic sulphides may also contain rich, basal sulphide accumulations should not be discounted. The Cliffs Mt. Keith prospect in the Wiluna area of Western Australia is such a high grade deposit which occurs at the base of a sill in proximity to the Mt. Keith deposit described above (Groves and Lesher, 1982). It is noteworthy that the basal contact of the Dumont intrusion has not been explored in detail.

REFERENCES

Alsac, C.
1977: Pétrographie et géochimie de formations volcaniques minéralisées de l'Abitibi et de l'Estrie; Ministère des Richesses Naturelles du Québec, DPV-519, 93 p.

Appleyard, E.C.
1980: Mass balance computations in metasomatism: metagabbro/nepheline syenite pegmatite interaction in northern Norway; Contributions to Mineralogy and Petrology, v. 73, p. 131-144.

Arndt, N.T.
1976: Melting relations of ultramafic lavas (komatiites) at 1 atm and high pressure; Carnegie Institute of Washington Yearbook, v. 75, p. 555-562.

1977: Thick, layered peridotite-gabbro lava flows in Munro Township; Canadian Journal of Earth Sciences, v. 14, p. 2620-2637.

Arndt, N.T., Francis, D., and Hynes, A.J.
1979: The field characteristics and petrology of Archean and Proterozoic komatiites; Canadian Mineralogist, v. 17, p. 147-164.

Arndt, N.T., Naldrett, A.J., and Pyke, D.R.
1977: Komatiitic and iron-rich tholeiitic lavas of Munro Township, northeast Ontario; Journal of Petrology, v. 18, p. 319-369.

Baragar, W.R.A. and McGlynn, J.C.
1976: Early Archean basement in the Canadian Shield: a review of the evidence; Geological Survey of Canada, Paper 76-14, 20 p.

Barnes, I. and O'Neil, J.R.
1969: The relationship between fluids in some fresh Alpine-type ultramafics and possible modern serpentinization, Western U.S.; Geological Society of America, Bulletin, v. 80, p. 1947-1960.

Barnes, S.J.
1980: Petrology and geochemistry of the Katiniq nickel deposit and related rocks, Ungava, northern Quebec; unpublished M.Sc. thesis, University of Toronto.

Barrett, F.M., Binns, R.A., Groves, D.I., Marston, R.J., and McQueen, K.G.
1977: Structural history and metamorphic modification of Archean volcanic-type nickel deposits, Yilgarn Block, Western Australia; Economic Geology, v. 72, p. 1195-1224.

Besson, M.
1979: Les roches encaissantes des gisements sulfurés de nickel: petrochimie des series magmatiques hôtes; Canadian Mineralogist, v. 17, p. 201-216.

Besson, M. and Capitant, B.
1976: Note sur le chimisme de roches ultrabasiques minéralisées en sulfures de nickel dans l'Abitibi (Province Supérieure archéenne, Canada); Bulletin du Bureau de Recherches géologiques et Minières, France (2), sect. II, v. 4, p. 349-378.

Bickle, M.J., Ford, C.E., and Nisbet, E.G.
1977: The petrogenesis of peridotitic komatiites: evidence from high pressure melting experiments; Earth and Planetary Science Letters, v. 37, p. 97-106.

Binns, R.A., Groves, D.I., and Gunthorpe, R.A.
1977: Nickel sulphides in Archean ultramafic rocks of Western Australia; in Correlation of the Precambrian, v. 2, ed. A.V. Siderenko; Nauka, Moscow, p. 349-380.

Bliss, N.W. and MacLean, W.H.
1975: The paragenesis of zoned chromite from central Manitoba; Geochimica et Cosmochimica Acta, v. 39, p. 973-990.

Bonneau, J.
1977: Minéralisations nickélifères et petrogenese du filon-couche Dumont Nickel; unpublished M.Sc. thesis, Laval University.

Bottinga, Y. and Weill, D.F.
1970: Densities of liquid silicate systems calculated from partial molar volumes of oxide components; American Journal of Science, v. 269, p. 169-182.

1972: The viscosity of magmatic silicate liquids: a model for calculation; American Journal of Science, v. 272, p. 438-475.

Burt, D.R.L. and Sheppy, N.R.
1975: Mount Keith Nickel Sulphide Deposit; in Economic Geology of Australia and Papua-New Guinea, v. 1, ed. C.L. Knight; Australian Institute of Mining and Metallurgy, p. 159-168.

Campbell, I.H.
1978: Some problems with cumulus theory; Lithos, v. 11, p. 311-323.

Campbell, I.H., Roeder, P.L., and Dixon, J.M.
1978: Plagioclase buoyancy in basaltic liquids as determined with a centrifuge furnace; Contributions to Mineralogy and Petrology, v. 67, p. 369-377.

Caruso, L.J. and Chernosky, J.V., Jr.
1979: The stability of lizardite; Canadian Mineralogist, v. 17, p. 757-770.

Clutten, J.M., Foster, R.P., and Martin, A.
1981: Nickel Mineralization in Zimbabwe; Episodes, v. 1981, p. 10-15.

Crook, W.W. and Jambor, J.L.
1979: Nickelbischoffite, a new nickel chloride hydrate; Canadian Mineralogist, v. 17, p. 107-109.

Dickey, J.S., Jr., Yoder, H.S., Jr., and Schairer, J.F.
1971: Chromium in silicate-oxide systems; Carnegie Institute of Washington Yearbook, v. 70, p. 118-125.

Dixon, T.H.
1981: Gebel Dahanib, Egypt: late Precambrian layered sill of komatiitic composition; Contributions to Mineralogy and Petrology, v. 76, p. 42-52.

Duke, J.M.
1976: Distribution of the period four transition elements among olivine, calcic clinopyroxene and mafic silicate liquid: Experimental results; Journal of Petrology, v. 17, p. 499-521.

1978: Serpentinization of the Dumont ultramafic intrusion, N.W. Quebec; Geological Association of Canada – Mineralogical Association of Canada, Abstracts with Program, v. 3, p. 392.

1979: Computer simulation of the fractionation of olivine and sulfide from mafic and ultramafic magmas; Canadian Mineralogist, v. 17, p. 507-514.

1980: Petrology and economic geology of the Dumont sill, N.W. Quebec; Geological Association of Canada – Mineralogical Association of Canada, Program with Abstracts, v. 5, p. 50.

1982: Origin of disseminated magmatic sulphide deposits of the Dumont type; Geological Association of Canada – Mineralogical Association of Canada, Program with Abstracts, v. 7, p. 46.

Duke, J.M. and Bonardi, M.
1982: Chromian andradite from Réaume township, Ontario; The Canadian Mineralogist, v. 20, p. 49-53.

Duke, J.M. and Naldrett, A.J.
1978: A numerical model of the fractionation of olivine and molten sulfide from komatiite magma; Earth and Planetary Science Letters, v. 39, p. 256-266.

1983: Lower grade nickel sulfide resources, in The Cameron Volume on Unconventional Mineral Deposits, ed. W.D. Shanks, American Institute of Mining, Metallurgical and Petroleum Engineers, p. 23-34.

Eckstrand, O.R.
1975: The Dumont serpentinite: a model for control of nickeliferous opaque mineral assemblages by alteration reactions in ultramafic rocks; Economic Geology, v. 70, p. 183-201.

Evans, B.W.
1977: Metamorphism of Alpine peridotite and serpentinite; Annual Review of Earth and Planetary Science, v. 5, p. 397-447.

Evans, B.W. and Frost, B.R.
1975: Chrome-spinel in progressive metamorphism – a preliminary analysis; Geochimica et Cosmochimica Acta, v. 39, p. 959-972.

Fleet, M.E., MacRae, N.D., and Herzberg, C.T.
1977: Partition of nickel between olivine and sulfide: a test for immiscible sulfide liquids; Contributions to Mineralogy and Petrology, v. 65, p. 191-197.

Francis, D.M. and Hynes, A.J.
1979: Komatiite-derived tholeiites in the Proterozoic of New Quebec; Earth and Planetary Science Letters, v. 44, p. 473-481.

Frisch, W. and Keusen, H.
1977: Gardiner intrusion, an ultramafic complex at Kangerlugssuaq, East Greenland; Grønlands Geologiske Undersogelse Bulletin 122, 62 p.

Gates, T.M. and Hurley, P.M.
1973: Evaluation of Rb-Sr dating methods applied to the Matachewan, Abitibi, Mackenzie, and Sudbury dike swarms in Canada; Canadian Journal of Earth Sciences, v. 10, p. 900-919.

Goodwin, A.M.
1979: Archean volcanic studies in the Timmins-Kirkland Lake-Noranda region of Ontario and Québec; Geological Survey of Canada, Bulletin 278, 51 p.

Goodwin, A.M. and Ridler, R.H.
1970: Abitibi orogenic belt; Geological Survey of Canada, Paper 70-40, p. 1-24.

Gray, N.H. and Crain, I.K.
1969: Crystal settling in sills: model for suspension settling; Canadian Journal of Earth Sciences, v. 6, p. 1211-1216.

Green, D.H., Nicholls, I.A., Viljoen, M., and Viljoen, R.
1975: Experimental demonstration of the existence of peridotitic liquids in earliest Archean magmatism; Geology, v. 3, p. 11-14.

Gresens, R.L.
1967: Composition-volume relationships in metasomatism; Chemical Geology, v. 2, p. 47-65.

Grove, T.L.
1978: Experimentally determined FeO-MgO-CaO partitioning between pyroxene and liquid in lunar basalts; EOS, v. 59, p. 401.

Groves, D.I. and Lesher, C.M.
1982: Regional geology and nickel deposits of the Norseman-Wiluna belt, Western Australia; University of Western Australia, Geology Department, Publication 7.

Harris, D.C. and Nickel, E.H.
1972: Pentlandite compositions and associations in some mineral deposits; Canadian Mineralogist, v. 11, p. 861-878.

Hébert, R.
1982: Géologie du complexe de filons-couches d'Amos, Québec; Ministère de l'Énergie et des Ressources, Québec, DPV-786, 28 p.

Hess, G.B.
1972: Heat and mass transport during crystallization of the Stillwater igneous complex; Geological Society of America, Memoir 132, p. 503-520.

Hostetler, P.B., Coleman, R.G., Mumpton, F.A., and Evans, B.W.
1966: Brucite in Alpine serpentinites; American Mineralogist, v. 51, p. 75-98.

Hyde, R. and Walker, R.G.
1977: Sedimentary environments and the evolution of the Archean greenstone belt in the Kirkland Lake area, Ontario; in Report of Activities, Part A, Geological Survey of Canada, Paper 77-1A, p. 185-190.

Imreh, L.
1980: Variations morphologiques des coulées méta-ultramafiques komatiitiques du sillon Archéen de La Motte-Vassan, Abitibi-est, Québec; Precambrian Research, v.12, p. 3-30.

Irvine, T.N.
1965: Chromian spinel as a petrogenetic indicator. Part 1, theory; Canadian Journal of Earth Sciences, v. 2, p. 648-672.

1967: Chromian spinel as a petrogenetic indicator. Part 2, petrologic applications; Canadian Journal of Earth Sciences, v. 4, p. 71-103.

1970a: Heat transfer during solidification of layered intrusions, I. sheets and sills; Canadian Journal of Earth Sciences, v. 7, p. 1031-1061.

1970b: Crystallization sequences in the Muskox intrusion and other layered intrusions, I. Olivine-pyroxene-plagioclase relations; Geological Society of South Africa, Special Publication 1, p. 441-476.

1975: Crystallization sequences in the Muskox intrusion and other layered intrusions – II. Origin of chromitite layers and similar deposits of other magmatic ores; Geochimica et Cosmochimica Acta, v. 39, p. 991-1020.

1977: Origin of chromitite layers in the Muskox intrusion and other stratiform intrusions: a new interpretation; Geology, v. 5, p. 273-277.

1980: Magmatic infiltration metasomatism, double diffusive fractional crystallization, and adcumulus growth in the Muskox intrusion and other layered intrusions; in Physics of Magmatic Processes, ed. R.B. Hargraves; Princeton University Press, Princeton, p. 325-384.

1982: Terminology for layered intrusions; Journal of Petrology, v. 23, p. 127-162.

Jackson, E.D.
1961: Primary textures and mineral associations in the Ultramafic Zone of the Stillwater complex, Montana; United States Geological Survey, Professional Paper 358, 106 p.

Jambor, J.L.
1975: Secondary minerals in an ultramafic intrusion, Amos Area, Quebec; in Report of Activities, Part A, Geological Survey of Canada, Paper 75-1A, p. 261-263.

James, N.F. and Mawdsley, J.B.
1925: Mineral deposits in Desmeloizes and Trécesson townships, Quebec; Geological Survey of Canada, Summary Report, 1925, Part C, p. 78-81.

Jolly, W.T.
1978: Metamorphic history of the Archean Abitibi belt; Geological Survey of Canada, Paper 78-10, p. 63-77.

Kanehira, K.
1966: A note on the texture of pyrrhotite in some rocks of the Muskox intrusion; Canadian Mineralogist, v. 8, p. 531-536.

Krogh, T.E. and Davis, G.L.
1971: Zircon U-Pb ages of Archean meta-volcanic rocks in the Canadian Shield; Carnegie Institute of Washington Yearbook, v. 70, p. 241-242.

Kushiro, I.
1969: The system forsterite-diopside-silica; American Journal of Science, v. 267-A, p. 269-294.

Kushiro, I. and Schairer, J.F.
1963: New data on the system diopside-forsterite-silica; Carnegie Institute of Washington Yearbook, v. 62, p. 95-103.

Latulippe, M.
1972: Val d'Or-Malartic Area; XXIV International Geological Congress Guidebook, Excursion A41-C41, p. 33-41.

McBirney, A.R. and Noyes, R.M.
1979: Crystallization and layering of the Skaergaard Intrusion; Journal of Petrology, v. 20, p. 487-554.

MacLaren, A.S.
1953: Peridotites of northwestern Quebec; unpublished Ph.D. thesis, McGill University, 113 p.

MacRae, N.D.
1969: Ultramafic intrusions of the Abitibi area, Ontario; Canadian Journal of Earth Sciences, v. 6, p. 281-303.

Miller, A.R.
1977: Petrology and Geochemistry of the 2-3 ultramafic sill and related rocks, Cape Smith-Wakeham Bay Fold Belt, Quebec; unpublished Ph.D. thesis, University of Western Ontario.

Miura, Y., Rucklidge, J.C., and Nord, G.
1979: The structural occurrence of chlorine in serpentine; Geological Association of Canada – Mineralogical Association of Canada, Program with Abstracts, v. 4, p. 67.

1981: The occurrence of chlorine in serpentine minerals; Contributions to Mineralogy and Petrology, v. 76, p. 17-23.

Moody, J.B.
1976: An experimental study on the serpentinization of iron-bearing olivines; Canadian Mineralogist, v. 14, p. 462-478.

Naldrett, A.J.
1969: A portion of the system Fe-S-O between 900 and 1080°C and its application to sulfide ore magmas; Journal of Petrology, v. 10, p. 171-201.

1979: Partitioning of Fe, Co, Ni and Cu between sulfide liquid and basaltic melts and composition of Ni-Cu sulfide deposits – a reply and further discussion; Economic Geology, v. 74, p. 1520-1528.

1981: Nickel sulfide deposits: classification, composition and genesis; in Skinner, B.J., ed., Economic Geology, Seventy-fifth Annual Volume, p. 628-685.

Naldrett, A.J. and Mason, G.D.
1968: Contrasting Archean ultramafic igneous bodies in Dundonald and Clergue townships, Ontario; Canadian Journal of Earth Sciences, v. 5, p. 111-143.

Naldrett, A.J. and Turner, A.R.
1977: The geology and petrogenesis of a greenstone belt and related nickel sulphide mineralization at Yakabindie, Western Australia; Precambrian Research, v. 5, p. 43-103.

Nesbitt, H.W. and Bricker, O.P.
1978: Low temperature alteration processes affecting ultramafic bodies; Geochimica et Cosmochimica Acta, v. 42, p. 403-409.

Nesbitt, R.W. and Sun, S.S.
1976: Geochemistry of Archean spinifex-textured peridotites and magnesian and low-magnesian tholeiites; Earth and Planetary Science Letters, v. 31, p. 433-453.

Nesbitt, R.W., Sun, S.S., and Purvis, A.C.
1979: Komatiites: geochemistry and genesis; Canadian Mineralogist, v. 17, p. 165-186.

Nisbet, E.G., Bickle, M.J., and Martin, A.
1977: The mafic and ultramafic lavas of the Belingwe greenstone belt, Rhodesia; Journal of Petrology, v. 18, p. 521-566.

Nunes, P.D. and Jensen, L.S.
1980: Geochronology of the Abitibi Metavolcanic Belt, Kirkland Lake area – progress report; in Summary of Geochronology Studies 1977-1979, ed. E.G. Pye; Ontario Geological Survey, Miscellaneous Paper 92, p. 40-45.

Nunes, P.D. and Pyke, D.R.
1980: Geochronology of the Abitibi Metavolcanic Belt, Timmins-Matachewan area – progress report; in Summary of Geochronology Studies 1977-1979, ed. E.G. Pye; Ontario Geological Survey, Miscellaneous Paper 92, p. 34-39.

Pearce, T.H. and Birkett, T.C.
1974: Archean metavolcanic rocks from Thackeray Township, Ontario; Canadian Mineralogist, v. 12, p. 509-519.

Peredery, W.V.
1979: Relationship of ultramafic amphibolites to metavolcanic rocks and serpentinites in the Thompson belt, Manitoba; Canadian Mineralogist, v. 17, p. 187-200.

Porter, D.J. and McKay, K.G.
1981: The nickel sulfide mineralization and metamorphic setting of the Forrestania area, Western Australia; Economic Geology, v. 76, p. 1524-1549.

Pyke, D.R., Naldrett, A.J., and Eckstrand, O.R.
1973: Archean ultramafic flows in Munro Township, Ontario; Geological Society of America Bulletin, v. 84, p. 955-978.

Rice, A.
1981: Convective fractionation: A mechanism to provide cryptic zoning (macrosegregation), layering, crescumulates, banded tuffs and explosive volcanism in igneous processes; Journal of Geophysical Research, v. 86, p. 405-417.

Roeder, P.L. and Emslie, R.F.
1970: Olivine-liquid equilibrium; Contributions to Mineralogy and Petrology, v. 29, p. 275-289.

Ross, S.H.
1939: Launay Township, Abitibi County; Quebec Department of Mines, Geological Report 1, 26 p.

Rucklidge, J.C.
1972: Chlorine in partially serpentinized dunite; Economic Geology, v. 67, p. 38-40.

Rucklidge, J.C. and Patterson, G.C.
1977: The role of chlorine in serpentinization; Contributions to Mineralogy and Petrology, v. 65, p. 39-44.

Schairer, J.F. and Yoder, H.S. Jr.
1962: The system diopside-enstatite-silica; Carnegie Institute of Washington Yearbook, v. 61, p. 75-82.

Shaw, H.R.
1965: Comments on viscosity, crystal settling, and convection in granitic magmas; American Journal of Science, v. 263, p. 120-152.

Shima, H. and Naldrett, A.J.
1975: Solubility of sulfur in an ultramafic melt and the relevance of the system Fe-S-O; Economic Geology, v. 70, p. 960-967.

Skinner, B.J.
1966: Thermal expansion; in Handbook of Physical Constants, ed. S.P. Clark; Geological Society of America Memoir 97, p. 75-96.

Thayer, T.
1966: Serpentinization considered as a constant volume metasomatic process; American Mineralogist, v. 51, p. 685-710.

1970: Chromite segregations as petrogenetic indicators; Geological Society of South Africa, Special Publication, no. 1, p. 380-390.

Thompson, J.F.H., Barnes, S.J., and Duke, J.M.
1984: The distribution of nickel and iron between olivine and magmatic sulphides in some natural assemblages; Canadian Mineralogist, v. 22, p. 55-66.

Turner, J.S. and Gustafson, L.B.
1978: The flow of hot saline solutions from vents in the seafloor – some implications for exhalative massive sulfide and other ore deposits; Economic Geology, v. 73, p. 1082-1100.

Viljoen, R.P. and Viljoen, M.J.
1970: The geology and geochemistry of the layered ultramafic bodies of the Kaapmuiden area, Barberton Mountain Land; in Symposium on the Bushveld Igneous Complex and Other Layered Intrusions, ed. D.J.L. Visser and G. von Gruenewaldt; Geological Society of South Africa, Special Publication 1, p. 661-688.

Vogel, D.E.
1979: Canton de Trécesson; ministère de l'Energie et des Ressources du Quebec, Rapport géologique 194, 42 p.

Wager, L.R. and Brown, G.M.
1968: Layered Igneous Rocks; Oliver and Boyd, Edinburgh and London, 588 p.

Wager, L.R., Brown, G.M., and Wadsworth, W.J.
1960: Types of igneous cumulates; Journal of Petrology, v. 1, p. 73-85.

Weber, W.W. and Latulippe, M.
1964: Amos-Barraute Area, Abitibi-East County; Quebec Department of Natural Resources, Geological Report 109, 69 p.

Weeks, L.J.
1935: Amos Sheet, Abitibi County, Quebec; Geological Survey of Canada, Map 327A.

Wicks, F.J. and Whittaker, E.J.W.
1975: A reappraisal of the structures of the serpentine minerals; Canadian Mineralogist, v. 13, p. 227-243.

1977: Serpentine textures and serpentinization; Canadian Mineralogist, v. 15, p. 459-488.

Wicks, F.J., Whittaker, E.J.W., and Zussman, J.
1977: An idealized model for serpentine textures after olivine; Canadian Mineralogist, v. 15, p. 446-458.

Williams, D.A.C.
1978: Some geological and geochemical aspects of Archean komatiitic and tholeiitic volcanism in Rhodesia; Unpublished manuscript.

Wilson, J.F.
1968: The Mashaba Igneous Complex and its subsequent deformation; Geological Society of South Africa, Transactions, v. 71, Annex, p. 175-188.

1979: A preliminary reappraisal of the Rhodesian Basement Complex; Geological Society of South Africa, Special Publication, v. 5, p. 1-23.

Appendix 1 – Diamond-drill hole data

D.D.H. No.	Township	Range	Lot	Longitude	Latitude	L.O.H. (ft)	Inclination
DT-1	Trecesson	V	3	17+30E	1+00N	300	45°/0, 43°/300
DT-2	Trecesson	V	3	20+30E	1+00N	300	45°/0, 45°/300
DT-3	Trecesson	V	3	17+30E	3+50N	601	60°/0, 53°/200, 62°/400, 48°/600
DT-4	Trecesson	V	3	20+30E	3+50N	600	60°/0, 58°/200, 54°/400, 48°/600
E-5	Trecesson	V	2	17+30E	8+00N	1075	60°/0, 42°/300, 40°/600, 39°/900
E-6	Trecesson	V	2	12+00E	35+50N	1085	55°/0, 42°/300, 41°/600, 40°/900
E-7	Trecesson	V	1	4+00E	35+00N	1069	60°/0, 52°/300, 52°/600, 52°/900
E-8	Launay	V	62	4+00W	39+00N	1239	60°/0, 58°/200, 57°/600, 56°/900, 52°/1200
E-9	Launay	V	61	12+00W	43+50N	1306	60°/0, 54°/200, 54°/600, 55°/900
E-10	Launay	V	60	20+00W	44+00N	912	60°/0, 64°/300, 64°/600
E-11	Launay	V	59	28+00W	43+50N	521	70°/0, 73°/300
E-12	Launay	V	58	28+00W	39+00N	830	70°/0, 73°/300, 68°/600, 70°/800
E-13	Launay	V	58	36+00W	50+00N	225	70°/0
E-14	Launay	V	58	36+00W	52+00N	1498	70°/0, 70°/300, 67°/600, 69°/900, 65°/1200
E-15	Launay	VI	57	44+00W	10+00N	2136	70°/0, 61°/300, 60°/600, 58°/900, 54°/1500, 52°/1800
E-16	Launay	VI	58	36+00W	8+00N	2216	70°/0, 68°/300, 58°/600, 49°/900, 50°/1200, 47°/1500, 47°/1800, 44°/2100
E-17	Launay	VI	57	52+00W	18+00N	2004	65°/0, 61°/300, 60°/600, 57°/1200, 54°/1500, 49°/1800
E-18	Launay	V	59	28+00W	52+00N	1545	65°/0, 65°/300, 65°/600, 63°/900, 65°/1200, 63°/1545
E-19	Launay	VI	57	44+00W	11+00N	2759	80°/0, 75°/300, 77°/600, 77°/900, 77°/1200, 79°/1500, 76°/1800, 81°/2100, 76°/2400, 85°/2700
E-20	Launay	VI	58	36+00W	11+00N	2203	75°/0, 72°/300, 62°/600, 56°/900, 48°/1150, 44°/1200, 39°/1500, 34°/1800
E-21	Launay	VI	58	36+00W	14+00N	3105	82°/0, 80°/300, 77°/600, 65°/900, 54°/1250, 48°/1500, 45°/1800, 41°/2100, 38°/2400, 35°/2700
M-1	Launay	V	57	50+00W	46+10N	800	70°/0, 73°/200, 66°/600
W-1	Launay	VI	56	60+00W	32+00N	925	60°/0, 46°/300, 44°/600
W-2	Launay	VI	56	60+00W	24+00N	1020	70°/0, 66°/300, 66°/600, 68°/900
W-3	Launay	VI	54	68+00W	28+00N	1079	70°/0, 68°/300, 63°/600
W-4	Launay	VI	54	68+00W	37+00N	1416	70°/0, 64°/300, 64°/600, 64°/900, 66°/1200
W-5	Launay	VI	54	68+00W	44+00N	421	70°/0, 69°/300
W-6	Launay	VI	54	76+00W	45+00N	1265	70°/0, 70°/300, 69°/600, 69°/900, 69°/1200
W-7	Launay	VII	54	76+00W	4+00N	1107	70°/0, 70°/300, 64°/600, 62°/900, 57°/1100
W-8	Launay	VI	54	76+00W	52+00N	1431	65°/0, 62°/300, 62°/600, 62°/900, 61°/1200
W-9	Launay	VI	54	68+00W	45+00N	1498	70°/0, 67°/300, 66°/600, 64°/900, 60°/1200, 53°/1498
W-10	Launay	VII	53	84+00W	10+00N	1490	65°/0, 65°/300, 62°/600, 59°/900, 45°/1200, 45°/1485
W-11	Launay	VII	52	92+00W	19+00N	1795	65°/0, 66°/300, 64°/600, 58°/900, 53°/1500, 49°/1795
W-12	Launay	VII	51	100+00W	27+00N	2064	65°/0, 47°/300, 44°/600, 41°/1000, 42°/1200, 40°/1500, 37°/1900
W-13	Launay	VII	50	108+00W	35+00N	1551	65°/0, 62°/300, 61°/600, 54°/900, 55°/1200, 54°/1540
W-14	Launay	VIII	47	136+00W	1+20N	1758	65°/0, 61°/300, 58°/600, 57°/900, 56°/1200, 53°/1500
P-1	Launay	VI	57	44+00W	2+00N	1202	90°/0, 90°/300, 88°/600, 89°/900, 87°/1200
P-2	Launay	V	57	44+00W	52+00N	1000	90°/0, 90°/300, 85°/600, 80°/900
P-3	Launay	V	57	44+00W	48+00N	628	90°/0, 86°/300, 85°/600
P-4	Launay	VI	58	40+00W	5+00N	1501	65°/0, 63°/300, 61°/600, 57°/900, 59°/1200, 53°/1500
P-5	Launay	VI	57	44+00W	6+00N	700	90°/0, 90°/300, 90°/600
P-6	Launay	VI	58	36+00W	2+00N	1152	90°/0, 90°/300, 87°/600, 88°/900, 89°/1152
P-7	Launay	V	57	44+00W	44+00N	600	90°/0, 89°/300, 88°/600
P-8	Launay	V	58	36+00W	52+10N	1352	90°/0, 89°/300, 87°/600, 86°/900, 84°/1200
P-9	Launay	VI	58	40+00W	4+00N	1430	90°/0, 89°/300, 89°/600, 89°/900, 86°/1200, 87°/1430
P-10	Launay	VI	57	48+00W	10+00N	1646	90°/0, 88°/300, 86°/600, 89°/900, 38°/1200, 89°/1500
P-11	Launay	VI	58	40+00W	2+00N	1181	65°/0, 65°/300, 64°/600, 62°/900, 62°/1150
P-12	Launay	VI	58	36+00W	0+00N	980	70°/0, 65°/300, 63°/600, 58°/900
P-13	Launay	VI	58	40+00W	0+00N	758	65°/0, 60°/300, 58°/600
P-14	Launay	V	58	38+00W	0+00N	846	70°/0, 69°/300, 63°/600, 61°/846
P-15	Launay	VI	58	38+00W	3+00N	1054	65°/0, 60°/300, 57°/600, 52°/900
P-16	Launay	VI	58	42+00W	6+00N	1160	65°/0, 62°/300, 61°/600, 56°/900
P-17	Launay	VI	57	44+00W	0+00N	706	90°/0, 87°/300, 85°/600
P-18	Launay	VI	57	46+00W	10+00N	1201	65°/0, 66°/300, 65°/600, 64°/900, 60°/1200
P-19	Launay	VI	58	42+00W	3+00N	725	65°/0, 61°/300, 58°/600
P-20	Launay	VI	57	48+00W	8+00N	1100	65°/0, 60°/300, 59°/600, 54°/900, 53°/1100
P-21	Launay	VI	57	46+00W	7+00N	1000	65°/0, 63°/300, 62°/600, 57°/1000

Longitude is given in feet east or west of north-south boundary between Launay and Trecesson townships. Latitude is given in feet north of range line. L.O.H. is the length of the hole in feet. The trend (at the collar) of all inclined holes is 180°. The trend of initially vertical holes is unknown in those segments that deviate from the vertical. The inclination is given in terms of the angle of plunge/depth in the hole at which the measurement was taken. Thus hole P-21 plunged 65° at the collar, 63° at 300 feet, and so on.

Appendix 2 – Chemical analyses of whole rocks

Sample Numbers

Analyses are arranged in order of ascending sample number. Sample numbers prefixed by "DBA" are hand specimens collected from surface exposures. All others refer to drill hole number and intersection depth (in feet) as described in text.

Unit

The following abbreviations are used: C – Clinopyroxenite Subzone, D – Dunite Subzone, G – Gabbro Subzone, LP – Lower Peridotite Subzone, OG – Quartz Gabbro Subzone, UP – Upper Peridotite Subzone, V – volcanic host rocks.

Analytical Methods

SiO_2, TiO_2, Al_2O_3, total Fe, MnO, MgO, CaO, Na_2O, K_2O, and P_2O_5 were determined by standard x-ray fluorescence techniques. Where TiO_2, MnO or CaO are less than 0.5%, optical emission spectroscopy data were used. V, Cr, Co and Cu were also determined by optical emission. Rb, Zr, and Sr analyses were carried out by an energy dispersive x-ray fluorescence method. FeO was determined chemically by a modified Wilson method and Fe_2O_3 was obtained by difference. Cl was determined colorimetrically whereas H_2O, CO_2 and S were measured by infrared spectrometry. Ni analyses of 5 or 10 foot drill core intersections provided by the Dumont Nickel Corporation were used for samples from the Ultramafic Zone. Ni analyses for other samples were obtained by optical emission spectroscopy.

The concentrations of all constituents are tabulated as weight percent except those marked ppm which are in parts per million. The concentrations of V, Cr, Co, Ni, Cu, Rb, Sr and Zr were converted to the oxides for calculation of the totals.

Sample	DBA76109	DBA76110	DBA76114	DBA76115	DBA76117	DBA77016	DBA77017	DBA77018	E05-0300	E05-0340	E05-0380	E05-0420
Unit	QG	G	UP	UP	V	V	V	V	UP	UP	UP	UP
SiO2	50.300	48.900	38.300	41.100	50.100	49.870	51.270	48.000	35.300	35.500	34.800	37.200
TiO2	1.370	1.380	0.158	0.121	0.344	1.470	0.488	1.000	0.033	0.037	0.038	0.038
Al2O3	12.200	13.400	3.300	2.500	12.400	13.160	12.860	14.000	0.660	0.900	0.870	1.150
Fe2O3	1.300	2.300	7.600	6.700	1.300	2.510	0.981	3.000	5.500	3.900	6.000	2.900
FeO	11.100	12.500	6.700	5.600	7.400	10.400	4.740	9.100	2.300	1.700	2.400	0.900
MnO	0.234	0.226	0.174	0.176	0.164	0.178	0.124	0.253	0.130	0.140	0.140	0.110
MgO	5.900	6.500	31.300	31.400	10.800	7.220	5.470	5.000	41.100	41.300	40.000	41.600
CaO	8.950	7.900	2.700	3.880	12.400	7.390	9.620	14.000	0.060	0.050	0.060	0.050
Na2O	2.000	1.900	0.054	0.036	1.512	3.180	1.630	1.280	0.200	nd	nd	nd
K2O	0.120	0.800	nd	nd	0.200	0.330	1.300	1.000	nd	nd	nd	nd
P2O5	0.120	0.130	0.030	nd	0.060	0.100	0.150	0.060	0.030	0.040	0.020	0.020
H2O	5.000	3.000	9.500	8.300	1.700	4.300	4.300	3.500	14.300	13.900	12.500	14.000
CO2	2.200	nd	nd	nd	nd	0.900	7.800	0.100	0.300	0.500	0.300	0.300
S	0.200	0.300	0.100	nd	0.200	nd	nd	nd	0.090	0.090	0.070	0.080
Cl	0.010	0.410	0.020	na	0.020	na	na	na	na	na	na	na
V ppm	393.	404.	62.	56.	208.	355.	93.	259.	25.	36.	40.	32.
Cr ppm	96.	75.	2060.	3570.	533.	45.	319.	82.	1500.	8100.	6700.	7200.
Co ppm	51.	56.	142.	145.	53.	50.	22.	42.	110.	110.	140.	110.
Ni ppm	77.	74.	788.	662.	123.	43.	80.	43.	2550.	2400.	2300.	2200.
Cu ppm	111.	106.	35.	7.	257.	88.	11.	128.	5.	5.	nd	nd
Rb ppm	na	na	3.	2.	na	na	na	na	1.	2.	1.	1.
Sr ppm	na	na	5.	4.	na	na	na	na	2.	1.	1.	2.
Zr ppm	na	na	8.	7.	na	na	na	na	4.	4.	5.	4.
TOTAL	101.106	99.746	100.370	100.447	98.763	101.090	100.808	100.370	100.565	99.565	98.493	99.698

Sample	E05-0460	E05-0500	E05-0540	E05-0580	E05-0620	E05-0660	E05-0720	E05-0780	E05-0860	E05-0900	E05-0960	E05-1000
Unit	D	D	D	D	D	D	D	D	LP	LP	LP	LP
SiO2	35.600	36.100	35.900	36.500	35.900	34.400	34.000	36.800	31.400	30.500	36.400	35.700
TiO2	0.027	0.033	0.032	0.023	0.030	0.027	0.018	0.032	0.050	0.100	0.082	0.092
Al2O3	0.560	0.680	0.680	0.420	0.700	0.420	0.400	0.580	1.140	1.760	1.660	2.050
Fe2O3	3.600	4.000	5.100	3.400	4.800	7.800	5.000	5.200	6.700	2.700	7.900	2.100
FeO	1.600	1.600	1.700	1.200	1.200	2.900	1.700	1.400	3.300	5.900	3.500	6.300
MnO	0.110	0.130	0.110	0.121	0.110	0.120	0.120	0.090	0.240	0.170	0.120	0.110
MgO	42.100	41.500	41.000	41.400	41.700	40.200	43.600	39.700	33.100	30.700	36.000	30.000
CaO	0.140	0.060	0.050	0.860	0.220	0.290	0.070	0.170	5.850	4.070	0.930	2.730
Na2O	nd	0.300	nd	nd	nd	nd	nd	nd	nd	nd	nd	nd
K2O	nd	0.010	nd	nd	nd	nd	nd	nd	nd	nd	nd	nd
P2O5	0.030	0.040	0.020	0.040	0.040	0.040	0.030	0.010	0.030	0.030	0.020	0.040
H2O	14.400	14.400	13.900	14.300	14.200	13.400	14.800	14.200	10.200	4.400	11.700	5.500
CO2	0.400	0.300	0.300	1.000	0.400	0.400	0.200	0.900	7.200	18.700	1.600	15.000
S	0.090	0.080	0.040	0.040	0.030	0.040	0.060	0.090	0.070	0.060	0.040	0.070
Cl	na	na	na	na	na	na	na	na	na	na	na	na
V ppm	21.	27.	23.	23.	25.	31.	27.	28.	27.	63.	53.	63.
Cr ppm	980.	1700.	1500.	1700.	1400.	1700.	1500.	1900.	9200.	6700.	5300.	6500.
Co ppm	110.	100.	120.	110.	100.	160.	110.	120.	140.	100.	100.	99.
Ni ppm	2800.	5300.	2600.	2600.	3600.	3100.	3800.	2600.	1700.	2100.	2200.	1600.
Cu ppm	50.	48.	nd	8.	nd	nd	nd	5.	8.	12.	8.	8.
Rb ppm	3.	1.	1.	1.	1.	2.	1.	1.	2.	2.	2.	4.
Sr ppm	1.	2.	1.	5.	2.	4.	1.	3.	130.	270.	22.	120.
Zr ppm	4.	4.	4.	2.	4.	3.	3.	3.	3.	3.	8.	6.
TOTAL	99.180	100.178	99.401	99.902	100.009	100.705	100.718	99.800	100.878	100.391	101.031	100.882

Sample	E08-1160	E09-1165	E09-1215	E09-1255	E09-1275	E09-1285	E16-1425	E16-1550	E16-1600	E16-1830	E16-2185	E21-0060
Unit	LP	LP	LP	LP	LP	LP	D	D	D	D	LP	QG
SiO2	39.000	35.300	35.700	37.500	38.100	38.400	33.200	35.800	35.700	36.700	37.300	50.400
TiO2	0.142	0.085	0.108	0.162	0.200	0.153	nd	nd	nd	0.018	0.028	0.324
Al2O3	3.000	1.540	2.430	2.870	3.680	3.520	0.126	0.184	0.151	0.221	0.516	13.000
Fe2O3	5.500	7.500	9.100	8.000	6.500	7.200	6.000	3.200	2.700	3.500	3.000	2.300
FeO	4.100	3.000	3.700	3.300	3.800	4.700	3.300	3.300	3.900	6.000	6.500	8.700
MnO	0.115	0.160	0.200	0.220	0.220	0.250	0.091	0.105	0.108	0.134	0.175	0.181
MgO	34.000	37.300	35.700	33.200	30.700	29.000	41.700	44.100	45.100	43.900	44.200	8.440
CaO	4.160	1.030	0.220	2.650	5.110	6.690	0.403	0.427	0.307	0.389	0.505	12.100
Na2O	0.021	0.500	nd	0.100	0.200	nd	nd	nd	nd	nd	nd	1.100
K2O	nd	nd	nd	0.020	nd	nd	nd	nd	nd	nd	nd	0.030
P2O5	nd	0.030	0.020	0.040	0.050	0.040	0.010	0.050	0.010	0.010	0.040	nd
H2O	9.600	12.300	11.700	10.400	9.600	9.800	14.400	11.500	11.600	7.900	6.200	3.000
CO2	nd	0.300	0.200	0.100	0.100	0.100	0.300	0.200	0.200	0.100	0.100	0.100
S	nd	0.060	0.100	0.160	0.090	0.170	0.400	0.300	0.100	0.100	0.100	nd
Cl	na	na	na	na	na	na	0.380	0.320	0.290	0.300	0.170	na
V ppm	50.	61.	66.	90.	100.	82.	nd	nd	nd	nd	30.	212.
Cr ppm	5260.	7800.	6500.	5200.	5900.	3100.	1130.	890.	1030.	925.	7210.	401.
Co ppm	71.	120.	110.	150.	100.	55.	214.	101.	103.	136.	131.	50.
Ni ppm	2200.	2000.	2200.	1700.	1900.	1650.	2350.	7300.	4600.	2450.	2700.	60.
Cu ppm	7.	9.	10.	12.	5.	270.	187.	38.	14.	15.	12.	102.
Rb ppm	6.	1.	2.	3.	2.	1.	nd	na	nd	1.	nd	3.
Sr ppm	5.	2.	2.	3.	2.	3.	6.	na	17.	12.	12.	80.
Zr ppm	13.	6.	7.	10.	10.	9.	nd	na	1.	nd	3.	25.
TOTAL	100.706	100.524	100.433	99.733	99.483	100.740	100.825	100.561	100.918	99.739	100.254	99.805

Concentrations of constituents quoted as ppm of the element were converted to the oxide for calculation of the total.
nd - not detected; na - not determined

Sample	E21-0120	E21-0160	E21-0200	E21-0290	E21-0400	E21-0540	E21-0570	E21-0645	E21-0690	E21-0830	E21-0900	E21-0970
Unit	QG	QG	QG	QG	QG	QG	QG	G	G	G	G	G
SiO2	50.200	51.000	50.500	49.600	51.400	50.930	50.600	48.900	48.000	49.800	48.310	49.600
TiO2	0.429	0.630	0.332	0.317	0.289	0.260	0.890	0.234	0.214	0.162	0.157	0.194
Al2O3	15.200	12.400	16.900	15.400	14.700	13.250	13.900	14.000	16.600	14.700	11.430	11.300
Fe2O3	1.800	0.700	2.000	2.300	1.800	1.650	1.500	1.280	2.100	1.600	1.210	0.500
FeO	8.000	10.500	5.900	7.100	7.000	7.600	15.600	7.400	6.000	5.200	6.900	6.000
MnO	0.191	0.230	0.159	0.181	0.164	0.175	0.237	0.205	0.160	0.138	0.190	0.187
MgO	7.010	9.200	6.900	7.430	8.520	10.270	5.200	11.870	10.800	10.500	15.080	14.500
CaO	12.300	11.400	12.500	14.300	11.300	11.600	8.000	12.040	12.800	14.600	11.770	13.200
Na2O	1.400	1.100	1.600	1.200	1.300	1.320	1.240	1.680	1.100	1.030	0.730	1.060
K2O	0.060	0.220	0.100	0.040	0.430	0.160	0.100	0.050	0.160	0.060	0.090	0.080
P2O5	0.020	0.120	nd	nd	0.010	0.030	0.130	nd	nd	nd	nd	nd
H2O	2.900	2.600	2.500	2.400	3.100	2.300	3.500	2.800	3.700	2.700	3.700	3.800
CO2	nd	0.300	0.100	nd	nd	0.600	0.100	0.500	0.100	nd	0.800	0.600
S	nd	0.100	nd	nd	nd	nd	nd	nd	nd	nd	nd	0.100
Cl	0.020	0.030	na	na	na	na	0.040	na	na	na	na	na
V ppm	193.	272.	194.	185.	178.	134.	300.	141.	149.	138.	125.	147.
Cr ppm	16.	27.	33.	48.	75.	274.	30.	548.	427.	85.	177.	426.
Co ppm	48.	59.	36.	49.	34.	44.	75.	51.	36.	33.	53.	40.
Ni ppm	68.	75.	90.	81.	53.	108.	53.	133.	95.	75.	99.	99.
Cu ppm	87.	26.	95.	11.	63.	78.	11.	39.	59.	109.	78.	260.
Rb ppm	2.	6.	4.	5.	14.	na	6.	na	5.	nd	na	6.
Sr ppm	92.	65.	94.	121.	77.	na	66.	na	100.	82.	na	66.
Zr ppm	28.	40.	22.	28.	32.	na	82.	na	19.	4.	na	12.
TOTAL	99.601	100.608	99.567	100.339	100.084	100.234	101.123	101.088	101.857	100.560	100.440	101.265

Sample	E21-1075	E21-1100	E21-1135	E21-1155	E21-1200	E21-1295	E21-1599	E21-1734	E21-1837	E21-1947	E21-2048	E21-2150
Unit	G	G	C	UP	UP	UP	UP	UP	D	D	D	D
SiO2	46.470	49.600	53.500	38.360	35.600	35.400	34.000	37.000	34.100	33.100	34.000	33.500
TiO2	0.097	0.092	0.147	0.134	0.082	0.041	0.300	0.024	nd	nd	0.022	na
Al2O3	16.160	7.630	2.400	2.380	1.700	1.300	0.806	0.544	0.153	0.217	0.304	0.132
Fe2O3	0.511	0.250	0.800	8.860	10.000	5.200	4.600	3.000	4.400	4.400	4.700	3.800
FeO	3.000	4.300	5.000	5.100	5.200	3.400	3.700	2.600	2.600	2.600	2.300	2.500
MnO	0.112	0.142	0.177	0.209	0.113	0.114	0.090	0.088	0.096	0.098	0.100	0.096
MgO	11.380	19.200	19.700	32.060	34.800	40.200	41.700	43.000	42.000	41.300	42.000	41.700
CaO	16.880	17.000	16.800	2.780	1.100	0.560	0.137	0.144	0.329	0.242	0.242	0.260
Na2O	1.450	0.254	0.178	nd	0.014	nd	nd	nd	nd	nd	nd	nd
K2O	0.060	nd	nd	0.010	nd	0.050	nd	nd	nd	nd	0.030	nd
P2O5	nd	0.040	nd	nd	0.030	0.050	0.040	nd	0.050	0.050	0.060	0.020
H2O	3.600	2.000	1.700	6.700	10.800	13.800	14.900	10.300	15.100	16.100	14.800	15.100
CO2	0.600	nd	0.100	0.800	nd	0.100	0.100	1.100	0.200	0.200	0.100	0.200
S	nd	nd	nd	nd	0.200	0.100	nd	nd	nd	nd	0.200	0.200
Cl	na	0.010	na	na	0.080	0.100	0.100	na	0.400	0.440	0.420	0.480
V ppm	97.	117.	115.	59.	34.	28.	nd	nd	8.	nd	21.	nd
Cr ppm	1500.	2700.	4270.	5470.	3100.	4000.	5520.	8180.	1040.	1170.	1140.	1050.
Co ppm	17.	31.	39.	147.	127.	68.	101.	82.	74.	74.	141.	53.
Ni ppm	72.	238.	149.	530.	1100.	2300.	2700.	2700.	3200.	3000.	3300.	3700.
Cu ppm	48.	381.	8.	8.	21.	15.	12.	12.	9.	8.	21.	10.
Rb ppm	na	2.	nd	4.	5.	na	na	na	1.	na	nd	2.
Sr ppm	na	62.	11.	4.	4.	na	na	na	3.	na	2.	5.
Zr ppm	na	3.	7.	4.	8.	na	na	na	4.	na	4.	4.
TOTAL	100.571	101.020	101.169	98.289	100.337	101.306	101.636	99.349	99.999	99.309	99.888	98.621

Sample	E21-2234	E21-2378	E21-2583	E21-2886	E21-3079	W04-0140	W04-0220	W04-0280	W04-0370	W04-0400	W04-0440	W04-0530
Unit	D	LP	LP	LP	LP	D	D	D	LP	LP	LP	LP
SiO2	35.350	35.100	35.000	35.000	36.400	34.500	35.800	35.800	33.700	38.900	36.600	35.200
TiO2	na	0.020	0.018	0.033	0.037	0.017	0.011	0.008	0.013	0.042	0.048	0.023
Al2O3	0.206	0.361	0.319	0.620	0.714	0.350	0.250	0.470	1.430	0.620	0.910	0.680
Fe2O3	4.590	4.900	4.600	5.500	4.700	4.200	4.000	4.800	9.500	2.400	6.900	4.200
FeO	3.000	2.300	4.000	3.700	4.600	3.200	3.200	3.500	5.300	2.100	3.800	3.100
MnO	0.128	0.080	0.102	0.129	0.111	0.150	0.100	0.100	0.120	0.130	0.140	0.150
MgO	42.410	41.000	42.000	41.000	41.800	41.900	42.100	39.800	36.400	39.900	38.100	41.100
CaO	0.216	0.309	0.165	0.381	0.759	0.180	0.090	0.090	0.040	0.060	0.080	0.060
Na2O	nd	nd	nd	nd	0.011	0.100	0.300	0.200	nd	nd	nd	0.200
K2O	0.010	nd	nd	nd	nd	nd	nd	nd	nd	nd	nd	nd
P2O5	nd	0.020	0.050	0.060	0.040	0.020	0.030	0.040	0.020	0.030	0.020	0.030
H2O	13.200	14.100	12.800	12.800	9.200	13.800	12.400	13.100	12.200	13.200	12.400	14.100
CO2	1.300	0.100	nd	0.100	nd	0.400	0.200	0.300	0.400	0.300	0.200	0.300
S	nd	0.400	0.200	0.100	nd	0.060	0.130	0.070	0.050	nd	nd	nd
Cl	na	0.230	0.320	0.390	0.300	na	na	na	na	na	na	na
V ppm	nd	24.	25.	30.	27.	nd	nd	nd	nd	32.	58.	36.
Cr ppm	1360.	6650.	5170.	6660.	4930.	1100.	1100.	1400.	2800.	6100.	7300.	5800.
Co ppm	88.	148.	160.	102.	96.	90.	130.	87.	150.	66.	95.	140.
Ni ppm	2800.	2900.	2700.	2300.	2900.	3700.	4000.	3000.	2700.	2600.	2750.	3000.
Cu ppm	9.	77.	15.	11.	12.	17.	97.	33.	12.	10.	17.	13.
Rb ppm	na	nd	nd	2.	2.	2.	nd	2.	1.	2.	2.	1.
Sr ppm	na	4.	1.	2.	1.	2.	1.	1.	nd	2.	2.	2.
Zr ppm	na	4.	2.	3.	4.	2.	1.	2.	nd	7.	3.	2.
TOTAL	100.976	100.292	100.698	101.097	99.779	99.522	99.309	98.879	99.945	98.919	100.637	100.396

Concentrations of constituents quoted as ppm of the element were converted to the oxide for calculation of the total.
nd - not detected; na - not determined

Sample	W04-0690	W04-0935	W04-1175	W04-1215	W04-1271	W13-0245	W13-0345	W13-0425	W13-0520	W13-0665	W13-0765	W13-0905
Unit	LP	LP	LP	LP	LP	UP	UP	UP	UP	D	D	D
SiO2	32.200	34.600	26.700	36.700	35.400	35.800	37.000	35.400	33.100	34.400	34.300	36.100
TiO2	0.030	0.115	0.058	0.045	0.050	0.054	0.060	0.037	na	0.018	nd	nd
Al2O3	0.700	0.950	0.840	0.870	1.050	1.500	1.900	1.100	0.350	0.240	0.180	0.170
Fe2O3	10.700	8.400	24.400	4.400	6.500	6.300	5.200	4.800	4.500	4.100	4.400	3.200
FeO	5.400	3.900	10.600	2.700	2.900	4.100	3.700	3.400	2.400	2.600	2.900	3.800
MnO	0.170	0.200	0.180	0.180	0.160	0.170	0.120	0.130	0.097	0.088	0.098	0.110
MgO	37.000	38.200	27.700	40.100	38.900	38.000	40.000	41.200	41.200	42.500	43.400	45.200
CaO	0.050	0.130	0.070	0.110	0.150	0.570	0.640	0.630	0.047	0.097	0.112	0.230
Na2O	nd	0.200	nd	nd	0.100	0.100	0.010	0.010	na	nd	nd	0.007
K2O	0.010	nd	nd	nd	nd	0.040	0.060	nd	na	nd	nd	0.050
P2O5	0.030	0.050	0.010	0.020	0.020	0.050	0.070	0.040	0.050	0.010	0.020	0.060
H2O	12.900	12.000	8.600	12.900	13.700	11.400	10.400	12.300	15.400	15.200	14.100	11.000
CO2	0.300	0.200	0.200	0.300	0.300	0.100	0.100	0.100	0.200	0.100	0.200	0.100
S	nd	nd	nd	nd	nd	0.100	0.010	nd	nd	0.100	0.100	0.100
Cl	na	na	na	na	na	0.090	0.120	0.320	0.390	0.340	0.280	0.230
V ppm	nd	70.	48.	45.	52.	28.	35.	21.	nd	nd	nd	nd
Cr ppm	4800.	6300.	3700.	8800.	7500.	2660.	4500.	6750.	5950.	684.	1250.	1170.
Co ppm	150.	170.	160.	120.	130.	94.	94.	90.	69.	67.	76.	88.
Ni ppm	2200.	2500.	1900.	2100.	2100.	1900.	2050.	2600.	2650.	2900.	2850.	2950.
Cu ppm	8.	8.	11.	14.	11.	8.	7.	8.	8.	nd	nd	nd
Rb ppm	1.	3.	4.	nd	2.	nd	1.	na	1.	na	1.	nd
Sr ppm	nd	1.	5.	2.	2.	1.	nd	na	2.	na	3.	2.
Zr ppm	2.	4.	3.	5.	3.	4.	4.	na	4.	na	4.	3.
TOTAL	100.491	100.216	100.170	99.901	100.618	99.021	100.326	100.798	98.950	100.270	100.645	100.914

Sample	W13-1060	W13-1190	W13-1265	W13-1330	W13-1530	W14-0955	W14-1505	W14-1575	W14-1660
Unit	D	D	LP	LP	LP	D	V	V	V
SiO2	35.200	37.000	34.600	35.000	34.700	34.100	37.100	40.700	44.700
TiO2	0.019	0.018	0.020	0.017	0.028	0.027	1.240	0.940	1.500
Al2O3	0.290	0.280	0.493	1.200	0.620	0.433	10.900	12.700	13.000
Fe2O3	3.300	3.300	5.000	5.300	4.600	6.500	0.700	nd	nd
FeO	3.900	5.800	4.500	4.700	6.300	1.000	11.200	16.900	12.900
MnO	0.126	0.168	0.156	0.133	0.166	0.085	0.452	0.209	0.280
MgO	44.600	44.900	42.400	42.200	42.100	40.600	6.300	10.000	5.900
CaO	0.456	0.314	0.326	0.235	0.388	0.119	9.800	5.900	9.500
Na2O	0.008	0.007	nd	na	nd	nd	3.600	0.036	2.300
K2O	nd	nd	nd	na	nd	nd	1.900	0.130	0.140
P2O5	0.040	0.020	0.030	0.030	0.020	0.050	0.120	0.100	0.150
H2O	11.400	7.800	10.700	10.400	8.800	14.300	1.700	7.500	4.600
CO2	0.100	0.100	0.100	0.110	nd	3.000	15.100	5.500	5.200
S	nd	0.100	na	0.100	0.500	nd	0.300	0.300	0.400
Cl	0.280	0.210	0.250	0.260	0.230	0.040	0.040	0.020	0.010
V ppm	nd	nd	nd	na	35.	21.	313.	441.	441.
Cr ppm	777.	1110.	8990.	7960.	7530.	624.	28.	27.	42.
Co ppm	74.	97.	104.	98.	165.	85.	49.	61.	50.
Ni ppm	3050.	3100.	2550.	2450.	4200.	2900.	68.	57.	57.
Cu ppm	7.	7.	7.	12.	774.	15.	nd	131.	130.
Rb ppm	na	na	nd	1.	nd	na	na	na	na
Sr ppm	na	na	nd	1.	nd	na	na	na	na
Zr ppm	na	na	nd	nd	nd	na	na	na	na
TOTAL	100.230	100.586	100.225	101.172	100.208	100.729	100.517	101.035	100.681

Concentrations of constituents quoted as ppm of the element were converted to the oxide for calculation of the total.
nd - not detected; na - not determined